Glacial stratigraphy and micromorphology of the Pine Point Pb-Zn mining district, Northwest Territories

By

Jessey Rice B.Sc.

Department of Earth Science

Submitted

In partial fulfillment of the degree of

M.Sc. In Earth Science

Faculty of Mathematics and Science, Brock University

St. Catharines, Ontario

Abstract

This investigation aims to gain a better understanding of the glacial history of the Pine Point Mining district, Northwest Territories, by examining the sedimentological properties of the glacial sediments including, geochemical analysis, heavy mineral concentrate analysis, clast macro-fabrics, pebble lithologies, and micromorphological investigation. Four till units were identified, and three were associated with identified erosional bedrock features and streamlined landforms in the area, indicating a minimum of three ice flow directions. Sedimentological properties suggest that these units were all Type- B tectomict/mélange till, emplaced as part of a soft subglacial deformable bed. The lack of ice-marginal advance and retreat sequences within the studied till, suggests the Middle Wisconsinan Laurentide Ice margin was likely north and west of the Pine Point area, as opposed to along the margin of the Canadian Shield and Western Sedimentary Basin where it has been suggested to have existed.

Acknowledgements

First off, I wish to thank Dr. John Menzies. Thank you for picking me for this project, guiding me through it, and teaching more then I could ever imagine, you have given me the opportunities of a lifetime and I am very grateful, and will never forget it!

Thank you to Dale Hess and Graham Larson for their critical reviews of this work and agreeing to take the time and effort to review this thesis, your insights are greatly appreciated!

Roger Paulen and Beth McClenaghan, you guys helped me out more than I could ever put in words! The opportunities you have given me, the people you have introduced me to, and the lessons you have taught me are things I will be forever grateful for, thank you so much!

Natasha, ha ha, what can I say? I can't imagine spending so much time with just one other person and not going mad! Your assistance in the field was greatly appreciated! Thank you for being so awesome.

Mike Parkhill, I can't help but laugh just trying think of something to write, we have had too many good time, you have taught me some great things about geology but even better things about life! I can't wait to keep learning from you, and thank you for all your help and planning!

This project was funded by the Geological Survey of Canada's Geomapping for Energy and Minerals (GEM) program (2008-2013) under the Tri-Territorial Indicator Mineral Project, for which I am extremely grateful.

To all my friends at Brock (too many to mention) thank you so much for all the great memories, I will never forget the Geoclub, trivia night, epic monopoly games, etc. To

all my housemates 7 Culligan and 34 Thompson, you guys are amazing and thank you so much for making my time in St. Catharines so enjoyable!

The Argent family, Bob, Liz, and David, thanks for taking me in under your wing when I needed a home away from home, I will never forget the generosity you have shown me and I hope I get the opportunity to repay you somehow, someday.

Kaleb Wagner, I am thankful I had the opportunity to spend a year with you and share an office with you. I will really miss the great times we had in that office! Mary Spring, thanks for all the coffee talks, letting me crash at your place, and letting me play with Nelly, I greatly appreciate everything you did for me. Catherine Horrigan, thanks for always being there for me when I was getting stressed and making sure I did not lose my mind! Thanks for all the great times you truly are a great friend!

Most of all thank you to my family, Mom, Dad, Aron, and Grandma thank you for all the support throughout the years, I could not have done this without you! You have always been there for me and I will never forget it, you are the greatest family a perpetual student could ever have!

I am sorry if I missed anyone, I have so many people to thank I could not have mentioned you all!
This one is for you Grandpa!

-Jessey M. Rice

Table of Contents

List of Tables

List of figures

Chapter 1

1.0 Introduction

During the Last glacial epoch the Laurentide Ice Sheet (LIS) covered a large portion of Canada. Not surprisingly, the effects that the LIS had on the Canadian landscape were vast and profound, but are not yet fully understood. The importance of having a firm understanding of the glacial history at the regional context is becoming increasingly important, as it provides insight into the sedimentology of the region, allowing for more precise aggregate, groundwater, and contamination management, structural engineering planning, and development of more accurate mineral exploration methods.

Mineral exploration, especially glacial drift prospecting, has received increased focus over the last several years (e.g. McClenaghan and DiLabio, 1996; Parent et al., 1996; Paulen, 2009), especially in northern Canadian regions. Glacial drift prospecting involves the identification of indicator minerals and mapping their transportation from the source deposit. This method requires an accurate understanding of the mechanism, direction, and transport distance of glacial sediments. Clearly, a firm understanding of the glacial history and the changing glacial dynamics throughout glaciation are essential to accurately mapping glacial dispersal trains associated with economical grade mineral deposits. However, a paucity of ice flow history along the boundary of the Canadian Shield and Western Sedimentary Basin during the LGM, in the Great Slave Lake region, currently exists in modern research (Vincent and Klassen, 1989). Vincent and Klassen (1989) refer to this region as “terra incognita” due to the lack of Quaternary studies done in this region, largely because of the dense boreal forest cover in the region. However, with increased focus on the practical applications of glacial drift prospecting, especially in Northern Canadian regions, a firm understanding of the glacial history of this region will become increasingly important.

Although surficial landforms generally indicate the most recent paleo-ice flow, the exploration vectors needed for glacial drift prospecting requires a more detailed comprehension of ice flow/ice dynamics of more than just the last known erosional vector. One of the most common methods for re-creating the glacial history of a region is to examine the erosional (i.e. striations) and the sedimentological record. However, sediment sequences can often be thin or incomplete; fortunately the past producing Pine Point Mining District provides large sections of *in-situ* till, which overlie low relief bedrock, making it an ideal location for gaining a more in-depth understanding of the changing glacial dynamics of the LIS throughout the Late Wisconsinan.

Studying and understanding past glacial environments is difficult to approach, in part due to the lack of accessibility to comparable contemporary environments and the number of variables that control the dynamics of the ice-bed interface. These variables include ice sheet thickness, thermal regime, geometry, sediment permeability, sediment susceptibility to deformation, and pore water pressure.

All of these variables impact the transportation, deposition, and deformation of glacially deposited sediments, or till. Till is defined as non-sorted diamicton that has been transported and deposited directly by glacial ice with little or no sorting by water (Dreimanis, 1982). Traditionally, this definition is then separated into three primary till types: lodgement till, deformation till, and melt-out till, although melt-out tills are the result of "gradual release of glacial debris from ice that is not sliding of deforming internally," and has therefore not been transported (Dreimanis, 1982). However, since the classification schemed was developed by Dreimanis (1982) for the International Quaternary Association (INQUA) Commission on the Genesis and Lithology of Glacial Quaternary Deposits, criticisms of the macroscopic identifiable features used to differentiate between till types have been identified (Ruszczynsk-Saenajch et al., 2003; van der Meer et al*.,* 2003; Menzies et al*.,* 2006). The wide varieties of glacial deposits have too many characteristics that overlap with traditional classification schemes that make identifying till type in the field difficult.

There has been increased recognition of the importance of the deforming subglacial bed and its role in glacier movement and sediment transport (Boulton, 1976), and the recognition of different microstructures within macroscopically similar tills (van der Meer, 1993; Benn and Evans, 1996; Carr, 1999; Piotrowski and Tulczyk, 1999; Menzies, 1998, 2000; Menzies et al*.,* 2006; van der Meer and Menzies, 2011; Neudorf et al., 2013). Menzies et al. (2006) have suggested that some of the traditional classifications of "tills" are no longer valid. Instead, the use of micromorphological structure identification should been used to infer subglacial deformation and assist in the understanding of the depositional environment (Menzies and Maltman, 1992; Menzies et al., 1997; 2006; van der Meer et al., 2003; O'Cofaigh et al., 2005), and should be used to modify the INQUA classification system.

Since the increased understanding of the importance of the deformation of subglacial sediments has been recognized, the focus has recently switched to studying the strain imprinted upon on the diamict. Menzies (2012) has suggested three possible pathways responsible for the deformation of these sediments. These strain pathways, coupled with previous till classifications, has resulted in the classification of three general types of tectomict (Fig 1.). Type A having undergone significant strain, Type B have undergone varying degrees of strain, ranging from relatively low (but above yield strength) to comparatively high degrees of stress (close to the effective stress approaching zero), and Type C having little or no evidence of strain.

Therefore, with the ability to analyze the internal structures formed *in situ* as the sediment was deformed, an interpretation of deformation, and depositional processes imprinted upon glacial sediments can be made.

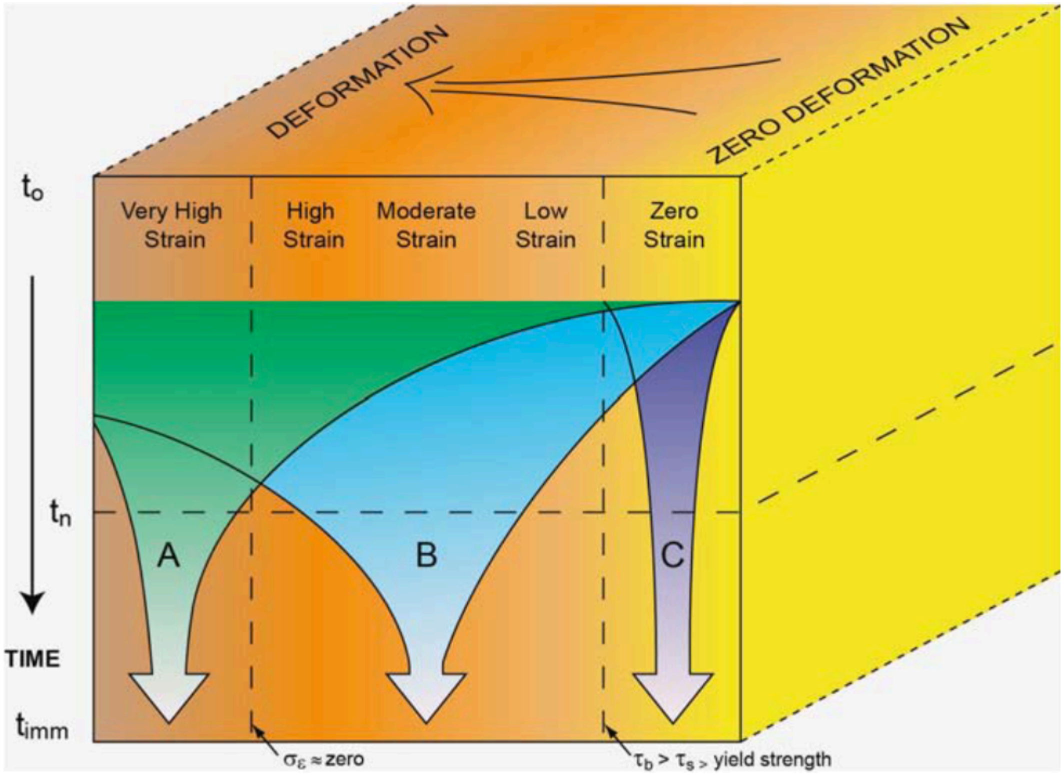

Figure 1. Strain pathways A, B, and C resulting from subglacial deformation over time.
(from: Menzies, 2012)

This approach, coupled with traditional sedimentological investigation methods, that was used to study a ~20 m vertical section of exposed diamicton at Pit-K62, within the Pine Point Mining District, Northwest Territories, to gain a better understanding of the erosion, transportation, deposition, and deformation of glacial sediments within this region. Through a detailed sedimentological facies investigation there will be a better understanding of the glacial history in terms of chronology and glacial vigour, ice-flow dynamics, and deposition mechanisms in the southern Great Slave Lake region.

1.1 Geological Setting

1.1.1 Location and Physiography

The past producing Pine Point Pb-Zn mine site is located on the southern shore of Great Slave Lake in the Northwest Territories (Fig. 2), approximately 800 km north of Edmonton, Alberta. It is located about 50 km east-southeast of the town of Hay River and about 180 km south across Great Slave Lake, from Yellowknife, located in the Buffalo Lake topographic map sheet (NTS 85B). Pine Point is located within the Great Slave Plain (Bostock, 1964; 1970) near the border of the eastern edge of the Western Canadian Sedimentary Basin (WCSB) and the western margin of the Canadian Shield. The mine closed in 1987 and, while the mine infrastructure and the town of Pine Point were removed, the open pits were never reclaimed. The former open pits allow relatively easy access to some bedrock outcrops, and large (up to ~ 22m high) exposures of undisturbed, continuous *in-situ* glacial sediment facies. Since the closing of the mine water has accumulated at the base of the open pits; however, accessibility and glacial sediment exposure has not been greatly affected. The Pine Point area has relatively low relief (less than 15 m), with a landscape dominated by Black Spruce peatlands (Lemmen, 1990). Black Spruce bogs, with discontinuous permafrost cover most of the vegetated areas (Heginbottom and Dubreuil, 1993) , however, former exploration cut lines and remaining mine infrastructure allows accessibility in summer months.

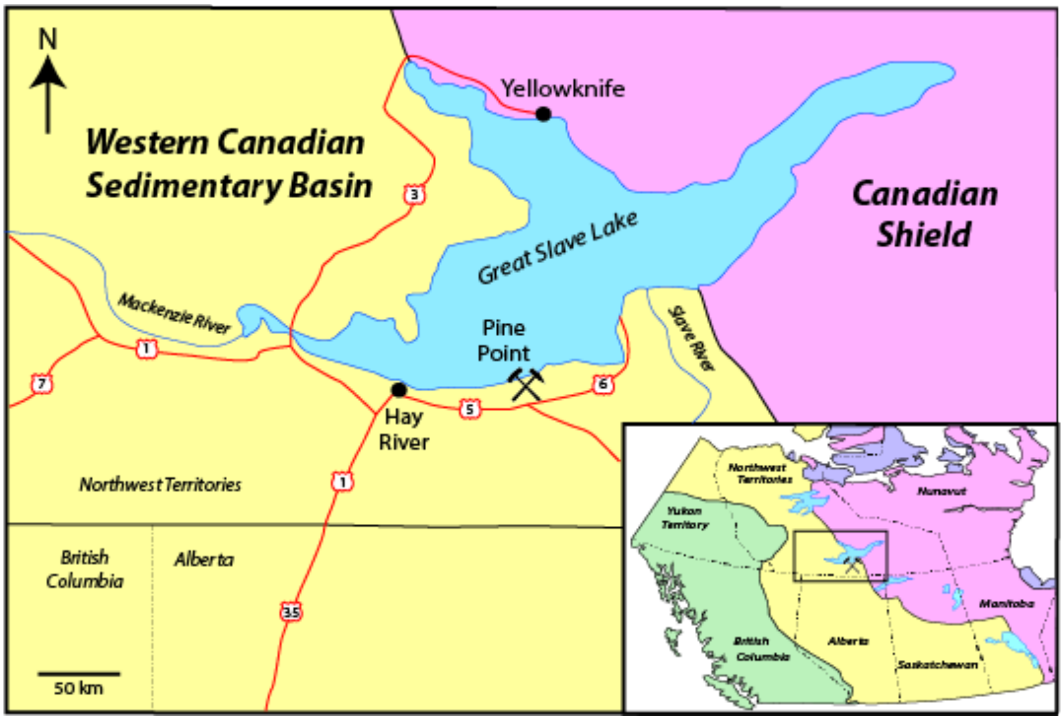

Figure 2. The geological and geographic setting of the past-producing Pine Point mine site, located on the southern shore of the Great Slave Lake, Northwest Territories. The study area is located near the eastern margin of the Western Canadian Sedimentary Basin and western margin of the Canadian Shield.

1.1.2 Bedrock Geology

The Pine Point mining district is located just west of the boundary between the WCSB and the Canadian Shield known as the interior platform (Rhodes et al*.,* 1984). The major Pine Point Pb- Zn ore bodies are hosted within Middle Devonian carbonates which are located in, or are in close proximity to, the dolomitized Presqu'ile barrier complex (Okulitch, 2006; Hannigan, 2007). The barrier complex is a reef-like complex that acts as the transition between the shallow marine sediments to the south and the deep marine sediments to the north. The reef complex extends west into the subsurface of the WCSB in northeastern British Columbia, subparallel to the McDonald Basement Fault (Kent, 1994). The Presqu'ile complex developed after the Devonian transgression of a carbonate-depositional sea across the platform of the north end of the Elk Point Basin, stretching south to North Dakota (Kent, 1994). The Presqu'ile Formation consists of Upper Keg River and Sulphur Point Formations. The Sulphur Point Formation overlies Keg River Formation, which is characterized by flat lensoid beds of carbonate mudstone and sandstones (Rhodes et al*.,* 1984). These Ordovician to Devonian age sedimentary units overlie a basement of Archean crystalline bedrock and Proterozoic sedimentary layers (Rhodes et al., 1984).

1.1.3 Mine Site Geology

The Pine Point deposit is considered a Mississippi Valley-Type (MVT) lead-zinc ore-deposit, where the deposition of pyrite, sphalerite, marcasite, and galena were deposited as hydrothermal fluids that percolated through the Presqu'le unit (Adams et al*.,* 2000). A number of studies have been conducted on the mineralization events at Pine Point and therefore will not be a focal point of this study (see Roedder, 1968; Krebs and Macqueen, 1984; Nelson et al., 2002; Paradis et al., 2006; Hannigan, 2007; Gleeson and Turner, 2007). The Pine Point barrier complex developed during the Givetian stage of the Devonian, and sub-crops gently (~ 2°) towards the west (Skall, 1975). The Sulphur Point Formation is composed of bioclastic limestones and carbonate sandstones that are the primary hosts of the ore bodies (Skall, 1975). There are more than 80 sulfide bodies within a 15 by 60 km geographical area at the mine site (Cumming et al*.,* 1990). The ore bodies are predominantly positioned along weakened bedrock planes associated with the Great Slave Lake Shear Zone (Eaton and Hope, 2003) with the primary control of ore deposition being karstification, which includes both surface and subsurface features and pore spaces (Rhodes et al*.,* 1984). The primary ore minerals are galena and sphalerite, which are the only minerals that occur at an economical level for lead and zinc at Pine Point (Hannigan, 2007).

1.1.4. Regional Quaternary Geology

The Late Wisconsinan advance of the Laurentide Ice Sheet (LIS) started from a Middle Wisconsinan interstadial minimum 27–30 $_{14}$C ka BP when the ice margin approximately followed the boundary of the Canadian Shield (Dyke et al., 2002). The Late Wisconsinan LIS reached its maximum extent ~ $_{14}$C 18 ka BP covering the majority of Canada (Dyke and Prest, 1987). Beget (1987) and Mathews (1974) suggests that the northwestern sector of the LIS consisted of low profile ice with streaming flow. Beget (1987) also suggested that ice streaming along the western and southern extents and thin overall thickness of the ice (~650 m) in Late Wisconsinan was responsible for rapid deglaciation in the region. The possibility of streaming ice has also been suggested in the northwestern section of the LIS by Kleman and Glasser (2007), and Winsborrow et al. (2004). More recent GIS investigations also suggest during deglaciation there were dynamic switches in ice flow orientation around the region to west and northwest of Pine Point (Brown et al., 2011). South of Pine Point there is evidence of a single glaciation during the Late Wisconsinan (Liverman et al., 1989; Paulen, 2009; Jackson et al., 2011). Wolfe et al. (2004) suggest through work on optical age data taken from stabilized sand dunes throughout northern Alberta and Saskatchewan, that the Pine Point region was deglaciated ~10.2 cal ka BP. This is similar to deglaciation estimates of the Pine Point region made by Dyke et al. (2002) and Dyke (2004) of ~10.0 - 9.6 $_{14}$C ka BP, and was based on location of the Cree Lake Moraine (Prest et al., 1968), which extends 300 km southeast from the western edge of Lake Athabasca, and the Slave Moraine which stretches 120 km along the same orientation as the Cree Lake Moraine, but occurs ~120 km north of Lake Athabasca (Bednarski, 1993). After the LIS retreated from the study area, glacial Lake McConnell inundated the region (Craig, 1965; Lemmen, 1990; Smith, 1994). Glacial Lake McConnell formed ~ 11.6 $_{14}$C ka BP in the Great Bear Lake region filling in a glacio-isostatic depression as the LIS retreated (Bednarski, 1999), and spread to the Great Slave Lake and Athabasca Lake regions covering 210 000 km^2 (Fig. 3) at its greatest extent, forming the second largest glacial lake known in Canada (Lemmen et al., 1994). The Pine Point region was inundated by the lake around ~ 10.5 - 9.9 $_{14}$C ka BP (Smith, 1994) and was confined by the LIS ice front to the east which Dyke and Prest (1987) estimated to be approximately along the edge of the Western Canadian Sedimentary Basin and the Canadian shield. Due to isostatic rebound the Lake was split into its current lake bodies: Great Bear Lake, Great Slave Lake, and Athabasca Lake ~ 8.3 $_{14}$C ka BP (Smith, 1994).

The LIS has had a profound effect on the geomorphology of the Pine Point mining district, especially in terms of glacial sediment deposition. The LIS had deposited till to thicknesses greater than 20 m in the region. In part due to the regionally gentle westward dip of the low relief bedrock surface, the sediment thickens westward from <1 m in the east to >25 m, where it is exposed in the westernmost open pits of the mine site. Thicker sections of glacial sediment occur as in-fillings of karst collapse structures. After the retreat of the LIS, the area was inundated by Glacial Lake McConnell, which winnowed the diamicton surface, and deposited a thin layer (<2 m) of beach and littoral glaciolacustrine sediments across the entire study area (Lemmen et al., 1994).

Figure 3. Maximum extent of Glacial Lake McConnell (shaded area) during the Late Wisconsinan ~ 10, 000 BP (Oviatt, 2013; Lemmen, 1990).

1.2 Previous Work

The natives of the southeastern edge of the Great Slave Lake region have long known of the metal-rich deposits at Pine Point (Bell, 1899; Bell, 1929). However, the deposits were not brought to the attention of people outside of the local settlement until first described by prospectors heading to the Klondike gold rush as they passed through the Great Slave Lake region (Bell, 1899; Campbell, 1966). In 1898 the first claim was staked at the site in hopes that the heavy lead and zinc sulphides would carry traces of gold or silver (Bell, 1929). The next year, Dr. R. Bell of the Geological Survey of Canada (GSC) was sent to the region to investigate prospector reports of lead and copper ores (Bell, 1899). In 1914, Gwynn G. Gibbins, a young mining engineer from the Huronian Belt Company staked another claim at the site, however, Gibbins lost his life on the front lines of WWI and nothing became of the claim (Bell, 1929). Little was done with the site until research was conducted at Pine Point in 1929 when the Northern Lead Zinc Company was formed, which included Cominco Limited (Campbell, 1966). The focus of Northern Lead Zinc Company's 1929-1930 exploration program was to determine if the known ore bodies were connected beneath the surface and to define the ore grade of the sub-cropping mineralization. The occurrence of the Great Depression in the 1930's halted all exploration in the area. After the depression, between 1940 and 1947, Cominco Limited directed a drilling program to delineate ore bodies associated with basement faulting (Campbell, 1966). In 1963, an induced polarization geophysical survey was conducted in the area, leading to the discovery of ore bodies that did not sub-crop (Hannigan, 2006). The Pine Point mine opened in 1964 and was one of the most profitable Pb-Zn mines in Canadian history (Hannigan, 2007). Cominco eventually shut down the mine in 1987 causing the mining town of Pine Point to close and slowly be removed from the location, with only some remnants such as roads and sidewalks still remaining. Between 1975 and 1981, Westmin Resources conducted drilling programs approximately 15 km west of Buffalo River and discovered nine additional deposits (Tamerlane Ventures Incorporated, 2013), however, none of these deposits have been mined to date. A soil survey was conducted by Brabec (1983), to distinguish anomalous Pb-Zn values in soil due to mineralization and those due to Zn-rich shales that occur in the area. This study was completed in order to examine proper methodology for conducting geochemical exploration in carbonate-hosted lead-zinc deposits.

GSC scientists carried out surficial mapping in the Pine Point area between 1989 and 1994. The main focus of the mapping projects was undertaken to expand the knowledge of Glacial Lake McConnell and its associated deposits (Lemmen et al., 1994). Detailed descriptions of Lake McConnell deposits and landforms were recorded. A diamicton was described by Lemmen (1990) as ranging from < 1 m to > 12 m thick, slightly-stony to stony with calcareous silt to silty-clay matrix, with total carbonate content ranging from 12-81%, and was concluded to be till (Lemmen, 1990). Glacial lacustrine sediments that commonly overlie the till were derived in part from the till, with wave activity being the predominant geomorphic process controlling the distribution of sediments (Lemmen, 1990).

Surficial geology maps of the Pine Point Mining District and surrounding area (Buffalo Lake (NTS 85B/15) and Klewi River (NTS 85B/16)) were compiled during the investigation of glacial Lake McConnell (Lemmen, 1998a,b). During these mapping compilations a single phase of ice flow to the west was identified. There is very little other published information on the ice flow history of the region (Prest et al., 1968; Paulen et al., 2008). Surficial geology of the western half of the Pine Point mining district has been mapped on a 1:50 000 scale which indicates that the predominant surficial sediments are glaciolacustrine (NTS 85-B/15)(Oviatt and Paulen, 2013), which are described in detail by Oviatt et al. (2013).

GSC fieldwork conducted in 2010 had documented cross-cutting striations on bedrock surfaces on the shoulders (bedrock benches) of the exposed open pits (Oviatt et al*.,* 2011; Oviatt, 2013). Documented striation measurements (Fig. 4), taken in the field, coupled with aerial photo and satellite imagery landform analysis, have determined a minimum of three ice-flow trajectories (Oviatt, 2013). The earliest flow indicated by the striations, was to the southwest (~230°), an intermediate flow to the northwest (~300°), and a later west-southwest (~250°) flow also occurred. There was a single striation record that indicated a flow toward the northwest (~330°), cross cutting relationships indicates that this phase must have taken place before the intermediate northwest (~300°) phase and the late west-southwest (~250°) phase (Oviatt et al., 2011). Landforms in the region are streamlined parallel to the last phase (~250°) of ice flow (Fig. 5), that reshaped older oriented landforms that were formed during the intermediate (~300°) glacial event.

Figure 4. Striation records found at pit O-28 indicating three flow directions: (1) 230° to the southwest, (2) 330° to the north-northwest, and (3) 297° to northwest. Measurements were completed by Oviatt et al., (2011), during reconnaissance work around the region in summer 2010. Field of view is approximately 1 m.

1.3 Classification of Sediments

Lemmen (1990) described a nearly continuous cover of a diamicton characterized as being slightly-stony to stony with calcareous silt to silty-clay matrix and was concluded to be till. This interpretation is supported by the nature of the sediment's matrix, which exhibited slight variation in composition throughout the study area, but usually consists of sandy-silt matrix with varying fissility, and contains sub-rounded to sub-angular, faceted and striated clasts, ranging in size from granules to boulders. Based upon Lemmen's (1990) interpretation, and field observations already published in conjunction with this thesis (Rice et al., 2013) the diamicton sampled from Pine Point discussed in this thesis will be henceforth referred to as till and this classification and justification will be examined in the following sections.

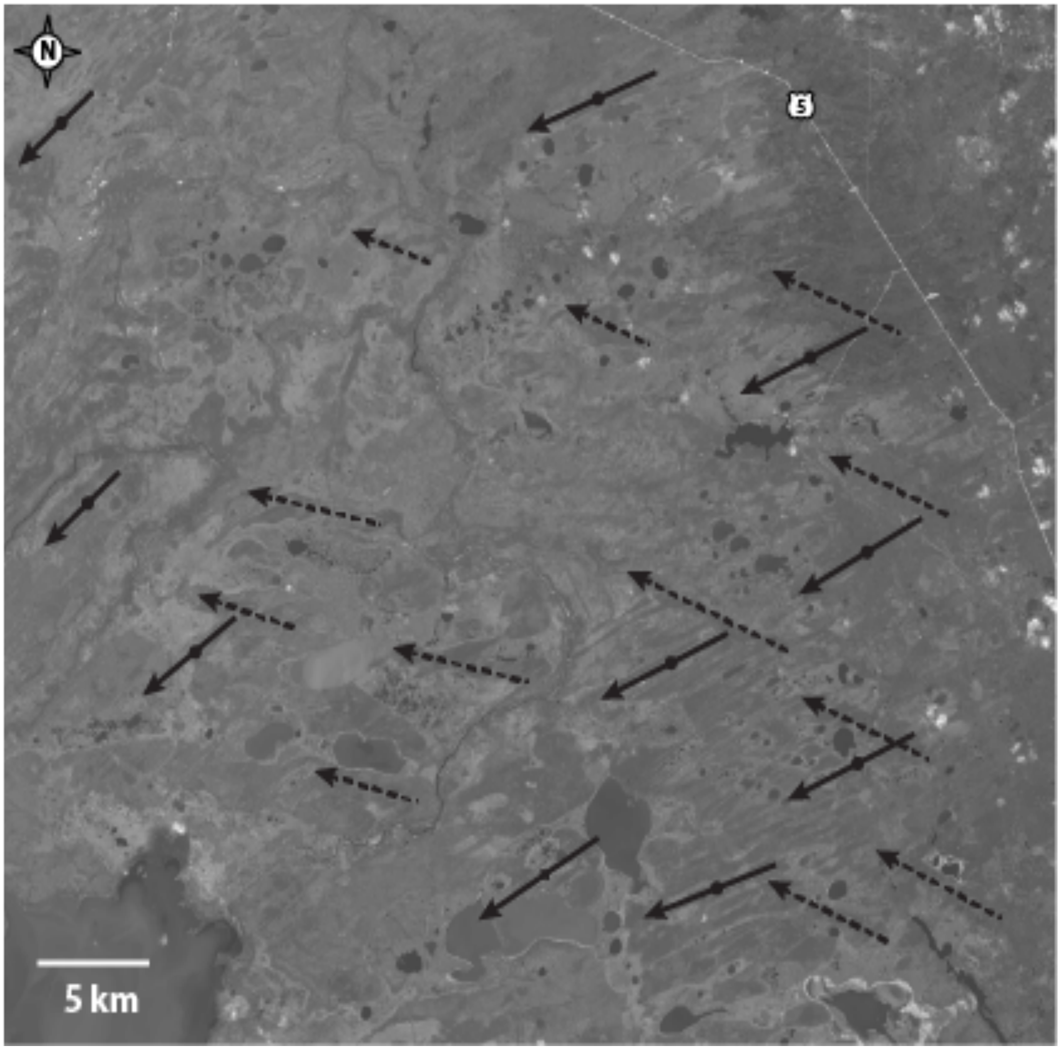

Figure 5. SPOT satellite image of Highway 5, southwest of the mining district, showing older, large northwest-trending glacial landforms (dashed arrows) crosscut by finer southwest-trending flutings.

1.4 Research Objectives

This thesis aims to gain a better understanding of the changing glacial dynamics that resulted in the deposition of till in the Pine Point mining district, in order to better understand the provenance of sediments deposited during the last glaciation. Through this investigation, a better understanding of the overall glacial history of the region will be obtained. A comparison between surficial landforms and reported striations in the region to the depositional record at pit K-62 will also be examined.

In summary the overall goal of this thesis is:

1. Investigate the changing ice dynamics throughout the Wisconsinan glacial history of the past producing Pine Point mining district through a detailed sedimentological examination of Pit K-62.
2. Determine whether the erosional record (surficial landforms and striations) observed in the Pine Point Region correlates with the deposited sedimentological record found at Pit-K62.
3. Investigate the relationship between previous ice margin hypotheses during the extent of the LIS and the sedimentary sequence at Pit-K62.

Chapter 2

2.0 Methods

2.1 Field observations

Initial site selection was based on reconnaissance fieldwork conducted in summer 2010 (Oviatt et al., 2011) around the Pine Point mining district. Several well-exposed sections in open pits were available for detailed study and Pit K-62 was selected for analysis (Fig. 6), as it displayed the largest

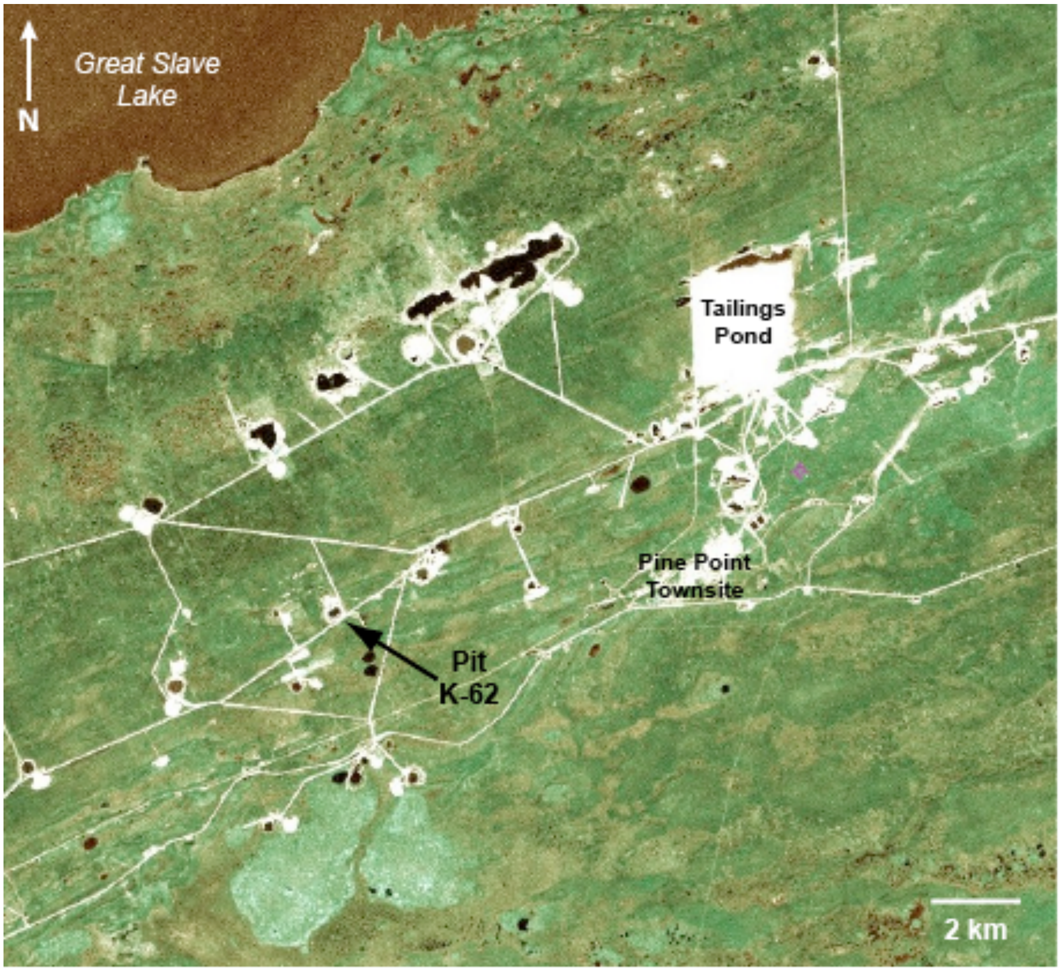

Figure 6. Landsat image of part of the past producing Pine Point mining district showing the location of open pit K-62, the focus of this research project.

depositional record (>20 m) and the northern face of the section was safely accessible to allow detailed sedimentological logging and also allows samples to be collected by hand.

This section (UTM 630160E, 6745706W NAD83) consists of a ~22 m vertically exposed face with six distinct units that can be distinguished with the naked eye by colour and sharp contacts (Fig. 7). A stratigraphic log was completed for the study site followed by detailed data collection including photographing the field site, photographing the specific study face, and photographing each individual sample. A GPS (NAD83) location was recorded for each sample collected, as well as the estimated clast content, clast roundness, oxidation, fissility, and any other general comments on the till. Any macroscopic diamicton architecture was also photographed and noted (i.e. shearing contact, rip up clasts, etc.). The units showed a large variance in clast size, ranging from large boulders to clay-sized fractions, and showed signs of reworking (mixing units), with many clasts being striated, faceted, and polished. Munsell colours were measured in the field on moist sediment, in natural light.

2.2 Bulk Sampling

A series of 3 kg and 12 kg samples were collected from four of the units that were believed to be till (Unit A- Unit D). The samples were collected after clearing any slope wash to reveal overconsolidated, fissile, *in situ* till. Once the surface debris was removed, the till was collected from each of the sample sites following procedures outlined by Spirito et al. (2011). Great care was taken to limit cross-contamination of samples, with the collection buckets being washed before use and the shovels used to remove the samples being washed before collection of each sample. All large pebbles and cobbles were removed from the collected sediments in order to maximize the amount of matrix material collected. In total, six bulk samples were collected throughout the section.

The 3 kg samples were submitted to the GSC Sedimentology Laboratory, Ottawa, for sample preparation, geochemical analysis, grain-size analysis, dry Munsell colour determination, and GSC archiving. Each sample was then put though standard procedure for the Sedimentology Laboratory, whereby each sample is dried at 105°C for 15 to 30 minutes, then each separate sample is laid out on dry Kraft paper and disaggregated using a rubber mallet (Girard et al., 2004). The < 0.063 mm fraction are isolated by dry sieving and sent for geochemical analysis (see Chapter 2.3). Grain-size analysis was conducted on a separate aliquot using a combination of wet and dry methods. The classes of sizes > 0.063 mm were determined by wet sieving in a stack of sieves, and the classes of sizes < 0.063 mm were determined using a Lecotrac LT-100 Particle Size Analyzer. Sediment classification was determined based on Shepard (1954) system for determining sand-silt-clay ratios. Munsell colour (dry) was determined for each till-matrix sample using a Spectrophotometer link to IQC colour software using dry samples.

2.3 Geochemical analysis of <0.063 mm fraction

Geochemical analysis has been used in unit correlation and provenance studies (Shetsen, 1984; Bell et al., 1989), but can also be used to determine depositional process (Walden, 2004), and assist in the identification of any

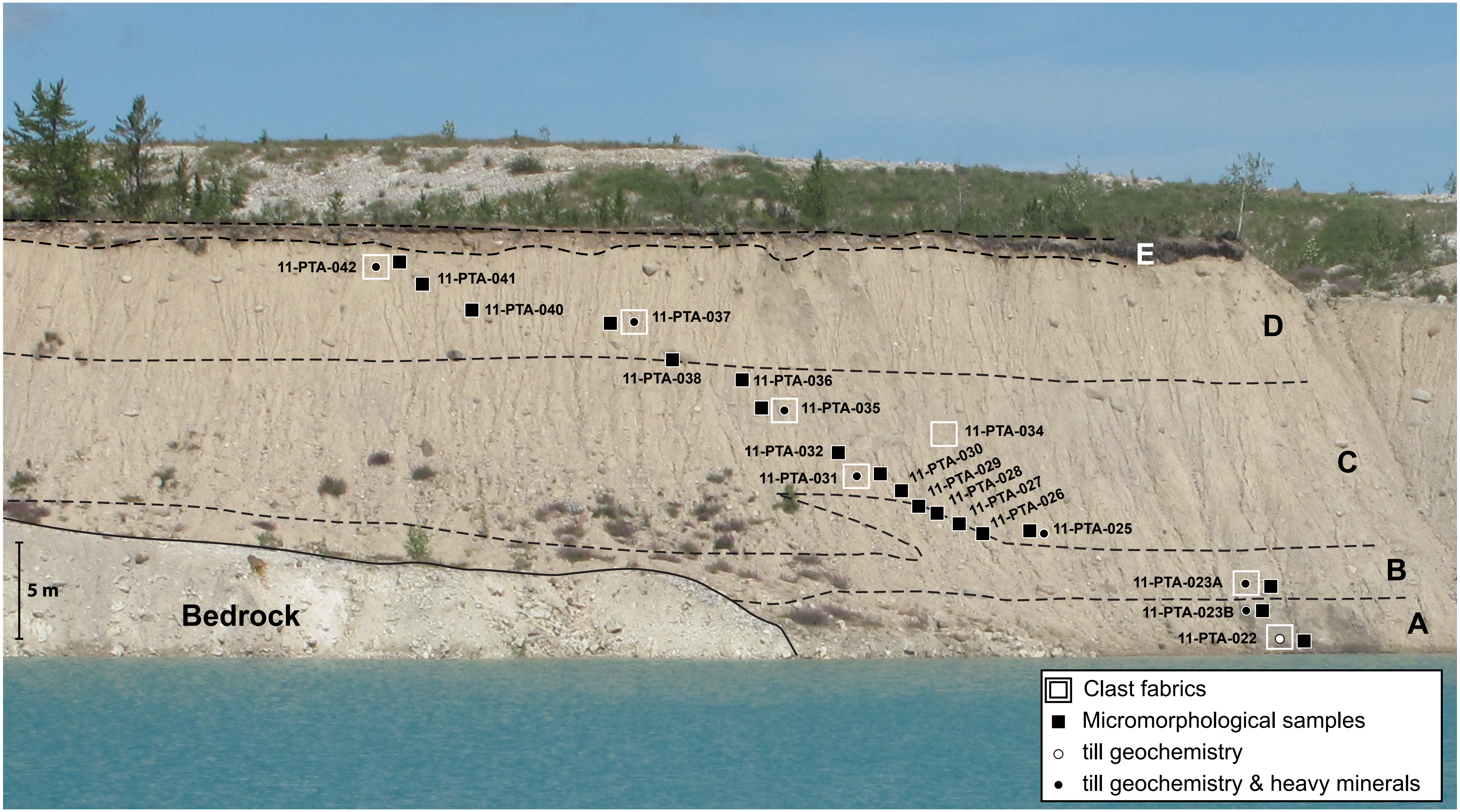

Figure 7. North face of open pit K-62, with four different till units (A to D) overlain by glacial Lake McConnell littoral sediments (Unit E). Total height of the section is 23 m. Dashed lines indicate the approximate till contacts. Sample locations and labels are indicated.

post-depositional weathering (Shilts and Kettles, 1990). The application of $CaCO_3$ analysis has been used for decades (Dreimanis, 1962) and also been used in provenance studies and stratigraphic correlation (Walden, 2004).

The < 0.063 mm till fraction was sent to Acme Analytical Labs, Vancouver, British Columbia, for analysis by aqua regia digestion/ICP-MS (Group 1F package). Thirty grams of sample material were weighed into a beaker and the aqua regia solution of HCl and HNO_3 (1:1) and demineralized water was added. This mixture was then placed in a boiling-water bath (> 95°C) for 60 minutes. After cooling, the solution was made up to a final sample volume, with a solution ratio of 0.5 g for 10 ml. Samples were then placed in a PerkinElmer ELAN® 6000 or 9000 ICP-MS and analyzed for 65 elements, including rare-earth elements. Samples were also analyzed by total digestion using borate fusion/ICP-MS methods (Group 4A + 4B package).

Total carbon, organic and inorganic carbon contents, and loss on ignition (LOI) were determined on < 0.063 mm fractions using the LECO® RC-412 Carbon Analyzer at the GSC in Ottawa. Samples were heated to 1350°C to determine percentages of total inorganic carbon and total carbon through infrared detection of CO_2. Samples were then heated for 1 hour at 500°C to determine the LOI. Detailed methodology can be found in the GSC Sedimentology Laboratory Manual (Girard et al., 2004). Additional portions of the < 0.063 mm fractions were used for determining calcite and dolomite concentrations. Concentrations were determined through analysis by the UIC CM5015 coulometer and acid evolution. The CM5015 exposes the sample to a temperature of approximately 950°C in an oxygen-rich atmosphere, rapidly oxidizing all carbon within the sample to CO_2. Concentrations are then automatically measured using absolute coulometric titration. During the acid evolution, samples are mixed with hydrochloric acid (1:1 concentration) and the concentration of calcite and dolomite is determined through analysis of the volume of CO_2 evolved in a Chittick gasometric apparatus, with the calcite being liberated and measured first and the slower-reacting dolomite being liberated and measured second. Detailed methodology of the procedure is described in the GSC Sedimentology Lab Manual (Girard et al., 2004).

2.4 Heavy mineral concentrates

Heavy mineral concentrates have been used for decades for the study of sedimentary rocks (Krumbein and Pettijohn, 1938; Milner, 1962; Carver, 1971; Lindholm, 1987), and sediments, which include rock fragments (Dreimanis et al., 1957; McClenaghan et al., 2000). The identification of heavy minerals has been used in a similar manner to pebble lithologies in determining provenance (Gwyn and Dreimanis, 1979; Lindholm, 1987). The heavy mineral concentrates found within a till unit are representative of the source rock they originated from, therefore allowing correlation between similar concentrates throughout a section, and assisting in provenance studies. However, density variations between minerals and destruction of less stable minerals must be taken into consideration. For example, some minerals such as calcite are fairly soft (H=3) and will break down rather quickly and may not be transported as far as a more robust mineral such as pyrite (H= 5-6) and therefore may have higher concentrations down ice from the bedrock source then the softer calcite, skewing the geochemical results. Therefore having an understanding of the local bedrock geochemistry is vital (McClenaghan et al., 2012).

Each facies unit identified in the field was sampled for heavy-mineral analysis (11-PTA-023A, -023B, -025, -030, -035, -037, -042). These samples (~12 kg) were submitted to Overburden Drilling Management Limited, Nepean, for disaggregation and production of heavy-mineral concentrates. Each sample was disaggregated in water then wet sieved to 2.0 mm. The > 2.0 mm fraction was washed with oxalic acid to remove iron staining and discolouration, and set aside for pebble-lithology analysis (see Chapter 2.6). The < 2.0 mm till fraction was passed over a shaking table separating the light and heavy minerals resulting in a table concentrate. The table concentrate was then panned, and precious metals and sulphide grains counted and set aside. The heavy fraction was then dried and sieved to remove the < 0.25 mm fraction. The 0.25 to 2.0 mm fraction was concentrated using heavy-liquid separation in methylene iodide diluted to a specific gravity of 3.2. The > 3.2 specific gravity fractions are then run through a ferromagnetic separator. The non-ferromagnetic fractions are subjected to an oxalic-acid wash to remove iron stains and secondary coatings, and then dry sieved into 0.25, 0.5, and 1.0 mm fractions. The 0.25 to 0.5 mm fraction then undergo paramagnetic separation. The paramagnetic fractions, along with the 0.5 to 1.0 mm and the 1.0 to 2.0 mm fractions, are selected and analyzed for abundance, composition, and paramagnatism. The sample-processing procedure is summarized in Figure 8.

When the results from ODM were obtained, the grain counts reflected results from the actual weight of the submitted samples. However, the submitted samples were of varying weights; to compensate for this, the results were normalized to a 10 kg samples size, to allow comparison between the ODM values.

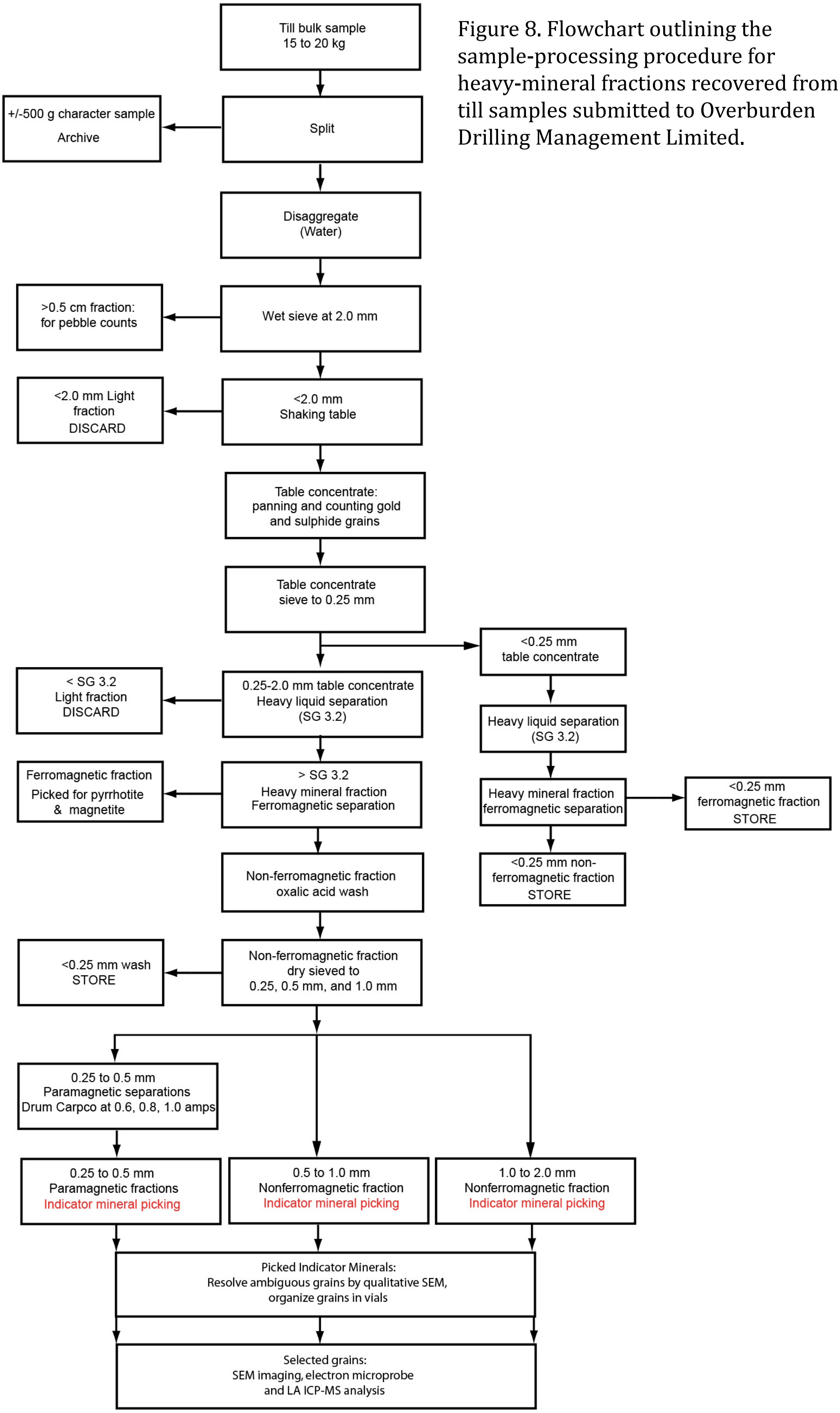

Figure 8. Flowchart outlining the sample-processing procedure for heavy-mineral fractions recovered from till samples submitted to Overburden Drilling Management Limited.

2.5 Clast macro-fabrics

Clast macro-fabric measurements were completed at seven of the eight aforementioned sites across the till face (Fig. 7). Using elongated-clast (minimum 20 mm) orientations to reconstruct former ice-flow directions has been practiced for more than a hundred years (e.g. Miller, 1884; Krumbein, 1938; and Holmes, 1941). This is a statistical exercise in which the a-axis orientation of multiple prolate (i.e. the a-axis is twice as long as the b-axis) clasts within a sample area is measured. The a-axis is the measured axis because it is susceptible to rotation under applied stress and the elongated axis aligns toward the direction of the applied stress (Hooyer and Iverson, 2000). These clasts typically dip up-ice as the particle orients itself to pose the least resistance to flow (Hooyer and Iverson, 2000); therefore, the dip of the clast is also measured. A minimum of 50 clasts were measured within an approximately 1 m^3 sample area, as recommended by Ringrose and Benn (1997). Only clasts with a minimum a:b ratio of 2:1 were selected, as these pebbles allow for the most practical measurement that is sensitive enough to indicate flow direction (Andrews, 1971).

A bench area was dug into the face at each sample area in order to remove any colluvium and slope wash and it allows for the measurements to be taken from a horizontal surface increasing the accuracy of the measurements (Andrews, 1971). Clasts were carefully uncovered and removed using a till knife and trowel. An aluminum knitting needle was then placed in the cast of the removed clast in the direction of the elongated axis and in the dip direction of the a/b plane (Fig. 9). Both the azimuth and dip of each clast were measured and recorded. This process was repeated for a minimum of 50 pebbles at each sample location (*cf*. Hirvas and Nenonen, 1990; McMartin and Paulen, 2009). No measurements were conducted in close vicinity to any large cobbles and boulders, as the strain patterns associated with the till near larger clasts would likely be complex (Boulton, 1976), and not reflect the

Figure 9. Knitting needles are used to indicate dip and azimuth of clasts that have been removed during clast fabric measurements.

overall ice flow direction.

The measurements were then imported into Rockworks® Earth Science and GIS Software for statistical analysis. Rose diagrams and stereonets were created using Stereonet 7© v. 7.3.5 for Mac OS (Allmendinger et al., 2013; Cardozo and Allmendinger, 2013). Eigenvector values were calculated to determine the strength of the orientations, and have been used in the interpretation of sediment facies, their depositional history and strain history (Hart, 1994; Benn, 1994; Benn and Evans, 1996). The principle eigenvalue (S_1) is a normalized vector magnitude of the degree of clustering within the fabric (see Woodcock, 1977 for detailed mathematical description). The correlation coefficient (R) and clustering (K) of each data set was also calculated using the Rockworks® software package, to aid in validating the macro fabric results.

The interpretation of these clast fabrics should be conducted with caution, as the type of shear/stress exhibited on the diamict will influence the strength of the fabric. Whether it is ductile deformation (Hicock and Dreimanis,1992), or a more brittle shear induced deformation (Iverson and Iverson 2001; Piotrowksi et al*.,* 2004), or a polyphase style of deformation (Lian and Hicock, 2000), the type of deformation will have a direct affect on the movement and alignment of clasts during deformation. A more brittle deformation would tend to behave according to the March (1932) style of rotation, whereas the more ductile style of deformation would exhibit more of a Jeffery (1922) style of rotation. The main difference between the two is the effect of increased shear on the strength of the resulting fabrics. Increased shear in March style rotation will increase the strength of the resulting fabric where as Jefferson style will occur perpendicular to the strain vector of the flow

(Iverson et al., 2003). However, increased shear in the Jeffery style rotation will weaken the fabric (Carr and Rose, 2003). Analysis of rotation style by Benn (1995) and Benn and Evans (1996) has indicated that March style rotation was the predominant style of rotation resulting in clast fabrics that paralleled local flutings and interpreted ice flow direction. This indicates that it is not merely shear-induced rotation but deformation-induced rotation, whereby the a-axis of the clasts passively rotates to parallel the strain axis. Therefore, interpretations based on clast fabric results were based on this assumption.

2.6 Pebble lithologies

Pebble lithologies are an effective tool used in determining relationships between stratigraphic units, till provenance, type of deposition, and chronology of sediment deposition (Walden, 2004). The lithologies of pebbles within a till unit reflect the bedrock geology of the area and of areas up-ice (Shetsen, 1984; Bell et al., 1989). By comparing the lithology, size, shape, and abundance of pebbles found within a till unit, a relative estimate of transport distance and source area can be made. The subcropping margin of the Precambrian Canadian Shield with the Paleozoic rocks at the eastern boundary of the Western Canada Sedimentary Basin, approximately 175 km due east (Fig. 2) of the Pine Point region, provides a unique opportunity for this type of study, as it defines a clear boundary between Paleozoic sedimentary rocks and Precambrian granites.

Samples collected in the field for heavy-mineral concentrate were also used for lithological analysis, and were processed as previously mentioned (see

Chapter 2.2). The > 2.0 mm fractions were received from Overburden Drilling Management Limited, and the 2.0 to 5.6 mm granules and clasts were removed and examined visually for sulphide minerals (Fig. 10). The > 5.6 mm fraction was counted by clast lithology following the general outline of Bridgland (1986). Each sampled yielded approximately 2 to 3 kg of 2.0 to 5.6 mm material. The remaining >5.6 mm fractions consisted of 800 to 900 clasts per sample, which were then coned and quartered, in order to randomly select 300 to 400 clasts. These pebbles were classified under nine categories (felsic intrusive, mafic instrusive, metavolcanic, medasediment, arkosic quartzite, vein quartz, limestone, dolomite, and other) based on bedrock lithologies known to occur in the Pine Point region and up-ice (*cf.* Skall, 1975).

Figure 10. Sorting and classification of pebble lithologies being completed at the GSC sedimentology lab, Ottawa, ON.

2.7 Micromorphology

2.7.1 Introduction

Micromorphology is a branch of soil sciences that uses low magnification examination of sediments to identify micro-features, microstructures, and micro patterns. Through examination of structures, patterns, and arrangements of individual components, and how they relate to each other microscopically, an indication of the internal and external stress applications can be identified and characterized (Menzies et al., 2010). Micromorphology allows for the examination of unconsolidated sediment samples without destroying the sample, and focuses on the examination of the relationships and patterns the grains exhibit, a unique process in comparison to traditional tools and methods used in the investigation of glacial sediments. Through micromorphological examination, an insight into the structures not visible to the naked eye can be obtained. This allows for an unique insight into processes responsible for the sediment's deposition, formation, and transportation. For this reason the use of micromorphology has increased over the last several decades (van der Meer, 1987; 1993; Menzies and Maltman, 1992; Carr, 2001; Hiemstra and Rijsdijk, 2003; Baroni and Fasano, 2006; Larsen et al*.,* 2007).

The study of sediments using microscopy has been used since the late 1930's, strongly influenced by the publication of Kubiëna's (1938) *Micropedology.* However, the use of microscopy was largely limited to the analysis of lithified sediments that are relatively easy to collect and grind down to thin section thickness (~ 30µm). It was not until the late-1960's that unlithified sediments were beginning to be collected *in-situ*, preserved through resin impregnation, and mounted for thin section analysis (Fitzpatrick, 1969).

With micromorphological examination, even massive, structureless diamicts at the macroscale can still give valuable information regarding the genesis, deposition, deformation, rheology and strain rate changes of the sediment (Carr, 2004). With the increased use of glacial micromorphology there have been improvements in identification of microstructures that give insights into transportation pathways, rheology, processes of deposition and deformation of glacially deposited sediments (Fig. 11; van der Meer, 1993; Menzies and Maltman, 1992; Menzies, 2000). These structures fall under four general classifications based on the type of deformation exhibited on the sediment: ductile, brittle, polyphase, and pore water.

Ductile deformation refers to the flow of the matrix/plasma (particles < 30μm thick making individual grains indistinguishable from one another) due to grain-boundary sliding and failure (Mohr-Coulomb failure) of over-pressured unlithified sediment. Brittle deformation refers to the grain-boundary sliding of dewatering sediment, displaying dislocation of sedimentary fabric along discrete planes (Passchier, 2000). Polyphase deformation refers to the presence of both brittle and ductile mechanisms. These structures could form simultaneous or within different portions of the sediment, or could have occurred at different times throughout the deformation history. Polyphase in this sense can be both spatial and temporal, or even both. Pore water structures indicate the presence of water within the sediment, giving an insight into pore water pressure, and in turn, effective pressures within the sediment (Boulton and Hindmarsh, 1987).

Since its inception, the study of micromorphology has constantly been evolving, and with that, the terminology used in describing micromorphological structures has also continued to evolve. The evolution of

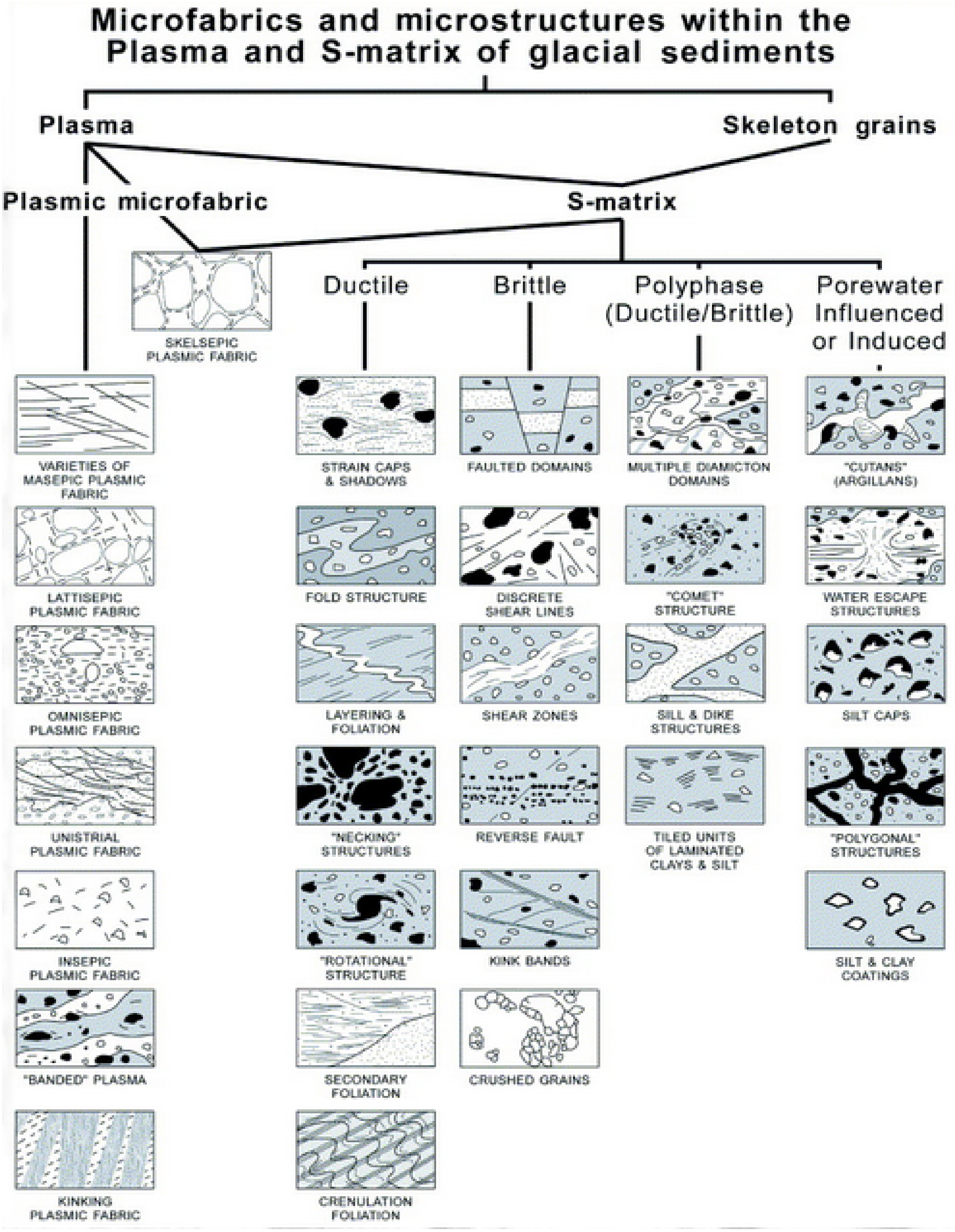

Figure 11. Chart of common microstructures within the plasma and S-matrix of glacial sediments, listed under th primary influence of their formation (Menzies, 2000; Menzies et al., 2006).

this language has been complicated by the fact that the terms used in micromorphology have been borrowed from sedimentology, structural geology, pedology, and glacial geology. This has created a unique set of terms and definitions used throughout different journals and studies. Therefore, a detailed description of these terms has been included in this research project.

2.7.2 Definitions

Each definition is listed under the deformation mechanism that the structure is most often associated with.

*Brittle Deformation*

Edge-to-edge

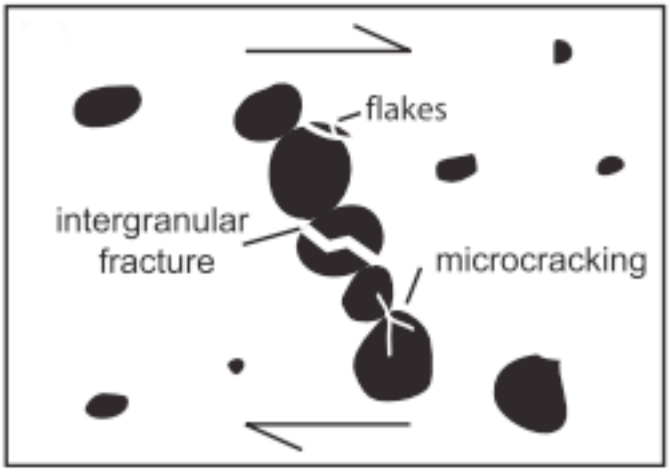

Figure 12. Edge-to-edge crushing displaying three types of grain fracturing under shear stress (Larsen et al., 2007).

Edge-to-edge crushing occurs when grains, under high strain, moving through a matrix come into contact with other grains with such force they crack or fragment the grains involved. There have been three main types of edge-to-edge crushing identified: internal grain fractures (microcracks), transgranular fractures, and chipped or fragmented transported "pieces" (Fig. 12) (Larsen et al., 2007). There has been a correlation between the pore water fracturing of grains and subglacial stress (Hiemstra and van der Meer, 1997).

Lineations/Grain Lineations

Lineations are indicative of stress application and readjustment of the fine particles within the sediment along the axis of least resistance, associated with discrete shear (Carr, 2004). This creates small "streaks" where stress has been exhibited on the sediment causing the grains to align in a single orientation, usually within the matrix/plasma. Grain lineations, are elongated grains that rotate and align within discrete shear zones (Hiemstra and Rijsdijk, 2003). This processes is similar to the mechanism involved in the alignment of the a-axis when conducting macro-clast fabrics (see Chapter 2.5). Lineations have been used to identify both the arrangement of plasma and skeletal grains, and have been suggested to reflect a sheet/plate like arrangement of the material (Reinardy et al., 2011). Lineations can exist in a single direction or multiple directions, and can become deformed post-formation and appear curved or shifted.

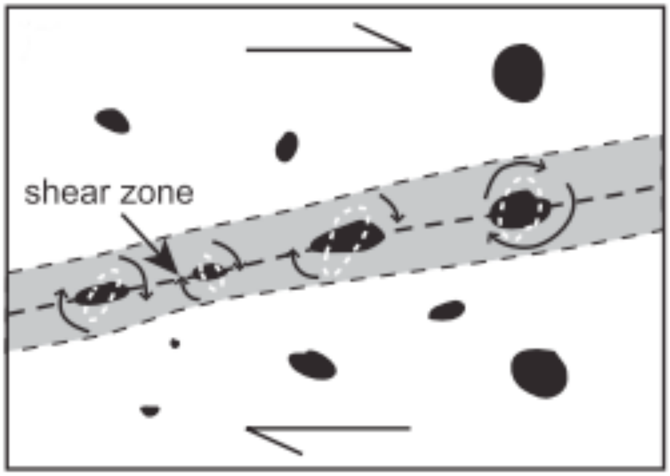

Figure 13. Grain lineations forming as the result of shear stress (Larsen, et al., 2007).

Shear Zones

Shear zones are domains of plasma that have a preferred orientation unlike that of surrounding plasma. These zones are often void of larger clasts and are predominantly composed of fine-grained matrix with a general single orientation.

<u>*Ductile Deformation*</u>

Grain stacks

Grain stacks are alignments of ~ 5 or more grains, usually with their elongated axis, oriented in a single direction, although grain stacks can cross cut existing grain stacks (Menzies et al., 2006). Grain stacks develop when discrete shear applied to the grains causes them to align elongated oblique to the strain direction (Fig. 13), unlike grain lineations (Cashman and Cashman, 2000; Hiemstra and Rijsdijk, 2003).

Necking Structures

Necking structures are the result of the movement of plasma being pinched between two clasts as it moves throughout the matrix of the sediment. The plasma appears as though it is flowing around the skeletal grains. Much like sand flowing through an hourglass, the plasma funnels between two skeletal grains.

Rotation/turbate structures

Rotational structures, or sometimes referred to as galaxy or turbate structures, involve a central resistant portion, usually a central-grain or less deformable matrix, surrounded by spiraling arrangements of finer grains (van der Meer, 1997). Rotation structures have been identified in subglacial (Menzies et al., 2010), glacial marine (Carr et al*.,* 2000), and debris flows (Menzies and Zaniewski, 2003). These structures occur when the nucleus of the rotation moves along a horizontal axis as a result of the different stress field above and below it. The finer particles align themselves parallel with the edge of the grain closest to them, and create a rotation alignment around the grain. van der Meer (1997) suggested that rotation structures act in a wheel like model whereby the rotation of one structure initiates the rotation of another rotation structure, much like the rotation of gears working in tandem. This style of rotation causes rotation structures to appear in clumps/groups or line up along a single plane. Hart et al*.* (2004) suggests larger grains create perturbations through stress fields. When these rotation structures occur without a core stone van der Meer (1997) suggests it is an indication of resistance to of material flowing around “sticky” spots. However, rotation/turbate structures are limited by grain abundance and grain size within the sediment (Hart, 2007). Larsen et al. (2006) noted that as deformation intensity increased so did the number of rotation structures.

Multiple domains

Multiple domains refer to the visually different zones of texturally unique domains within the sediment that can be differentiated from the surrounding matrix. These domains can indicate foreign sediment groups being reworked into the diamict (i.e. till balls/intraclasts; *cf.* Menzies and Ellwanger, 2011) or structurally induced zones in the diamicton (i.e. shear zones; *cf.* Thomason and Iverson, 2007).

Pore water influence

Cutans (Argillans)

During pore water movement thin laminations of fine particles, usually clay can be deposited along the sides of voids, clasts, or vugs and are referred to as Cutans or argillians. These layers can accumulate becoming layered and thicken. In some instances, these units can be reworked, in tact, into other domains.

Water escape

Water escape structures indicate the movement of pore water through the sediment. Characterized by the washing away of fine particles, these structures are dominated by coarser grain material, but can have fine grain deposition along the edges. A general sense of flow is also observed within the domain of these structures, but is not always evident, possibly due to deformation of the initial structure, or the flow direction could be perpendicular to the viewing plane (cross-cut by the thin section) making it difficult to determine flow direction. Water-escape structures generally result from the dewatering of pore fluid from the sediment during consolidation (Evans and Benn, 2004).

Silt and clay coatings

Silt and clay coatings are similar to cutans/argillans, however, do not appear as layered and can appear sparsely along the edges of grains. These structures tend to indicate the flowing of fluid around the grains, resulting in the finer grains sticking to the larger grains. 2.7.3 Field Collection

Thin section analysis first requires the collection of undisturbed bulk samples in the field. There are multiple methods for collecting samples in the field, all following the general outline of van der Meer (1996). First the existing slump was removed to reveal *in situ* sediment (Fig. 14A) and one lid from a Kubiëna tin is removed (Fig. 14B) and the Kubiëna tin is inserted into the sediment using a till knife to clear space for the tin to enter the face (Fig. 14C), making sure not to force the tin and disturb the sediment (Fig. 14D). Azimuth, up direction, sample number, and front of the sample is recorded. When field conditions, such as fissility, hardness, clast content, etc., do not allow for the use of Kubiëna tin, a section of diamict is carefully etched out of the face, and removed and wrapped in a plastic bag. If the Kubiëna tin is removed and diamict does not completely fill the container, well-sorted sand is added to pack the sample and prevent disturbance during transport (Fig. 14E). Sand is used as it is easily identified in thin section. The filled Kubiëna tin or cleaved samples are then individually placed in separate plastic bags, to retain moisture, wrapped in masking tape, and transported back to field camp to be vacuum-sealed (Fig. 14F), packed and shipped to Brock University for processing.

Selection of sample locations for micromorphological investigation was determined to allow adequate sampling from each identified unit. A minimum of one micromorphological sample was collected from each unit, with additional samples being collected in ~ 0.5 m vertical increments from one another within the same unit. Specific care was taken when collecting samples not to samples in close proximity to large boulders, which may affect the structures found within the sediment, and not accurately represent the true dynamics of the diamict (Boulton, 1976).

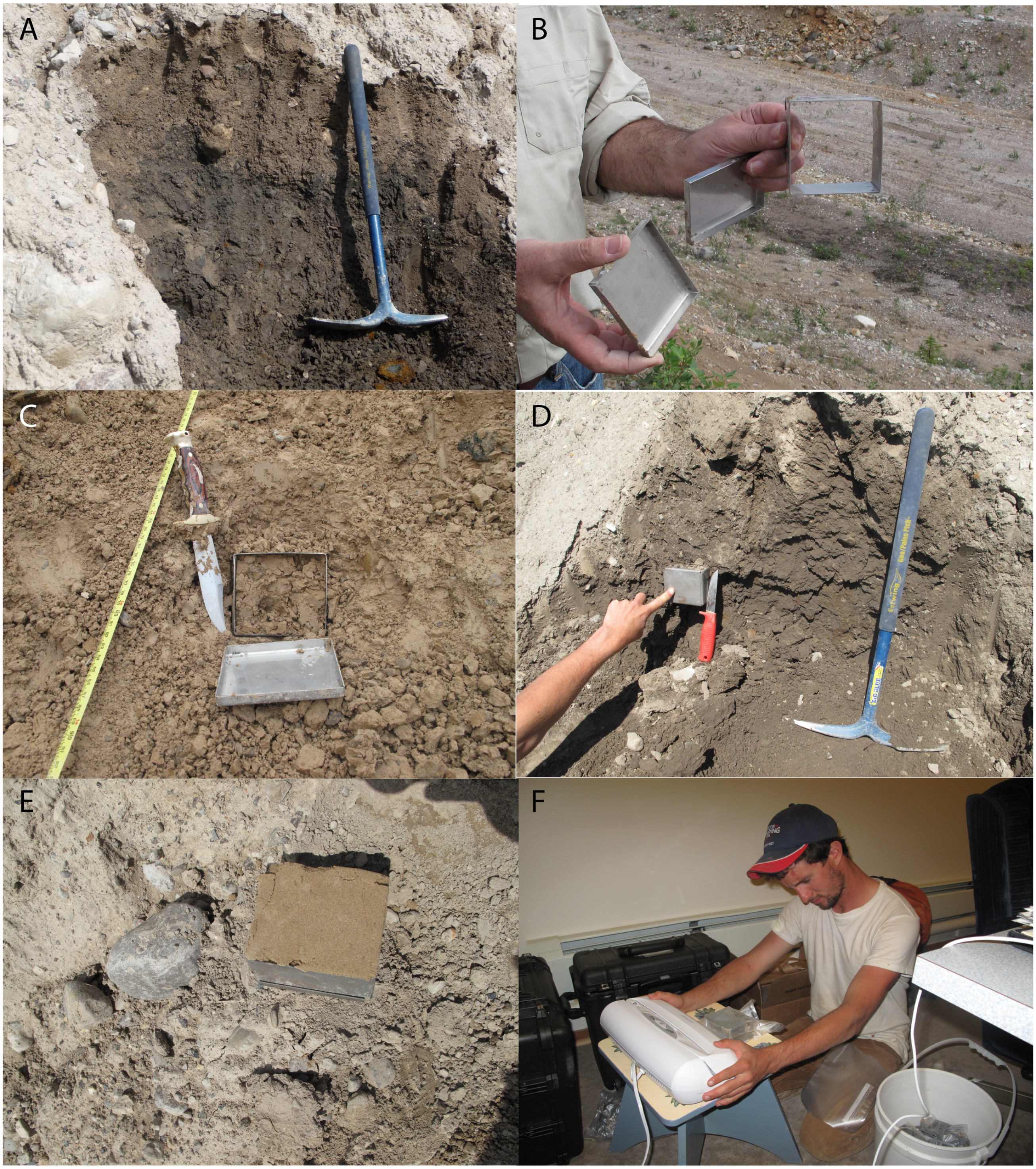

Figure 14. Field stages of collecting samples for micromorphological investigation: (A) Exposure of in situ diamicton. (B) An empty Kubiëna tin with both ends removed (75 mm x 55 mm x 40 mm). (C) Kubiëna tin inserted into the diamict using a till knife to ease its entry. (D) Completely inserted Kubiëna tin just before removal; the surrounding diamict has been removed to allow the sample to be cut out. (E) An incompletely filled Kubiëna tin packed with well-sorted sand to ensure the sample is not disturbed in transport. (F) Samples are vacuum-sealed prior to shipment and processing.

2.7.4 Thin section production

Sample preparation and thin section production was carried out at Brock University, Petrography Thin-sectioning Laboratory. Production of thin sections follows the steps and techniques outlined by Fitzpatrick (1984), Murphy (1986), van der Meer (1993), Lee and Kemp (1993), Carr and Lee (1998), and Menzies (2000). Once received samples are unwrapped and checked for any damage that may have occurred during shipping. The undamaged samples are allowed to air dry for approximately 2-3 weeks. The samples are then wrapped in aluminum foil, with sample number and orientation marked on the wrapped sample (Fig. 15A) the foil is then perforated (Fig. 15B) allowing resin to completely surround the sediment. A plastic lining is then inserted into a cardboard box, which will be used as a resin bath for the samples (Fig.15C). Samples are placed into the box and enough resin is added to completely submerging the samples (Fig. 15D). The resin is a mix between acetone and Ecopoxy©, an organic based hardening solvent. The hydrophobic acetone acts to drive out any existing moisture within the sediment, which, is then replaced with the resin. The resin slowly solidifies and allows for cutting and mounting of the sample (Kemp, 1985; Lee and Kemp, 1993; Carr and Lee, 1998; van der Meer and Menzies, 2006).

The chemicals are mixed manually with a rubber policeman until the two chemicals have completely mixed (~ 5 minutes). After hand mixing, the solution is placed on a magnetic stirring plate for an additional 5 minutes, then additional Ecopoxy© slow hardener is added and is mixed for an additional 30 minutes. The samples are immersed in resin and allowed to impregnate for ~ 1 week in a vacuum chamber (12-17 kg/cm). The over consolidation and stress experienced by most glacial sediments results in

Figure 15. Initial lab stages of thin section production: A) Samples are received vacuum-sealed in plastic bags, are removed and wrapped in tin foil, leaving the top open. (B) The bottom of the tin foil wrap is perforated to allow the flow of resin around the sample. (C) A plastic bag is placed around a cardboard box for impregnating the samples. (D) Samples are placed submerged in resin and allowed to cure for 2 weeks. (E) Samples after curing in vacuum hood for 2 weeks. (F) Excess resin is removed from samples. (G) Samples are then cut into manageable blocks. (F) Resulting impregnated sample.

relatively high porosity but low permeability, making resin impregnation difficult. The transportation of resin through the sample requires grain-to-grain transportation of the fluid through the sediment often leaving the central portion of the slide lacking full impregnation (Carr and Lee, 1998). Furthermore, as with most sediments, higher clay content within a sample often reduces the permeability, which causes difficulties for even resin distribution, thus the requirement of a vacuum oven. The resin bath is checked daily and topped up with additional resin when needed. Once impregnated (Fig. 15E), the samples are broken by hand to remove excess resin (Fig. 15F) and allowed to cure for another 4 – 5 days in a sparkless lab oven at 40- 45°C, then cooled in a fume hood for 24 hours. After the samples have solidified they are cut in half using a Servocut®-M250 (Fig. 15G), and analyzed for successful resin penetration (Fig. 15H). If needed, surface impregnation is applied to the sample to insure cohesion of the material during the mounting process. Once complete impregnation has been successful, a block ~ 1 cm thick is cut (Fig. 16A) from the hardened sediment (Fig. 16B). The small block is then ground down (Fig. 16C) and polished using a PM 2A® Polisher and is mounted on a glass plate (75 mm x 50 mm x 1 mm) the glass plate is etched with sample number and up direction. The excess block is then removed via a vacuum saw. Once the block is cut down to a reasonable thickness using a Petro-Thin® machine (Fig. 16D), it is hand ground to ~ 30μm thick (Fig. 16E). The samples are then analyzed under a microscope to ensure the thin section is an acceptable thickness, and if needed hand ground to the correct thickness. The thin section is then cleaned and a cover slip is added (Fig. 16F), sample number and up direction are added to the slide. The slide is then ready for microscopic examination (Fig. 16G). A flow chart of the entire process is presented in Figure 17.

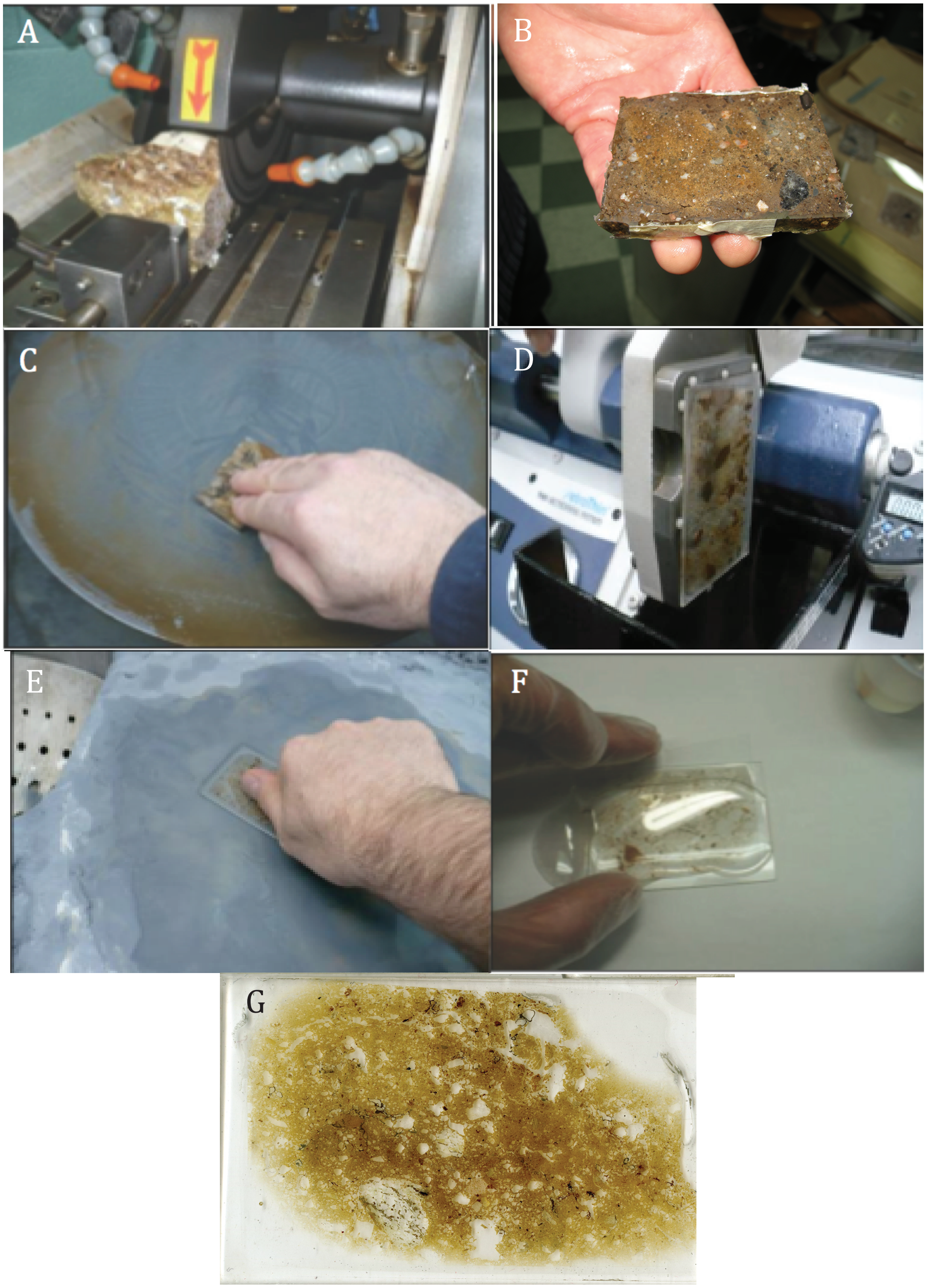

Figure 16. Final stages of thin section production: (A) Cutting down the larger solidified sample into ~ 1 cm thick slabs. (B) Resulting block that will be cut and trimmed to thin section dimensions. (C) The sample is ground down on a lap wheel and then mounted on a glass slide. (D) Mechanically grinding down the thin section to ~ 35 μm. (E) The sample is ground down by hand to ~30 μm and inspected under a low magnification microscope to ensure ideal thickness. (F) A cover slip is added to the finished thin section. (G) Resulting scan of completely finished thin section.

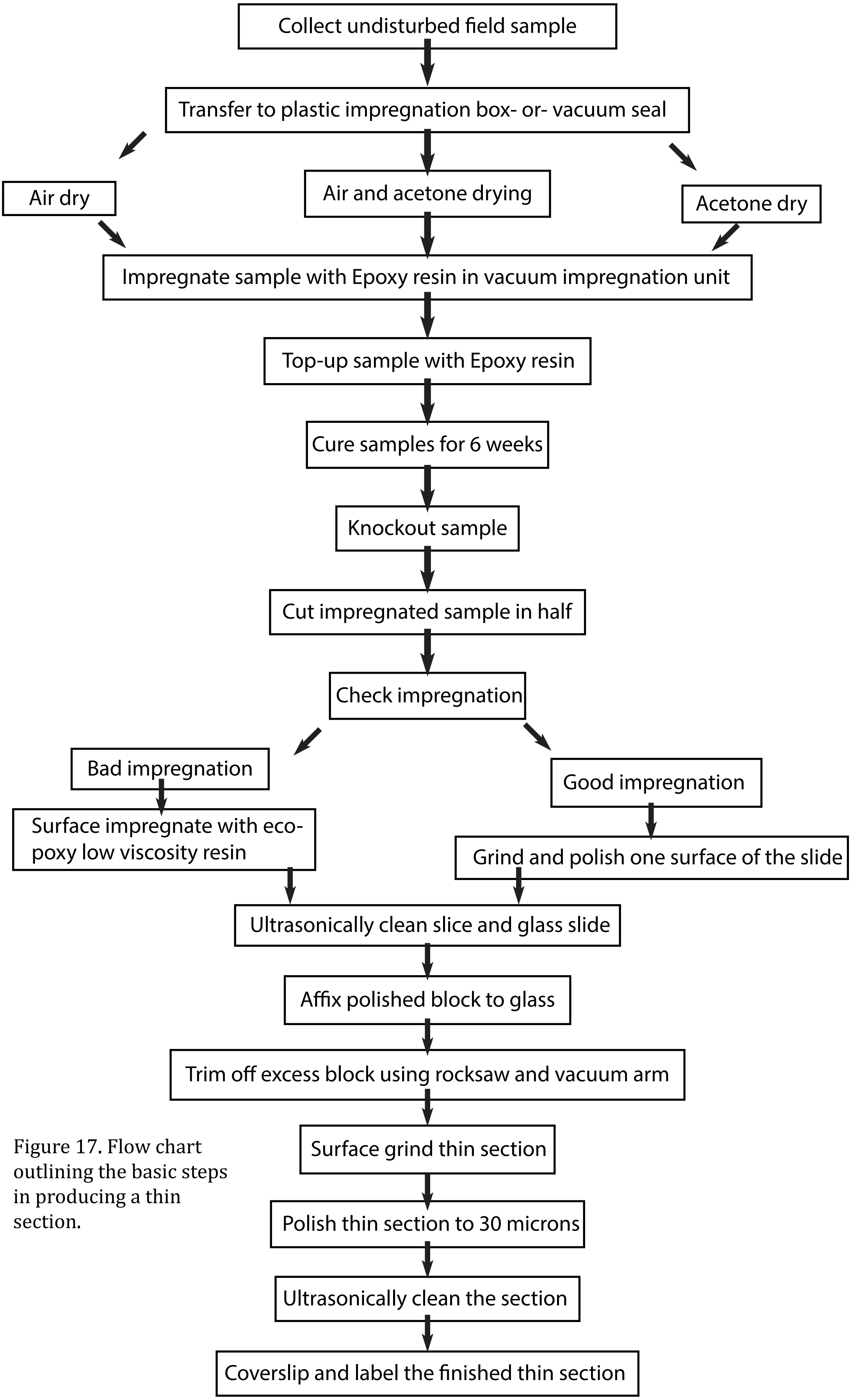

Figure 17. Flow chart outlining the basic steps in producing a thin section.

2.7.5 Analysis

Samples are first macroscopically examined with the naked eye and any visible structures, the range of grain size, and grain distribution are noted. Then the thin section is analyzed at low magnification (6.5-10X) in plain light using a Wild-Heerbrugg® M420 microscope, affixed with a Nikon® Digital sight DS-Fi1 digital imaging device. Nikon® NIS-Br imaging software was then used to measure grain orientation, grain length, sphericity of grains, and also used to determine texturally different areas within the plasma. This software is also utilized to stitch individual images to create a large composite of the slide. Images of the composite

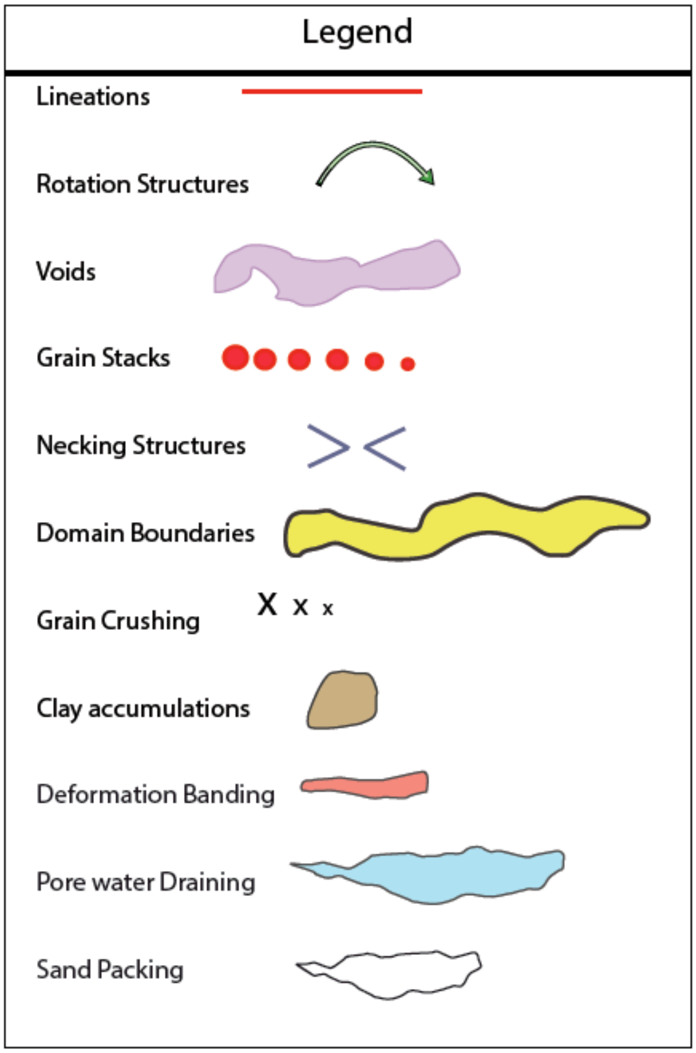

Figure 18. Annotations used to identify microstructures in thin section.

slides are printed off in high quality and a complete microscopic analysis is completed. Specific focus on size range, distribution, shape and general lithology of the skeletal grains within the thin sections is noted. A systematic analysis of the structures within the thin section is conducted starting with the upper right hand corner and working in a snake-like fashion until the end of the slide noting any voids (orientation, type, and distribution), or other microstructures (Fig. 18). As the structures are identified they are annotated on the high-resolution printed image of the thin section.

Once this initial microscopic analysis is completed, the thin sections are then placed on a PetroScope® projection macroscope under plane light (2X) and re-analyzed for confirmation of structures and to aid in the identification of any larger structures not identified in thin section or through microscopic analysis. Although there is an admitted amount of personal bias in microstructures identification, a study conducted Leighton et al. (2012) on observer bias and influence of experience on the identification of microstructures demonstrated there is little difference in identification of structures based on human bias.

Structures were annotated according to the legend (Fig. 18) and placed over a semi-transparent copy of the original image. Several of the slides contain perfectly spherical dark air bubbles which are a result of the resin impregnation, process likely during the application of the cover slip or an air bubble caught in the resin. It should also be noted that the arrows used to indicate rotation structure do not reflect direction of rotation, but are used to indicate the rotation of the material in general. The resulting annotated microstructures are not an exhaustive indication of microstructures in the diamict, but merely a representation of the major structures observed throughout the thin section. The annotated slides are then interpreted based on the specific microstructures within the thin section and their relation to one another. Through this examination a better understanding of the rheological conditions and the deformation of the diamict can be inferred (Menzies et al., 1997; Carr, 1999; Carr et al., 2000; Roberts and Hart, 2005; O'Cofaigh et al., 2005). By looking at the sedimentological relationships (e.g., overprinting, deformation of structures, abundance, etc.) the cycle of deformation can also be determined (Menzies et al., 2010).

Chapter 3

3.0 Observation and results

3.1 Field Observations and sedimentological analysis

Six distinct Quaternary units were identified in the field based on visually distinguishable differences in the units, including colour changes, grain size, and the distinct contacts between the units (Fig. 7). These six units were labeled in ascending stratigraphic sequence; Unit A is lowest in the sequence, and Unit F at the top of the section. The four lowest units (A-D) were classified, generally, as till. This classification was based on the diamicton's sandy-silty matrix, lack of apparent sorting, the presence of polished and faceted clasts, the presence of exotic pebble lithologies, and the unique set of microstructures identified within the units. These till units were separated into four separate units based on colour changes within the diamicton, grain size changes between the units, and also by visible contacts between the units. A layer of littoral beach sediments (Unit E), ~ 1 m thick overlie the four till units. Unit E was the focus of an in depth studies by Craig (1965) and Lemmen (1990) and will not be discussed in this study. The upper most layer is an organic-rich layer (Unit F) ~0.5 m thick, and are irrelevant to the focus of this study and will not be discussed in detail.

Two striation measurements were collected on the bedrock shoulder of the open pit of K-62 near the base of the section, trending from 223° to 232°, parallel to the oldest known striation direction mapped by Oviatt et al*.* (2011) at Pit O-28 (Fig. 6). Detailed grain size results can be found in Appendix A and Munsell colour results can be found in Appendix B.

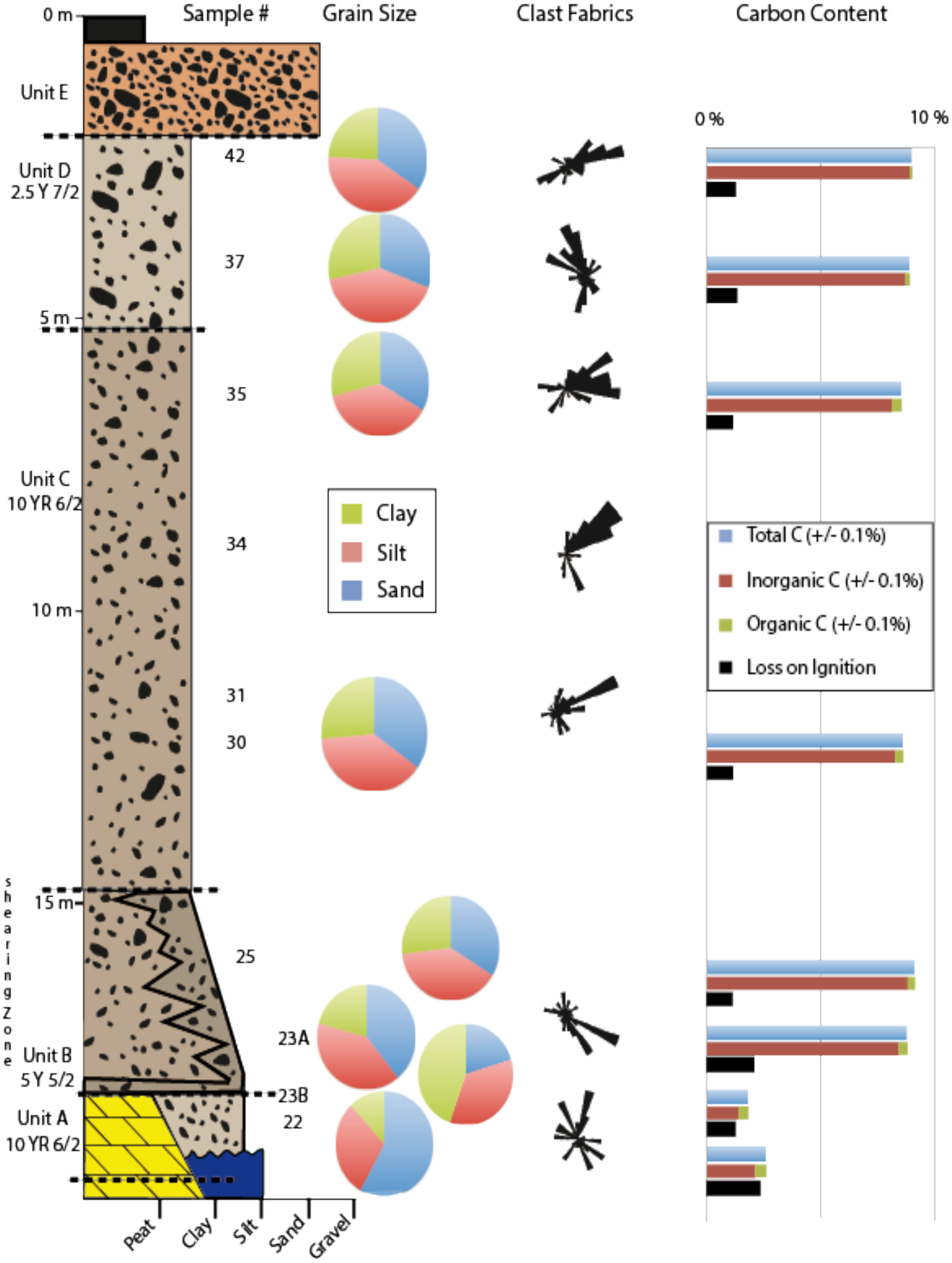

Figure 19. Stratigraphic and lithofacies of the northern exposure at open pit K-62 (Rice et al., 2013). Bedrock is depicted to include the karst-collapse structures seen in the open pits at Pine Point. Grain size, clast fabric, and carbon content results are displayed.

3.1.1 Unit A

Unit A is the lowest till unit in the till facies in Pit-K62. This unit is also only preserved in karst depressions in the bedrock, smeared along the bedrock, surface or in trace amounts re-worked into overlying units. Unit A is dark grayish brown (PTA-022- wet: 2.5 Y 3/2; dry: 10-YR 6/2; PTA-023B- wet: 10YR 6/3; dry 5 5/2) with clast content of 13%, of which are mostly subrounded, ranging in size from small pebbles to cobbles, some being striated and faceted. A silty-sand matrix supports the clasts (average 48.7% sand and 42.8% silt; Table 1; Fig. 19). Water levels in the open pit during sample collection made total thickness of this unit difficult to determine and also made obtaining multiple samples within this layer impractical.

Unit A is moderately fissile, with fissility planes running in both the vertical and horizontal plane. Macroscopically, the unit appears overconsolidated, massive, matrix supported, with no particle sorting, and, other than some minor sand lenses, structureless. Multiple well-rounded quartzite pebbles of Cordilleran origin were also located within this unit. Approximately two meters of till was exposed above the current water line.

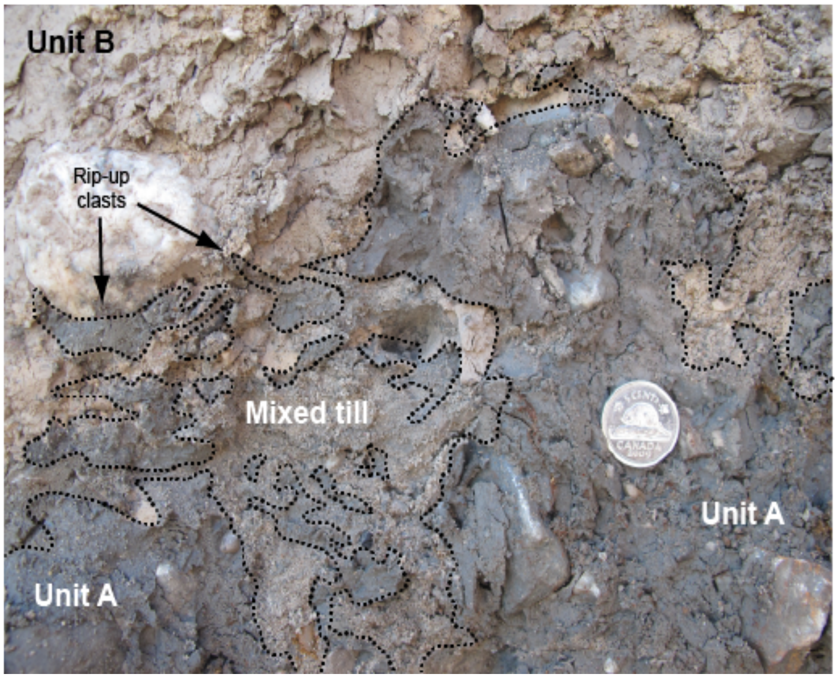

Figure 20. Shearing contact and mixed zone between the lowest tills, Units A and B. Intact sediment rip-up clasts of Unit A are commonly observed above the contact in Unit B. Canadian five-cent coin (21 mm) for scale.

Table 1. Summary of Data

Sample #	Till Unit	Top sample depth from surface (m)	Munsel Colour (dry)	Total C (+- 0.1%)	Inorganic C (+- 0.1%)	Organic C (+- 0.2%)	Loss on Ignition %	Description	Clast Content (%)
11-PTA-022	A	17	10YR 6/2	2.6	2.1	0.5	2.3	Llight brownish grey,slightly fissle, sand lenses	<5
11-PTA-023B	A	16.2	5Y 5/2	1.8	1.4	0.4	2.1	Olive gray, darker clasts, more fissile	5
11-PTA-023A	B	16.1	10YR 7/2	8.8	8.4	0.4	1.3	Light gray, iron stained clasts, lighter coloured clasts	5
11-PTA-025	C	12.5	10YR 6/2	9.1	8.8	0.3	1.1	Light brownish grey, more sand rich	<5
11-PTA-030	C	9.8	10YR 7/2	8.6	8.3	0.3	1.2	Light gray, more sand rich	~5
11-PTA-035A	C	6.2	10YR 6/2	8.6	8.1	0.4	1.2	Light brownish grey, fissile, clay rich	~5-10
11-PTA-037	D	4.2	2.5Y 7/2	8.9	8.7	0.2	1.3	Light grey with iron staining on joints	10
11-PTA-042	D	1.2	2.5Y 7/2	9.0	8.9	0.1	1.3	Light grey, highly fissile	>5

		Potential Indicators of Metamorphosed Cu-Zn-Pb-Ag Mineralization (Grains)(0.25-0.5 mm)							
Sample #	Till Unit	Pyrite/ Marcasite	Chalcopyrite	Sphalerite	Galena	Hercynite	Kyanite	Sillimanite	Staurolite
11-PTA-022	A	n/a	n/a	n/a	n/a	n/a	n/a	n/a	n/a
11-PTA-023B	A	3,333	0	80	0	4	167	167	7
11-PTA-023A	B	2,041	1	272	10	14	14	27	1
11-PTA-025	C	n/a	n/a	n/a	n/a	n/a	n/a	n/a	n/a
11-PTA-030	C	2,128	0	284	21	0	4	7	0
11-PTA-035A	C	2,256	1	75	8	2	2	113	1
11-PTA-037	D	7	0	3	5	15	41	7	1
11-PTA-042	D	16	0	0	0	3	62	0	0

Table 1. Summary of Data

					Concentrations		
Sample #	Till Unit	% Sand (63µm-2 mm)	% Silt (4-63 µm)	% Clay (<4µm)	Calcite CO2% (+-) 0.05%CO2+ 5% of concentration	Dolomite CO2% (+-) 0.1%CO2+ 5% of concentration	Dolomite/ calcite ratio
11-PTA-022	A	58.2	35.9	5.9	1.63	5.89	3.61
11-PTA-023B	A	39.2	49.2	11.6	1.19	3.64	3.06
11-PTA-023A	B	32.0	49.6	18.4	7.94	22.63	2.85
11-PTA-025	C	33.7	48.1	18.1	7.65	23.94	3.13
11-PTA-030	C	34.9	47.6	17.6	7.74	21.84	2.82
11-PTA-035A	C	33.4	48.0	18.6	8.98	20.23	2.25
11-PTA-037	D	30.8	50.1	19.1	7.83	23.00	2.94
11-PTA-042	D	34.5	49.5	15.6	7.24	24.56	3.39

The contact between this unit and the overlying unit shows evidence of mixing (Fig. 20) rip-up inclusions, re-entrapment, and small-scale deformation.

3.1.2 Unit B

Unit B is pale-brown till (wet: 2.5Y 5/3; dry: 10YR 7/2) with a clast content of 8%, of which were mostly sub-rounded to subangular clasts, ranging in size from small pebbles to large cobbles, some of which are striated. A sandy-silt matrix supports these clasts (49.6% silt and 32.0% sand; Table 1; Fig. 19). The unit has much lighter colored, local bedrock clasts than underlying Unit A. There were also some clasts with iron and manganese staining the clasts and surrounding local matrix. Iron and manganese staining also appeared along joint fractures and fissility plains. No internal bedding was observed in this unit, which appeared macroscopically massive with no particle sorting. Several small inclusions, which appeared to be rip up inclusions from the underlying Unit A were observed (Fig. 20). The unit is ~ 1 m thick and a shearing contact between this till unit and Unit C is observed, indicating a substantial amount of syndepositional and/or post-depositional stress has been exerted on this unit during/after deposition.

3.1.3 Unit C

Unit C is light olive-brown till (wet: 2.5 Y 5/3; dry: 10 YR 6/2) with a clast content of 11-17%, of which are mostly subrounded to subangular clasts, ranging in size from small pebbles to small boulders, some of which were striated and faceted. A generally sandy-silt matrix supports this unit (average: 34.0% sand; 47.9% silt; Table 1; Fig. 19). No visible bedding or sorting was observed in this unit, which appeared macroscopically massive throughout its entirety. The unit was highly fissile with fissility planes running in the vertical and horizontal planes. No inclusions were visible in the till, and mixing of this unit and the underlying unit dissipated ~ 10 cm above the shearing zone. Unit C is the thickest unit in the section

(~ 12 m) and was continuous around the open pit. The upper boundary between Unit C and Unit D is defined by a weakly developed boulder horizon (Fig. 21; see Chapter 4.2.3), change in sediment colour, and an increase in fissility (Fig. 22).

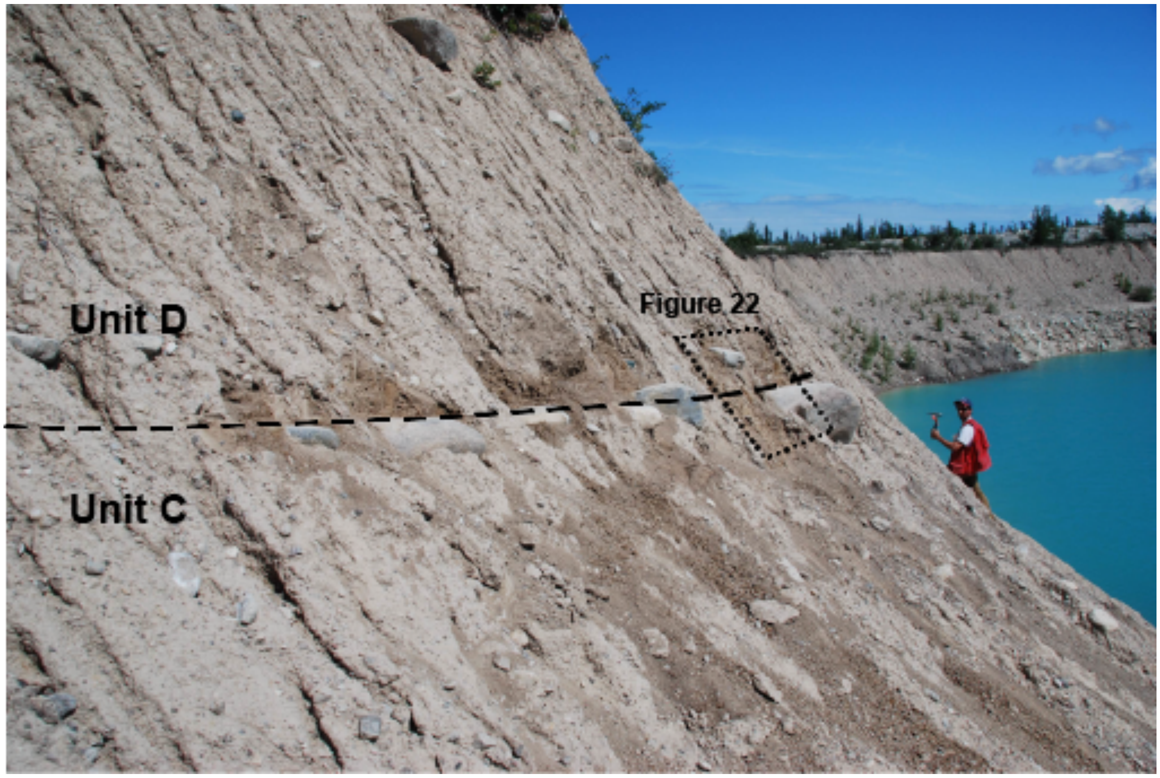

Figure 21. Oblique photo showing the boulder horizon between Units C and D. The location of Figure 22, showing the contact between the tills in detail is outlines.

Figure 22. Sharp planar contact between till Units C and D, showing the subtle differences in till colour and fissility. Boulders occur along this contact, with the tops of the boulders typically faceted and striated. Handle of the pick is ~ 60 cm long.

3.1.4 Unit D

Unit D is the upper-most till unit, characterized by it's brown appearance (wet: 10 YR 5/3; dry: 2.5 Y 7/2), this unit has a clast content of 12-18%, comprising mostly of sub-rounded to sub-angular clasts, which range in size from small pebble to boulders. A dominantly sandy-silt matrix supports these clasts (average: 32.7% sand and 49.8% silt; Table 1; Fig. 19). The unit is highly fissile with fissility planes running in both the horizontal and vertical planes. There is a small boulder/cobble horizon halfway through the unit, is comprised of abundant small (~ 40 cm a-axis) boulders and cobbles and occurring along a horizontal plane with a fine sandy-silt matrix in the interstices. Macroscopically the unit is massive, with little sorting, and no bedding features. The unit is ~ 3 m thick and is continuous around the open pit. The upper contact is a gradual transition showing evidence of reworked diamicton from underlying units into Glacial Lake McConnell Beach sediments, consisting of coarse sand, gravels, cobbles and some small boulders (Unit E) (Lemmen, 1990)(Fig. 23).

Figure 23. Uppermost till (Unit D) overlain by a thin veneer of stony glacial Lake McConnell littoral sediments.

3.1.5 Unit E

Deglaciation of the Pine Point region occurred near the end of the Late Wisconsinan ~ 10 ^{14}C ka BP (Dyke, 2004). The LIS margin retreated to the east of the Slave River, and the Pine Point mine site was inundated by Glacial Lake McConnell (Fig. 3), a large proglacial lake that covered present day Great Bear Lake, Great Slave Lake, and Lake Athabasca at its greatest extent (Dyke and Prest, 1987; Lemmen et al., 1994). Clast lithologies from the Lake McConnell deposits surrounding the Pine Point region are dominantly till derived. Reworking and deposition of the till through wave action, except where wave action has eroded exposed bedrock, was the predominant mechanism for littoral beach sediment deposition in the region (Lemmen, 1990).

The Glacial Lake McConnell sediments found overlying Units A-D have a high clast content (Fig. 22), and the clasts within this unit reflect the underlying units, indicating the till has been reworked by wave action. Wave erosion has resulted in removal of most of the finer material leaving cobbles, boulders, small clasts, and a sandy matrix, indicative of littoral beach sediments. Unit E is ~ 1.5 m thick along the northern face of Pit K-62.

3.1.6 Unit F

Overlying the Glacial Lake McConnell sediments is ~ 0.5 m of organic material deposited by the broad peatland that covers most of the land surface in the mining district. Mining construction and operation of the open pit has disturbed much of the peatland surface. Present day vegetation includes small black spruce trees and other small bushes and plants. Due to the anthropogenic influence, relative young age of this unit, and its irrelevance to the glacial sedimentological analysis, no further investigation was conducted on this unit.

3.2 Geochemical analysis of <0.063 mm fraction

Results for the geochemical analysis of < 0.063 mm grain fractions can be found in Appendix C; LOI results can also be found in Appendix C, and $CaCO_3$ results can be found in Appendix D. For a detailed description of the geochemical properties of the sediments found throughout the Pine Point and surrounding region see McClenaghan et al. (2012) and Oviatt et al. (2013a).

3.2.1 Unit A

Calcite and dolomite concentrations within this unit are significantly lower (calcite = 1.63 -1.19%, and dolomite = 5.89 - 3.64%) in comparison to overlying units (Table 1); However, Unit A has the highest calcite/dolomite ratio (~3.25:1). This unit also contained the lowest total carbon (1.8- 2.6%) than any other sample, and slightly lower LOI percentages (2.1-2.3%) than the overlying units (Table 1). Unit A is geochemically the most unique of all till units (Fig. 24-26), specifically when analyzing the relationship between Ca and Mg percentages (Fig. 24). Additionally, separation between this unit and the overlying unit is highlighted when comparing Ni and Cr vs. Ti, Pb vs. Zn, and %Mg and %Ca (Fig. 25; Fig. 26). However, there are some concentration fluctuations between the two samples taken from within Unit A (Fig. 7) when comparing Ni and Cr vs. Ti, Pb vs. Zn (Fig. 25; Fig. 26). This is due the fact that the lower sample (PTA-022) was sampled from within a karst collapse, whereas the upper sample (PTA-023B) was taken just above the karst collapse feature. The diamict within the collapse is sheltered from re-working of later glacial events, unlike the upper sample (as it was sampled just below observed mixing contact between the two units (Fig. 20)). It is also possible that the upper sample was taken from a portion of the unit that incorporated more of the local bedrock then the lower sample causing differences in concentrations (*cf.* McClenaghan et al., 1992). This sample was taken laterally parallel to the bedrock

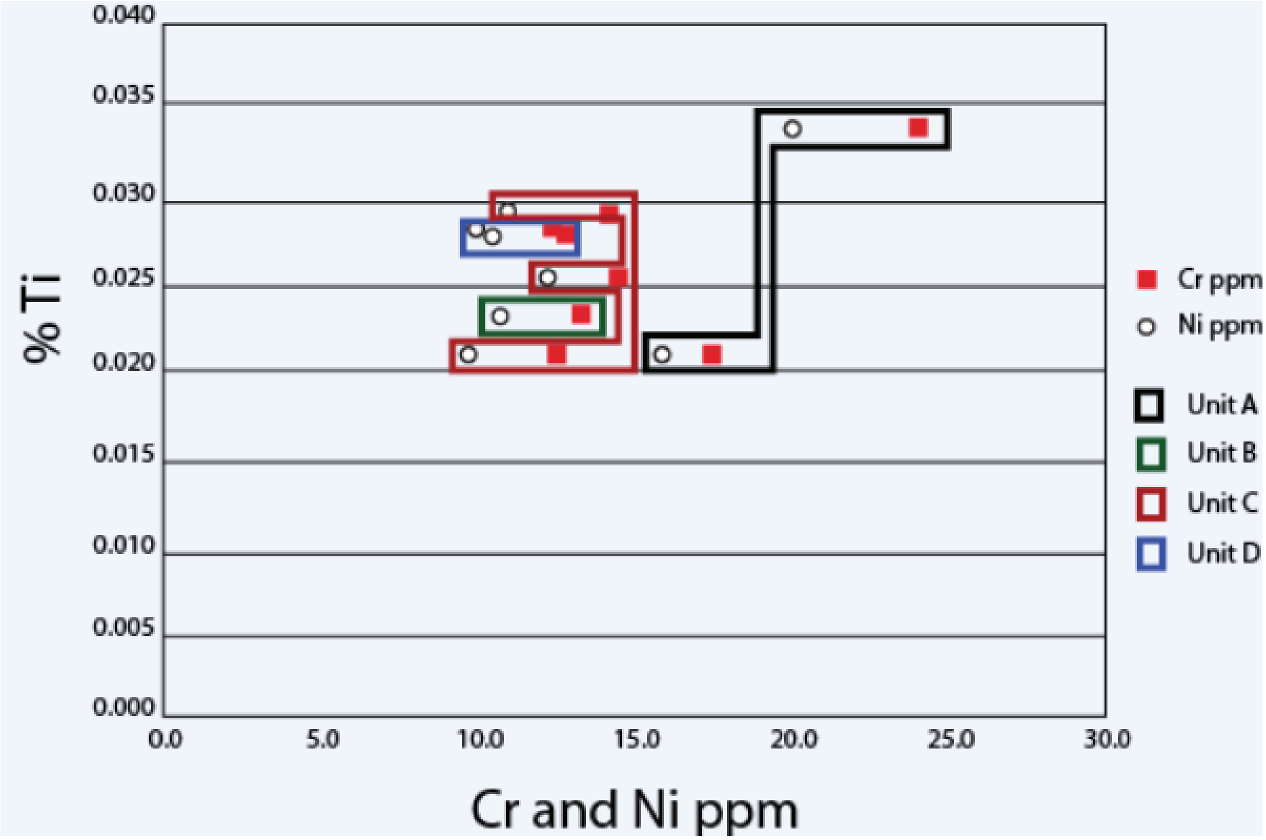

Figure 24. Concentrations of Cr and Ni (ppm) compared to % of Ti from each sample. Samples are grouped into their appropriate stratigraphic unit from which they were sampled.

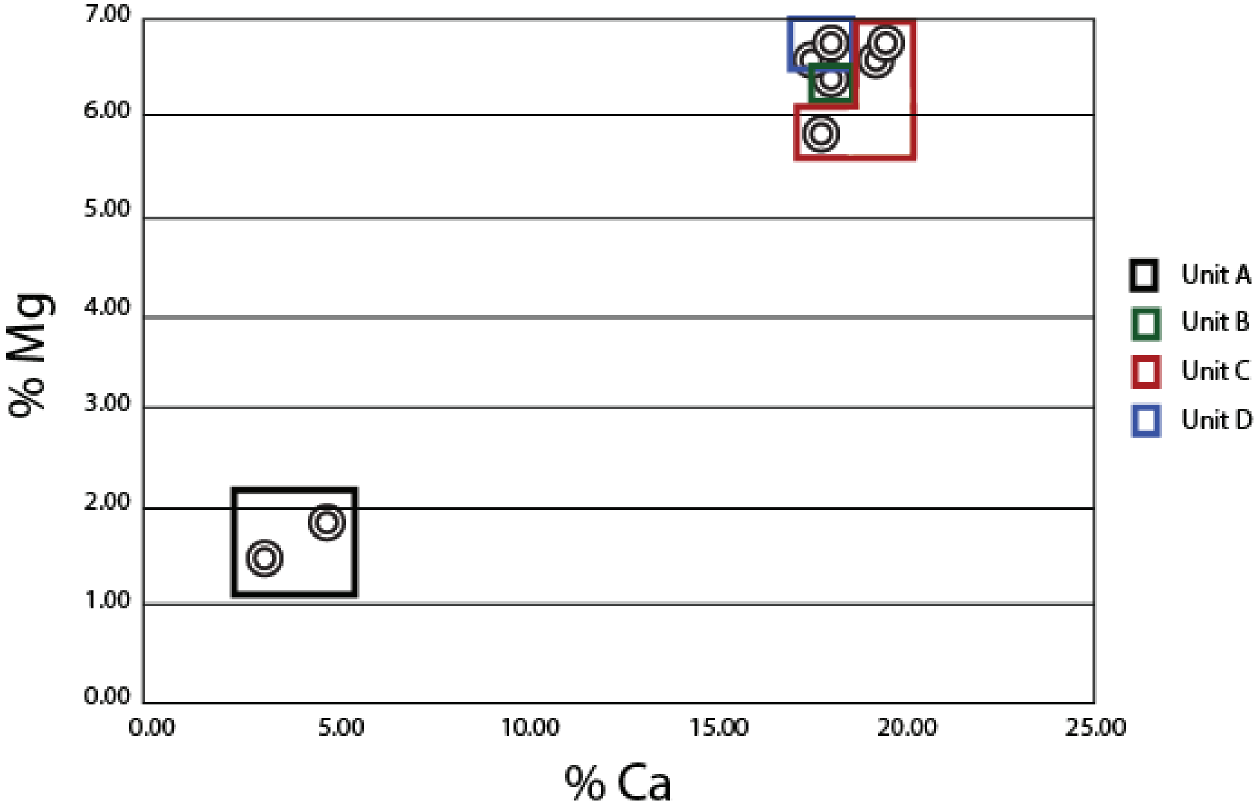

Figure 25. Geochemical results for %Ca and % Mg. Samples are grouped into their appropriate stratigraphic unit from which they were sampled.

outcrop nearby and therefore the increased inclusion of local bedrock is highly likely. Therefore, it was likely a combination of inclusion of local bedrock, and increase mixing with overlying samples that caused this discrepancy in some geochemical signatures between these two samples.

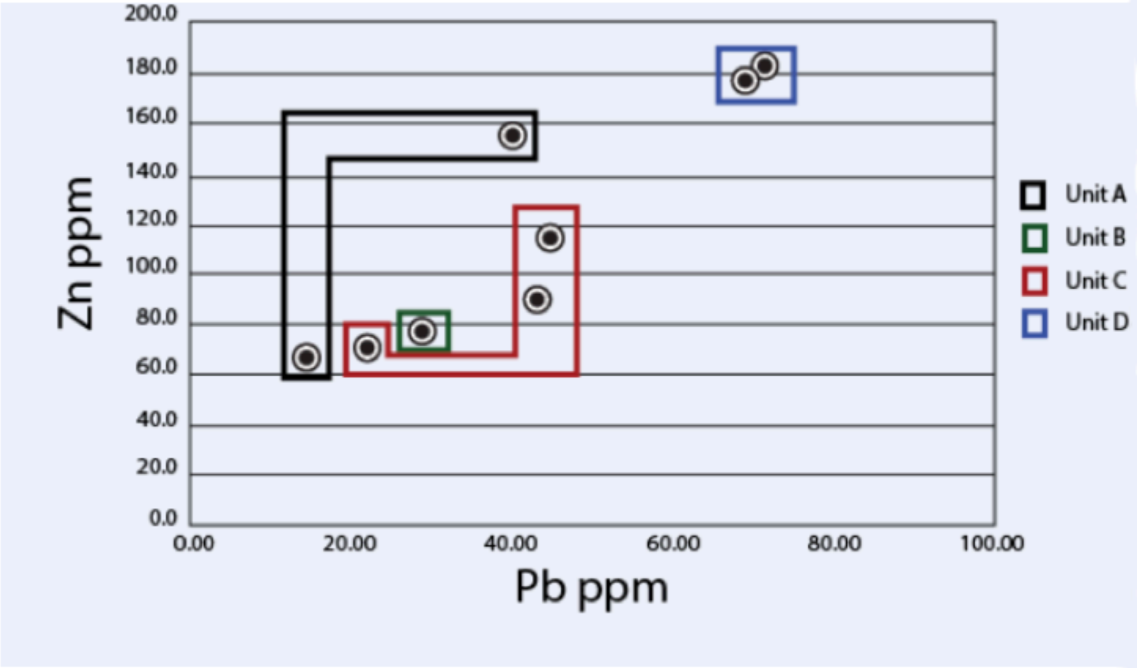

Figure 26. Concentrations of Pb (ppm) compared to concentrations of Zn (ppm) grouped into their appropriate stratigraphic units.

3.2.2 Unit B

Calcite and dolomite concentrations in this unit (7.94% calcite; 22.63% dolomite) are significantly higher than in the underlying unit, but close to those of overlying units (Table 1). This unit has similar LOI and total C results as the two overlying units as well (Table 1). Geochemically, Unit B is also very similar to the overlying unit C (Fig. 24-26).

3.2.3 Unit C

Calcite and dolomite concentrations in this unit are similar to those of Unit B and Unit D, ranging from 7.65 - 8.98% calcite and 20.23 - 23.94% dolomite, with the concentration of calcite increasing slightly toward the top of the unit, and dolomite decreasing (Table 1). This unit has very similar LOI and total C results throughout the unit, again, similar to the underlying and overlying units. Geochemically, Unit C was identical to the underlying unit and very similar to the overlying unit (Fig. 24-25), except when comparing Pb/Zn values (Fig. 26).

3.2.4 Unit D

Calcite and dolomite concentrations within this unit are similar to those in underlying Unit C and Unit B, with calcite concentrations of 7.84- 7.24%, and dolomite concentrations of 23.00-24.56% (Table 1). This unit has LOI and total C values that coincide with the two underlying units (Table 1). Geochemically Unit D was also very similar to both the underlying units (Fig. 24-26), except when comparing Pb/Zn concentrations, which were much higher than amounts found in underlying units (Fig. 26).

3.3 Heavy mineral concentrates

The results of heavy mineral concentrates can be found in Appendix E. For detailed description of heavy mineral concentrations throughout the Pine Point and surrounding region see McClenaghan et al*.* (2012) and Oviatt et al. (2013a).

3.3.1 Unit A

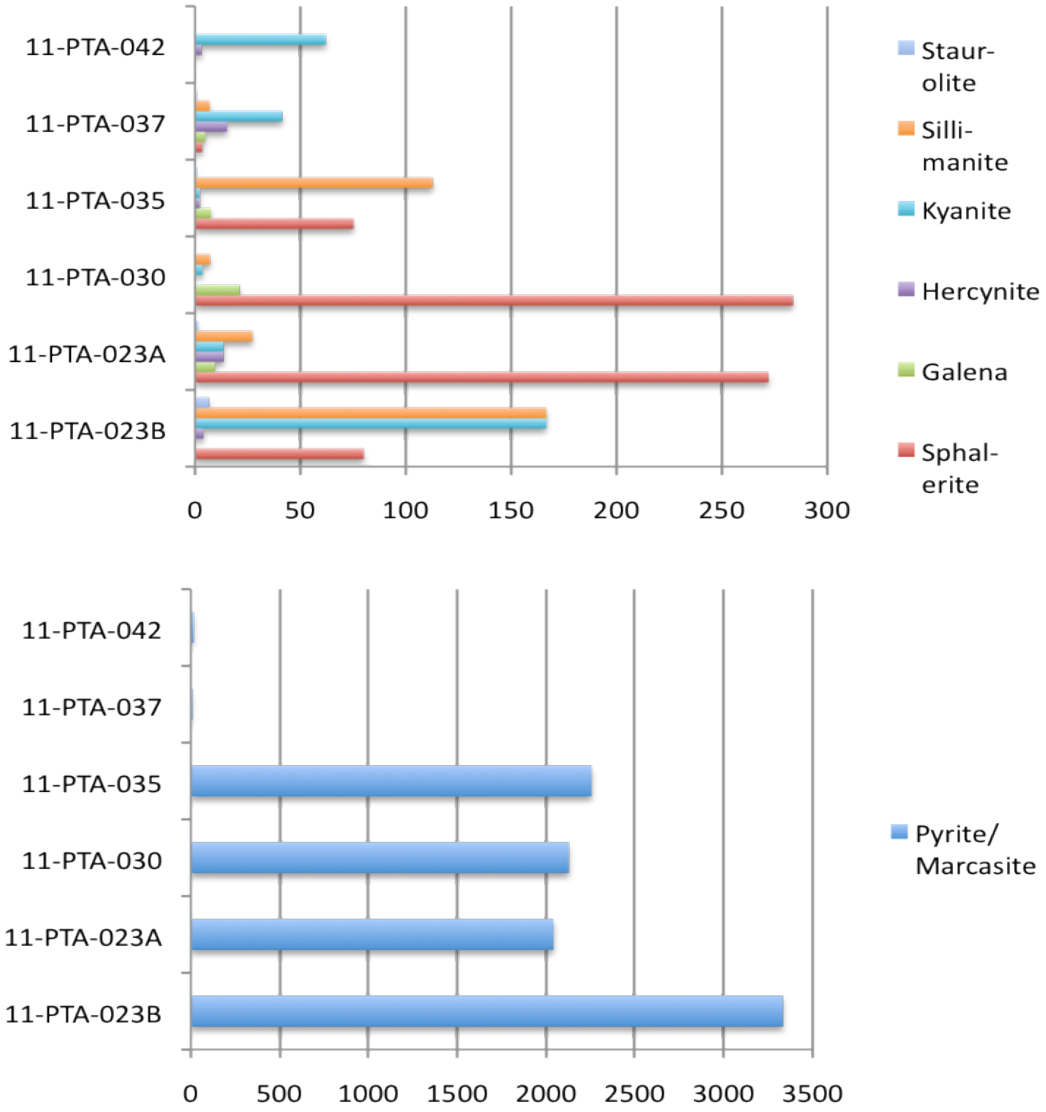

Figure 27. Graphical representation of heavy mineral concentrations of various minerals throughout the northern face at pit K-62.

This unit contains higher amounts of pyrite/marcasite grains (3333 gr/10 kg) in comparison to the other units (ranging from 7 – 2256 gr/10 kg). A similar pattern emerged when analyzing kyanite grains in which higher amounts (167 gr/10 kg) were observed in Unit A in comparison to the other units (2 - 62 gr/10 kg; Table 2).

There were no significant amounts of hercynite, staurolite, or galena (Fig. 27).

Table 2. Normalized (to 10 kg) table of base metal indicator grains

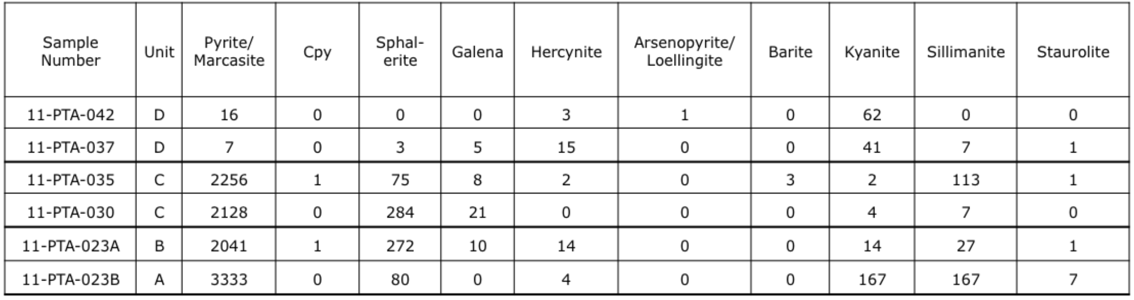

Sample Number	Unit	Pyrite/ Marcasite	Cpy	Sphal-erite	Galena	Hercynite	Arsenopyrite/ Loellingite	Barite	Kyanite	Sillimanite	Staurolite
11-PTA-042	D	16	0	0	0	3	1	0	62	0	0
11-PTA-037	D	7	0	3	5	15	0	0	41	7	1
11-PTA-035	C	2256	1	75	8	2	0	3	2	113	1
11-PTA-030	C	2128	0	284	21	0	0	0	4	7	0
11-PTA-023A	B	2041	1	272	10	14	0	0	14	27	1
11-PTA-023B	A	3333	0	80	0	4	0	0	167	167	7

3.3.2 Unit B

This unit contained higher amounts of sphalerite (272 gr/10 kg) than the underlying units and Unit D, however was comparable to the lowest sample in Unit C (11-PTA-030 284 gr/10kg). This unit had no other geochemically unique signatures associated with it. All of the grain counts were similar to the overlying Unit C, with marginally lower concentrations of pyrite/marcasite, kyanite, sillimanite, and staurolite, or marginally greater concentrations of sphalerite, galena, and hercynite than Unit A.

3.3.3 Unit C

Unit C contains the lowest concentrations of Kyanite (2-4 gr/ 10kg) in comparison to any other Unit (14-167 gr/ 10 kg). There were also slightly elevated amounts of sillimanite in the upper portion of the unit (PTA-035 113 gr/10kg) and there is a slight increase in pyrite/marcasite and sillimanite abundances moving up through the unit (Fig. 27). Unit C also has moderate amounts of sphalerite and pyrite/marcasite (75 and 2256 gr/10 kg respectively), in comparison to the rest of the units (Table 2). However, there was a decrease in the abundance of sphalerite and galena between the lower sample (11-PTA-030) and the upper sample (11-PTA-035).

3.3.4 Unit D

The amount of kyanite and pyrite/marcasite increased toward the upper part of Unit D (Fig. 27), however, the amount of all other detectable heavy minerals decreased in the upper portion of the unit (Table 2). It is the lack of heavy minerals within this unit that make it distinctive from the underlying units.

3.4 Clast fabrics

A table of all clast orientation measurements taken in the field, completed rose diagrams and stereonets can be found in Appendix F. Results and statistical analysis of these clast fabrics can be found in Table 3. Stratigraphic changes in clast orientations (rose diagrams) can be found in Figure 19.

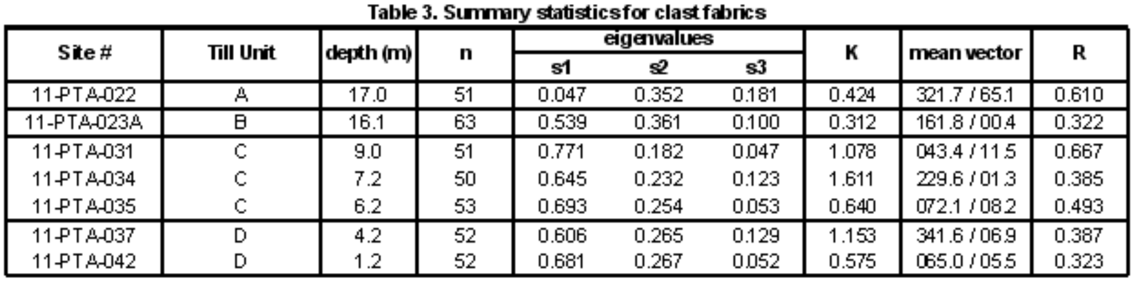

Table 3. Summary statistics for clast fabrics

Site #	Till Unit	depth (m)	n	eigenvalues			K	mean vector	R
				s1	s2	s3			
11-PTA-022	A	17.0	51	0.047	0.352	0.181	0.424	321.7 / 65.1	0.610
11-PTA-023A	B	16.1	63	0.539	0.361	0.100	0.312	161.8 / 00.4	0.322
11-PTA-031	C	9.0	51	0.771	0.182	0.047	1.078	043.4 / 11.5	0.667
11-PTA-034	C	7.2	50	0.645	0.232	0.123	1.611	229.6 / 01.3	0.385
11-PTA-035	C	6.2	53	0.693	0.254	0.053	0.640	072.1 / 08.2	0.493
11-PTA-037	D	4.2	52	0.606	0.265	0.129	1.153	341.6 / 06.9	0.387
11-PTA-042	D	1.2	52	0.681	0.267	0.052	0.575	065.0 / 05.5	0.323

3.4.1 Unit A

Due to the water levels at Pit-K62, only a single site was selected for clast fabric analysis within this unit. No clear trend was obtained, (S_1 = 0.05; Fig. 19) and the high angularity of the clasts and low clustering (K= 0.424) do not allow for accurate ice flow trajectory interpretation. In total 51 clasts were measured to complete this fabric (Table 3).

3.4.2 Unit B

Due to the thin nature of this unit, only a single sample site was used for clast fabric analysis, which indicated an ice flow direction to the NW (S_1= 0.54; Fig. 19). The clasts within this unit also had a significant variation in the dip-direction of each clast, and had weak clustering within the data points (K= 0.312). 63 clasts were selected from this unit for analysis (Table 3).

3.4.3 Unit C

Due to the thickness of unit C, three clast fabrics were completed at equal intervals throughout the unit (Fig. 7). The two lower clast fabrics tend to the SW (S_1=0.65-0.77; Fig 23), whereas the clast fabric completed near the top of this unit indicated a stronger correlation to the NW (S_1= 0.70). Clustering of the clasts within the unit was weakest in the top sample (PTA-035: K=0.640), strongest in the middle sample (PTA-034: K= 1.611), and moderately strong in the lowest sample from the unit (PTA-031: K=1.078). There were between 51- 53 clasts selected for analysis during the completion of the clast fabrics (Table 3).

3.4.4 Unit D

Two clast fabrics were completed in this unit, suggesting a WSW and NNW flow direction (S_1 = 0.60 - 0.68; Fig. 19). Again, the clustering of the data points plotted weakened toward the top of this unit (PTA-037 K= 1.153 and PTA-042 K=0.575). In total 52 clasts were selected for each fabrics within this unit (Table 3).

3.5 Pebble lithologies

A table of results from the clast lithology analysis and images of sorted pebble lithologies can be found in Appendix G. Graphical representations of results can be found in Figure 28.

3.5.1 Unit A

Table 4. Pebble-count categories and results from > 5.6 mm fraction of the till samples from pit K-62

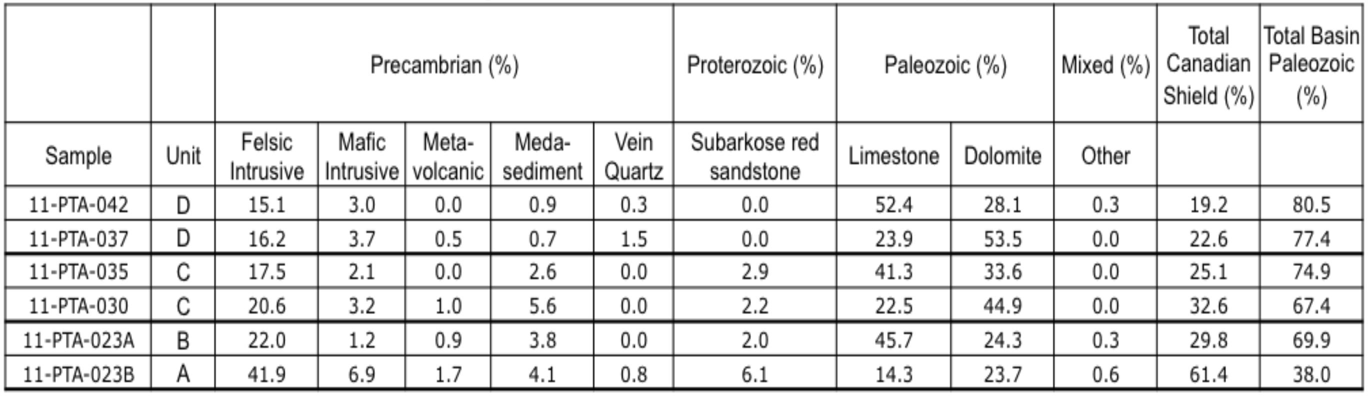

		Precambrian (%)					Proterozoic (%)	Paleozoic (%)		Mixed (%)	Total Canadian Shield (%)	Total Basin Paleozoic (%)
Sample	Unit	Felsic Intrusive	Mafic Intrusive	Meta-volcanic	Meda-sediment	Vein Quartz	Subarkose red sandstone	Limestone	Dolomite	Other		
11-PTA-042	D	15.1	3.0	0.0	0.9	0.3	0.0	52.4	28.1	0.3	19.2	80.5
11-PTA-037	D	16.2	3.7	0.5	0.7	1.5	0.0	23.9	53.5	0.0	22.6	77.4
11-PTA-035	C	17.5	2.1	0.0	2.6	0.0	2.9	41.3	33.6	0.0	25.1	74.9
11-PTA-030	C	20.6	3.2	1.0	5.6	0.0	2.2	22.5	44.9	0.0	32.6	67.4
11-PTA-023A	B	22.0	1.2	0.9	3.8	0.0	2.0	45.7	24.3	0.3	29.8	69.9
11-PTA-023B	A	41.9	6.9	1.7	4.1	0.8	6.1	14.3	23.7	0.6	61.4	38.0

Unit A contains the highest amount of Canadian Shield clasts (61.4%) double that of the second most abundant sample collected (Table 4). The vast majority of these Precambrian Canadian Shield clasts (41.9%) (Fig. 28) were felsic intrusive clasts (Fig. 29). Overall, this unit displayed the highest amounts of felsic, mafic, and arkosik quartzite clasts, but had the lowest abundance of limestone and dolomite clasts.

3.5.2 Unit B

Unit B contains the third highest concentrations (29.8%) of Precambrian Canadian Shield clasts compared to the rest of the samples (Table 4). This unit also has the third lowest percentage of Basin Paleozoic clasts (69.9%). Unit B also contains the second highest abundance of felsic and limestone clasts, and the lowest abundance of mafic clasts, but has average abundances for all other lithologies categorized (Fig. 28).

3.5.3 Unit C

This unit has, on average, lower levels of Canadian Shield clasts (25.1-32.6%) than underlying layers and more Paleozoic clasts (67.4 – 74.9%; Table 4). The concentration of dolomite clasts is slightly less in the upper sample, in comparison to the lower samples within this unit, with the lower sample (PTA-030) containing 44.9% dolomite clasts and the upper sample (PTA-035) containing 33.6%. A reverse trend is observed between these samples when comparing the lower (PTA-030) limestone concentration (22.5%) and the upper (PTA-035) limestone concentration (41.3%; Fig. 29).

3.5.4 Unit D

Unit D contains the lowest concentration of Canadian Shield clasts (19.2 - 22.6%) and the highest concentration of Paleozoic clasts (77.4 - 80.5%). A similar trend observed in Unit C with increasing concentrations of limestone clasts is evident in this unit as well (Fig. 28), with the lower sample (PTA-037) having limestone clasts percentages (23.9%) in less then a half of the abundance of the upper samples (PTA-042; 52.4%)

3.6 Micromorphology

Each stitched scanned image has been analyzed in detail as previously mentioned (see Chapter 2.7.3) and each sample description is given under the unit from which it was collected. See Figure 7 for sample distribution throughout the section.

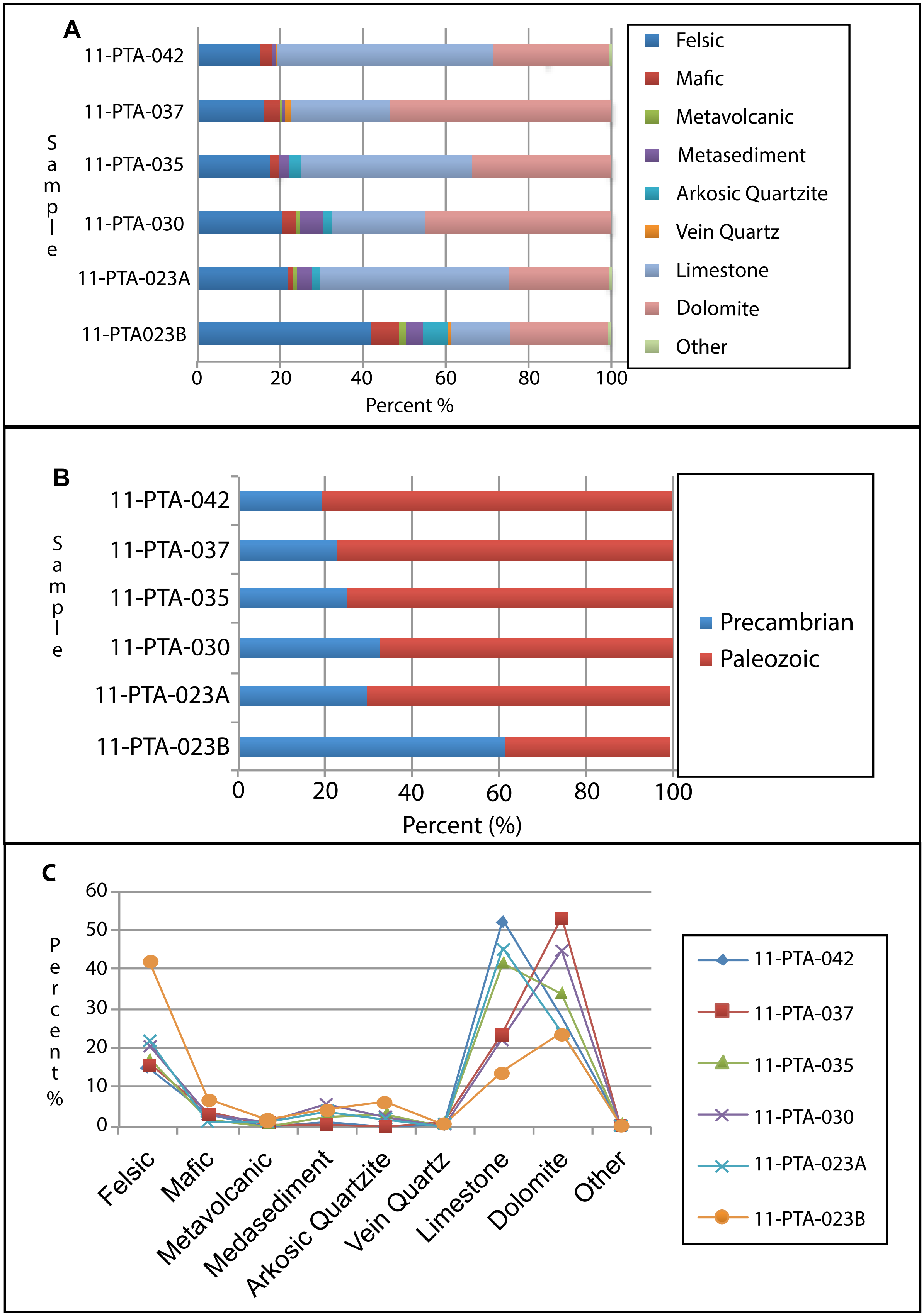

Figure 28. Results of the pebble-lithology counts: (A) relative percentages of each pebble lithology in stratigraphic sequence; (B) Simplified plot highlighting the percentages of clasts from the Canadian Shield and Paleozoic carbonate basin; (C) Line graph showing relative percentages of each lithology from each bulk sample.

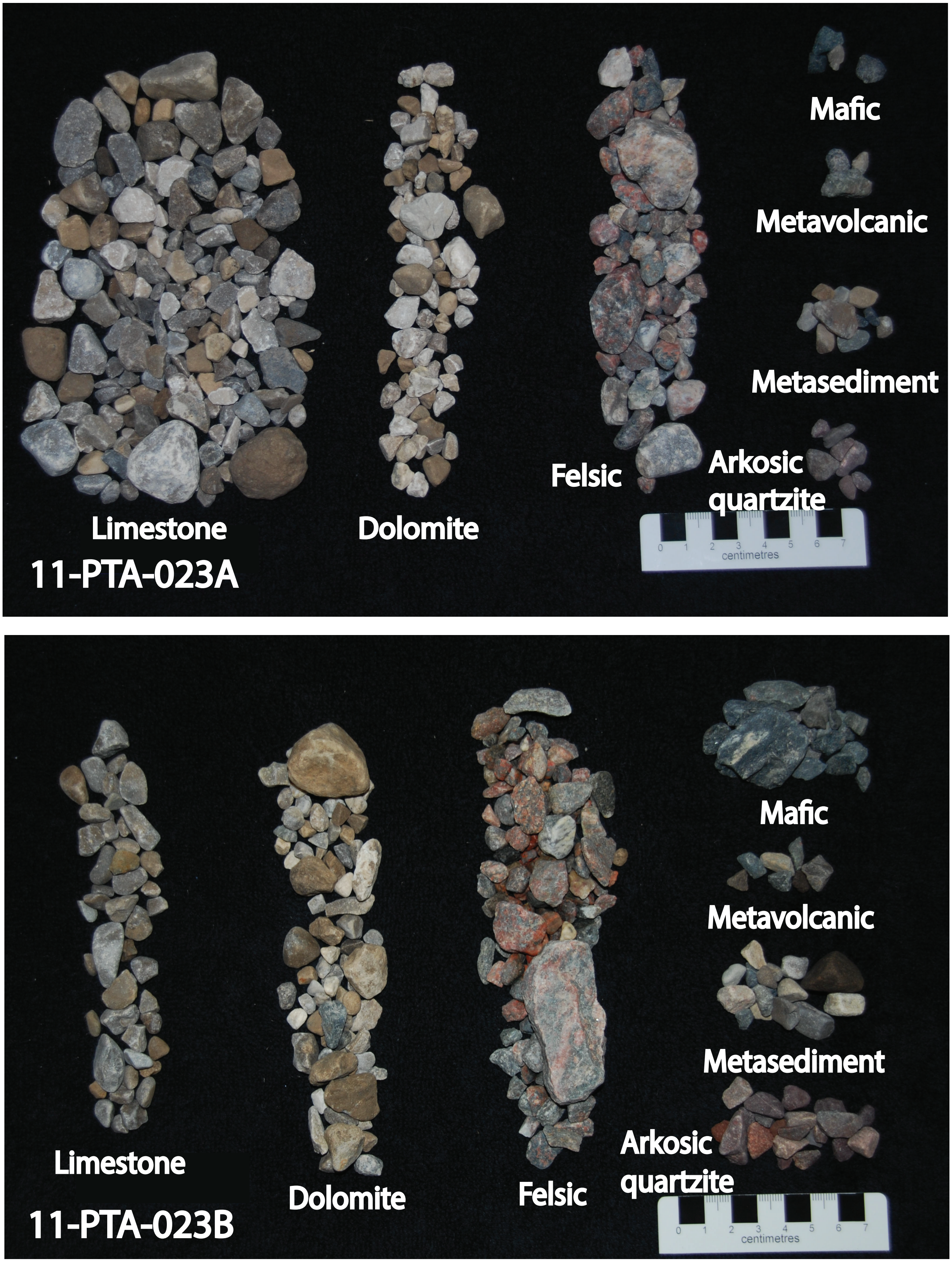

Figure 29. The difference in pebble lithologies between Unit a (bottom) and Unit B (top). Unit C has a much higher abundance of local limestone clasts and Unit A has a higher abundance of Canadian Shield derived clasts.

3.6.1 Unit A

11-PTA-022

There are two distinct domains, one is a darker more clay rich matrix (Fig. 30, highlighted in yellow) and there is a lighter more clast-rich matrix, the latter of which comprises the majority of the thin section. There are a small amount of vug-like voids found within this thin section. Lineations occur with two dominate directions, one trends in an upward northeast direction and the second tends down to the northeast, with some of these lineations showing deformational curving. Sets of grain-lineations parallel these lineations. Rotation structures have formed and transect the voids, that likely indicates the voids developed during the thin section production. Some necking structures are also identified.

11-PTA-022
This sample was collected at an azimuth of 315°

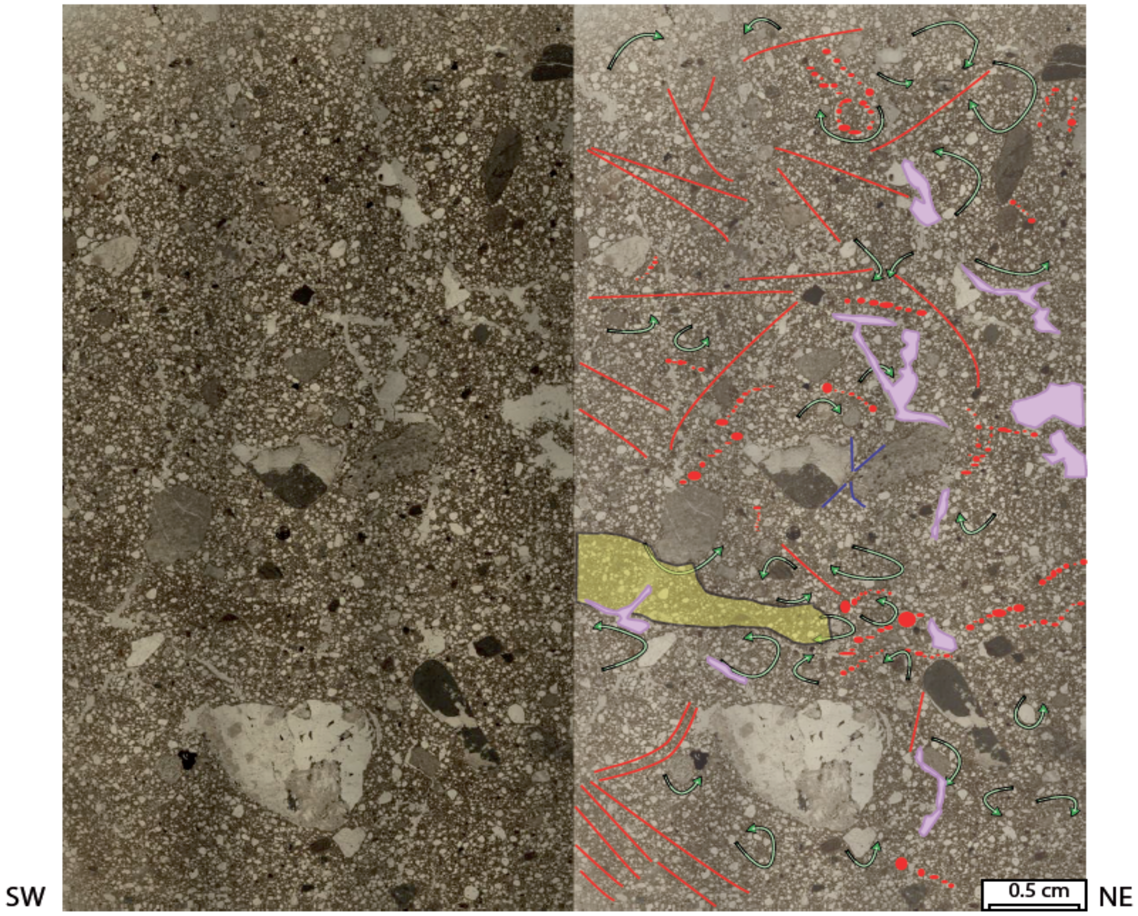

Figure 30. Annotated slide 11-PTA-022.

11-PTA-023B

This sample consists mostly of a single matrix domain with a minor secondary matrix that has a darker composition (Fig. 31, highlighted in yellow) observed around voids or clasts. There are numerous amounts of fracture voids, predominantly in the horizontal and vertical planes. Lineations are seen throughout the sample, with a higher clustering of lineations in the central portion of the slide. There are a number of rotation structure and grain-lineations that parallel the fracture voids and general lineations trend.

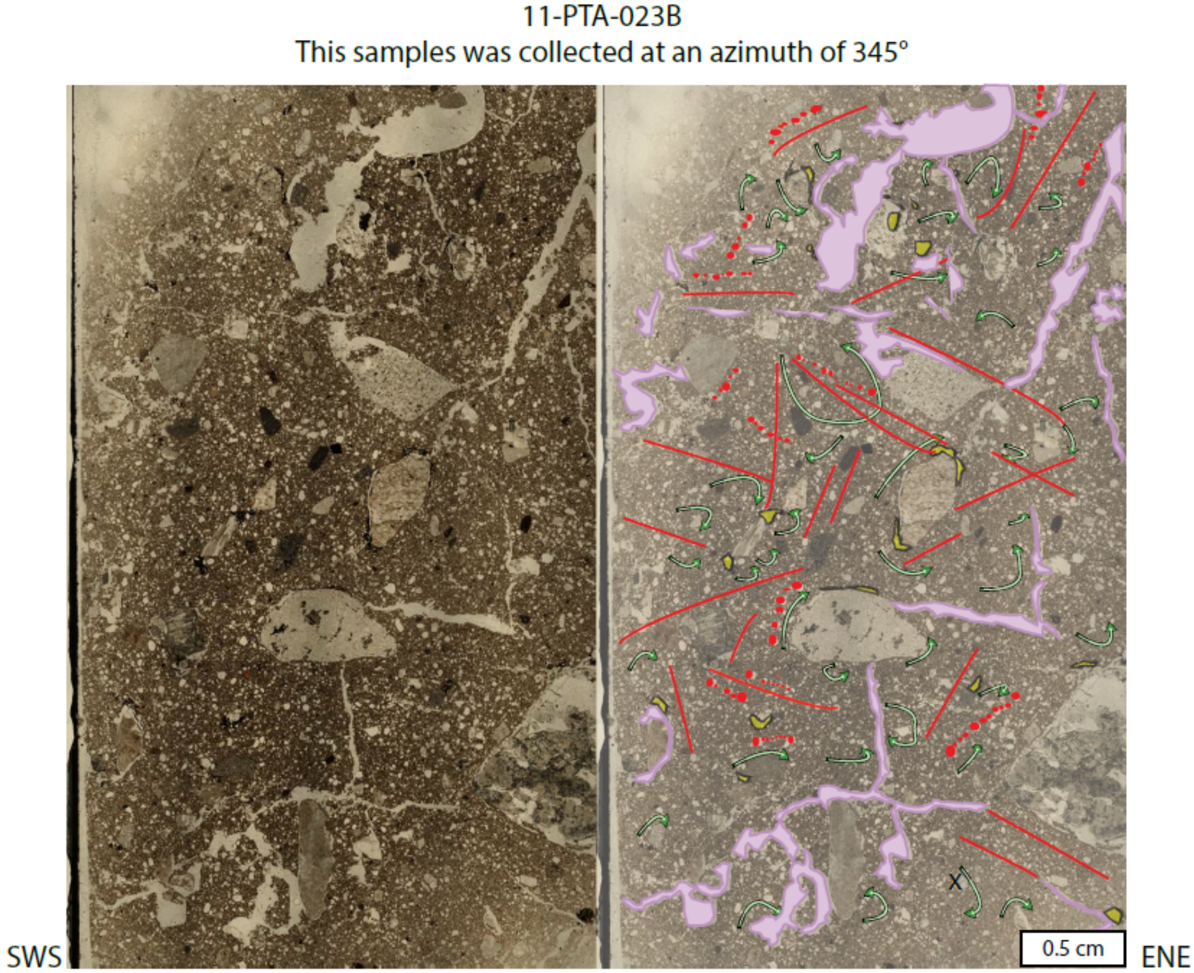

Figure 31. Annotated slide 11-PTA-023B.

11-PTA-023

This sample (Fig. 32) was collected at the contact between Unit A and overlying Unit B. Unit A has a silt-rich matrix (36.95% sand and 40.39% silt) while Unit B has a silty-sand matrix (58.17% sand and 29.86% silt). This difference in grain size is reflected in the till density, the matrix from Unit A has been ripped up and reworked into the overlying Unit B. Rotation of the matrix can be seen throughout the overlying and underlying matrix (Fig. 20).

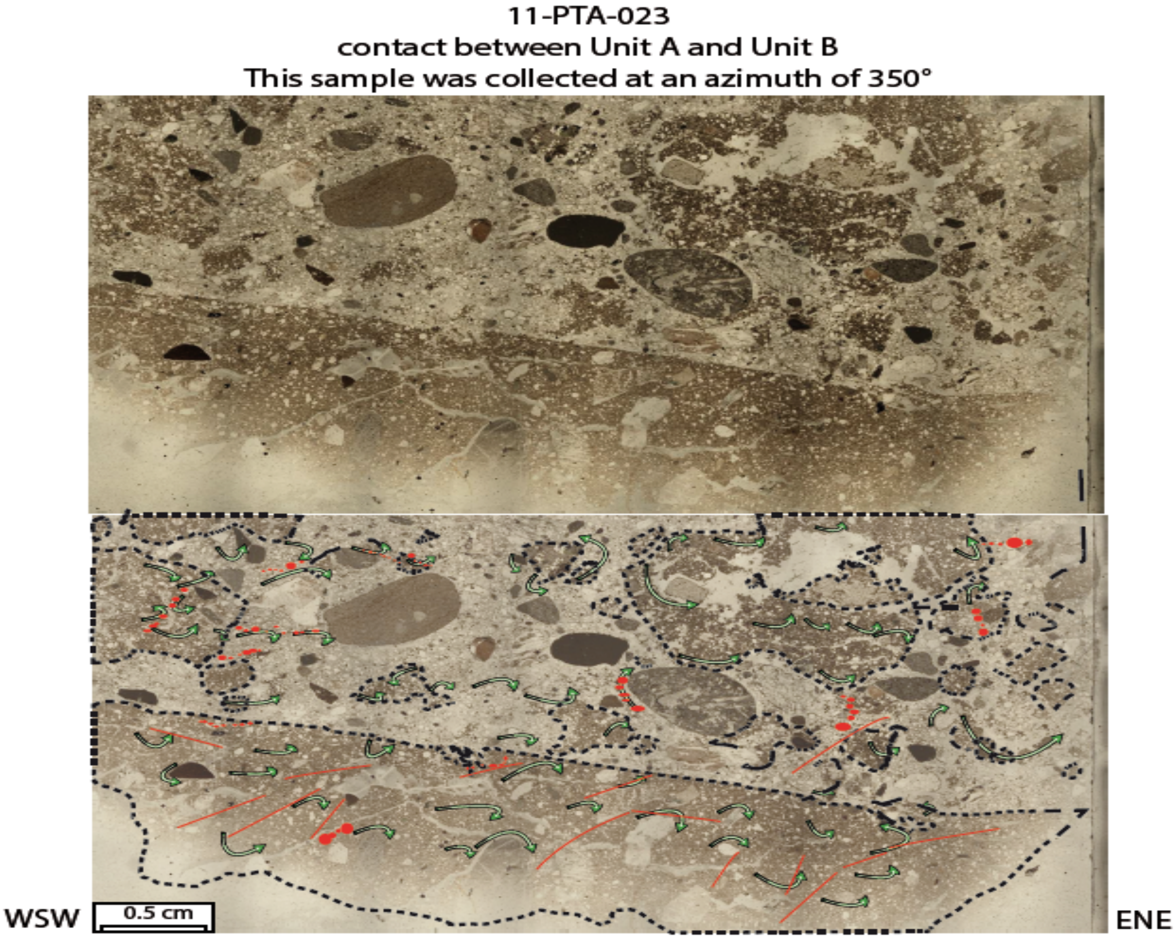

Figure 32. Annotated slide 11-PTA-023.

3.6.2 Unit B

11-PTA-023A

Two distinct matrix domains are observed, a dark, clay-rich matrix and a light coarser matrix (Fig. 33, highlighted in yellow). Abundant rotation structures are found throughout the entire thin section. There are several horizontal lineations and several grain stacks occurring perpendicular to these lineations; several of these structures appear to be deformed. There are also several microfractured grains, and garmented grains found in the dark clay-rich matrix. There are few voids found within this thin section.

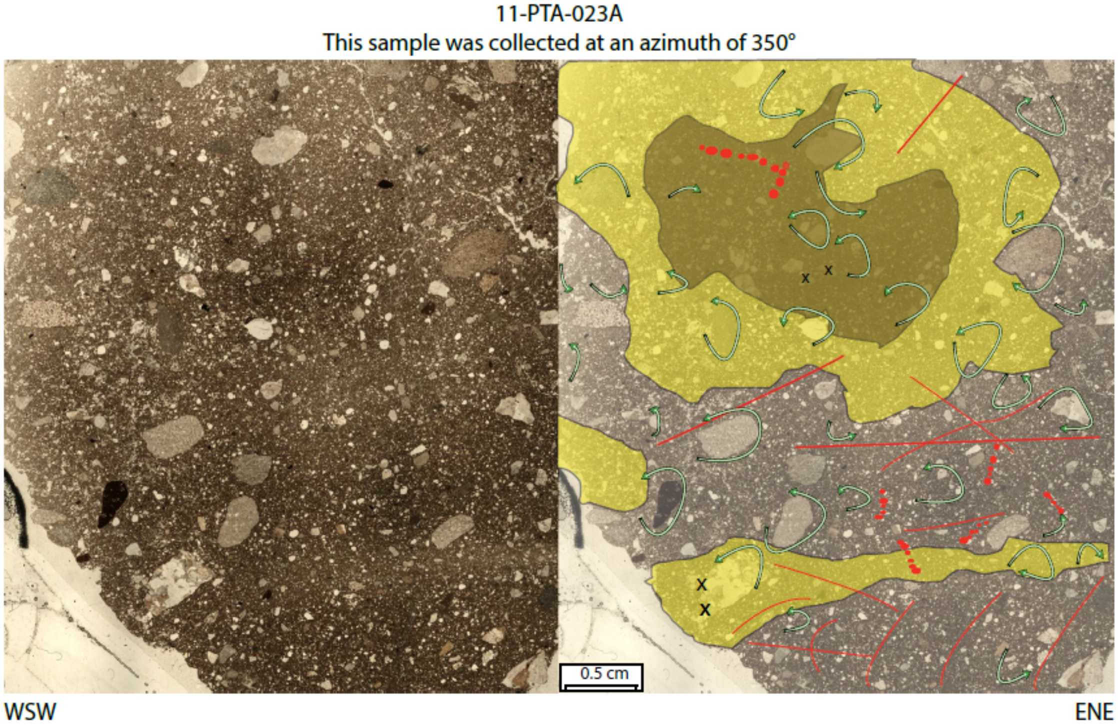

Figure 33. Annotated slide 11-PTA-023A.

3.6.3Unit C

11-PTA-025

Throughout Unit C, two distinct matrix domains are observed, a dark clay-rich matrix and a light coarser matrix (Fig. 34, highlighted in yellow). There are void spaces, some surrounding the larger clasts, horizontal and vertical lineations. A flow nose (Fig. 34, outlined in by purple lines) of densely packed grains is also observed. There are several rotation structures, which appear predominantly toward the top of the section, likely due to the highly voidal matrix at the base of the section. There are also zones of clay dominant matrix that is comprised of predominantly fine-grained material (Fig. 34, highlighted in yellow). There is also an inclusion of a foreign object within the slide, likely incorporated during the thin section production (Fig. 34, highlighted in green).

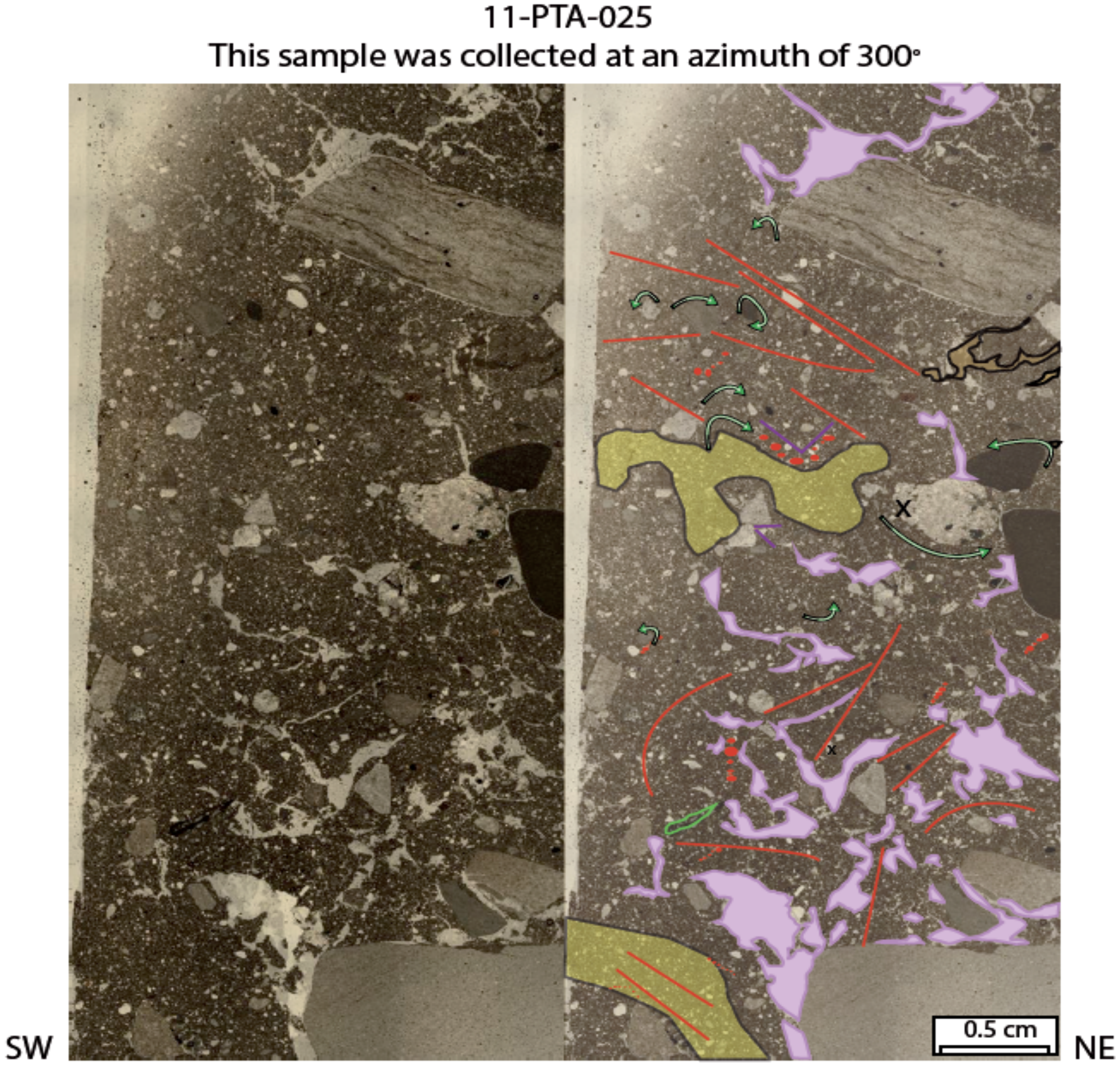

Figure 34. Annotated slide 11-PTA-025.

11-PTA-026

There are a thin fracture voids with no defined orientation found throughout the thin section, and some larger vug-like voids surrounding some of the larger grains. A thin shearing zone can be identified between the two separate matrix (Fig. 35, highlighted in red) that may be associated with the fracture void located directly beneath it. There are an abundance of rotation structures, some of which line the border of the two till domains. There are lineations within the thin section, orienting along two main orientations, to the upper south side corner, and the lower south side corner. A number of grain-lineations occur that parallel the lineation trends. Minor areas of clay accumulation are found throughout the thin section.

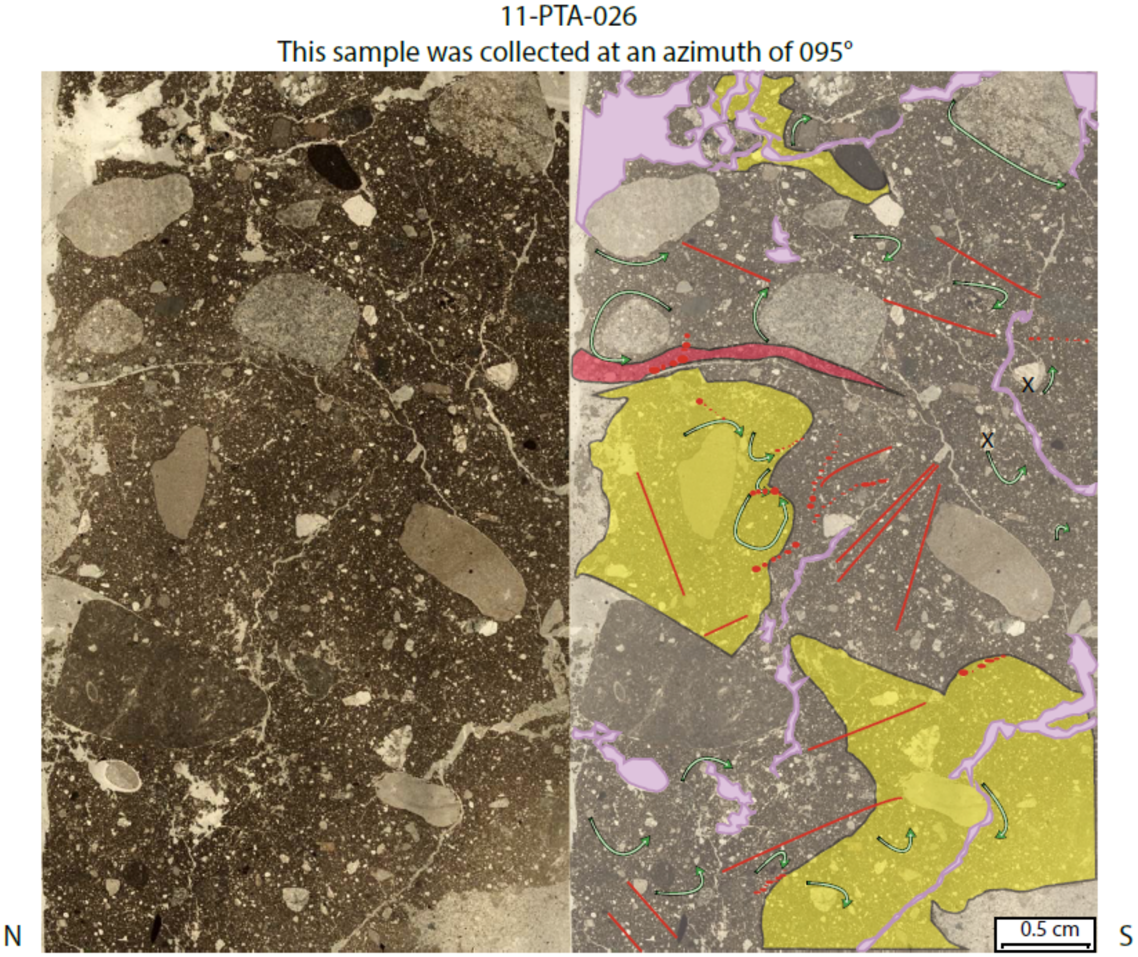

Figure 35. Annotated slide 11-PTA-026

11-PTA-027

There is a zone of deformation banding to the right of the largest clast in the thin section (Fig. 36, highlighted in red), which exists between the darker and lighter matrixes. There are a few fractural voids within the thin section that angle to the top south corner and bottom south side corner. There are few lineations and grain-lineations that parallel these voids. There are rotation structures that dominantly occur around core stones.

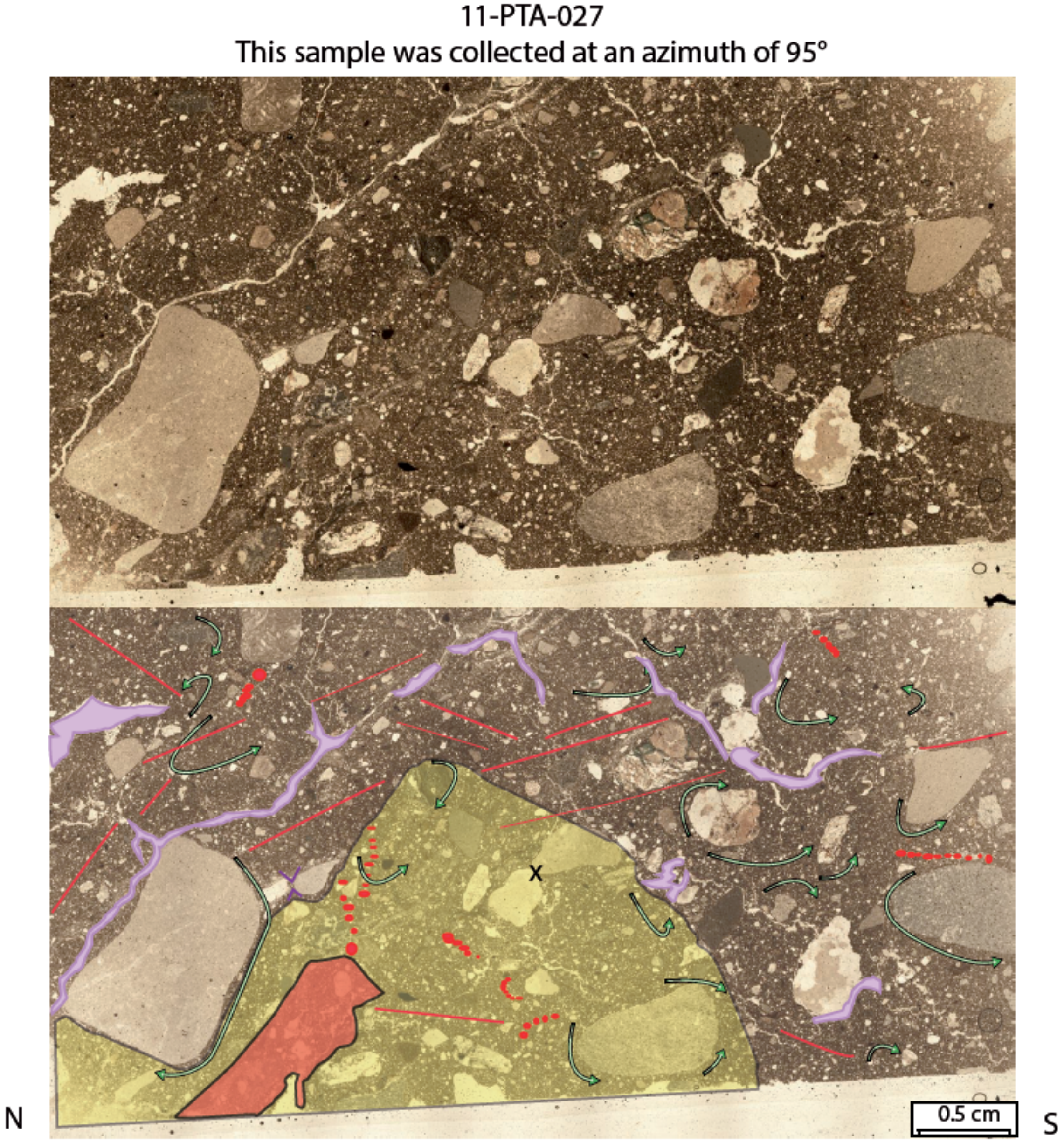

Figure 36. Annotated slide 11-PTA-027.

11-PTA-028

A zone of shear banding occurs in the upper north corner of the thin section. There are thin fracture voids that are clustered on the north side. There are also lineations, which appear to be more abundant in the finer-grained, darker domain and are predominantly oriented horizontally and to the top north and bottom north sides. Grain-lineations parallel these orientations, some having been affected by rotation. Rotation structures are evident throughout the entire thin section. There are also several microfractured grains (Fig. 37, marked with an X) appearing along a fracture void edge with other fractured grains appearing only in the darker, finer-grained matrix.

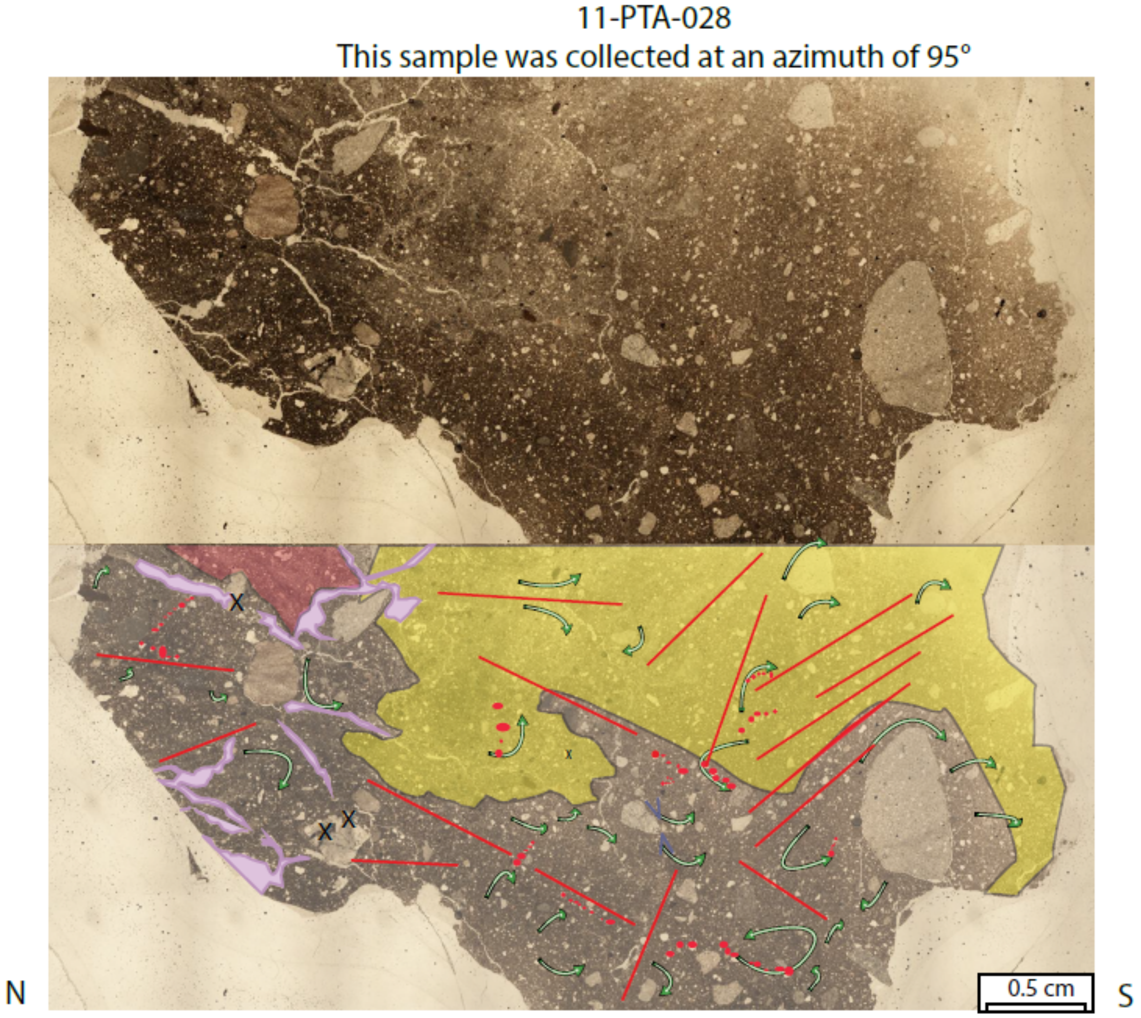

Figure 37. Annotated slide 11-PTA-028.

11-PTA-029

There are several large, vug-like voids within the sediment (Fig. 38), and several thin fracture voids that have no predominant direction. There are lineations oriented from the bottom north corner to the top south corner and the angle of these lineations lower toward the south near the base of the slide. Grain stacks found within the thin section tend to be oriented perpendicular to the surrounding lineations. There are some rotation, galaxy, and necking structures within both domains. There are some pressure shadows occurring on the north side of some clasts, in both domains.

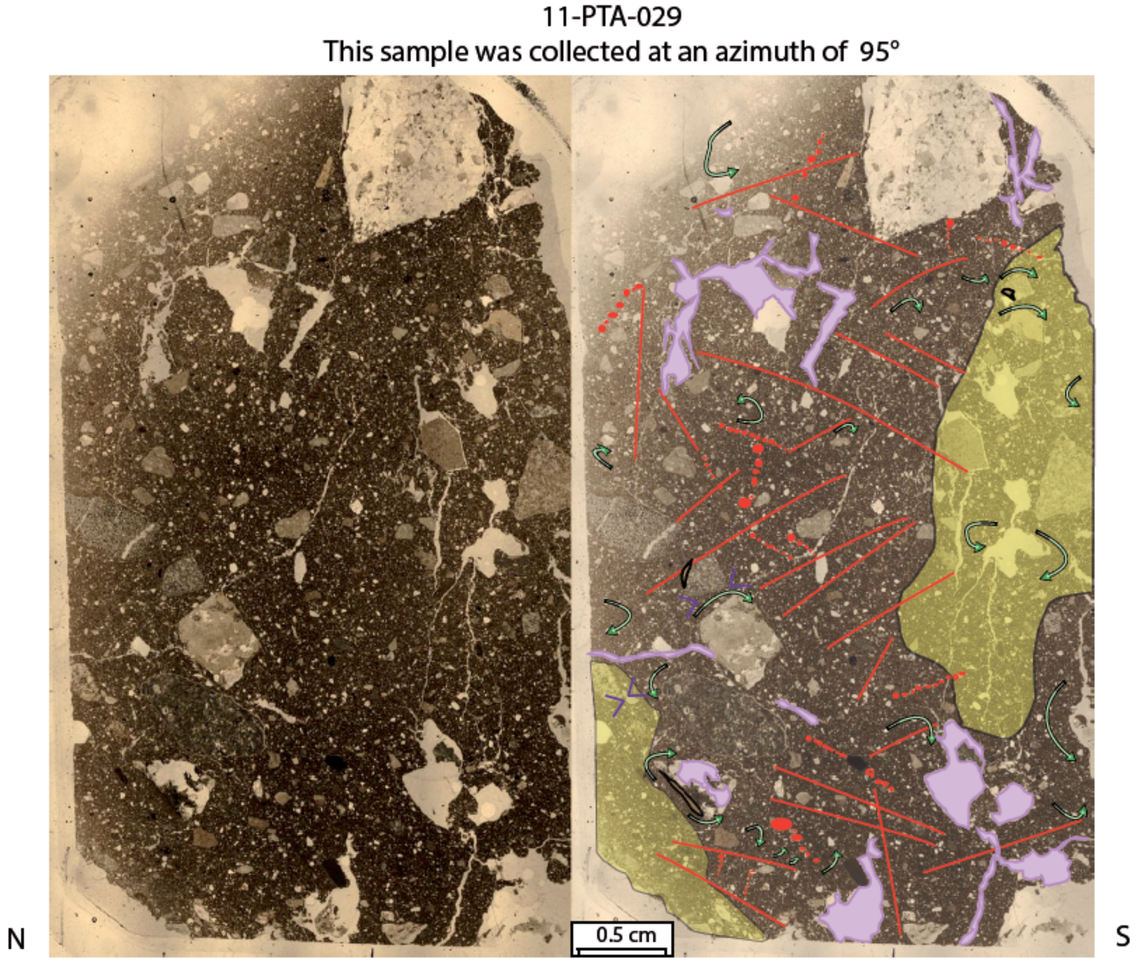

Figure 38. Annotated slide 11-PTA-029

11-PTA-030

Within this thin section there is a single domain with a small darker region (Fig. 39, highlighted in yellow) possibly bitumen from the bedrock in the region (*cf.* Rhodes et al., 1984; Lemmen, 1990; Gleeson and Turner 2007; Oviatt, 2013) or an accumulation of clay within that area of the slide. There are a large number of voids that have no clear orientation. There are a number of lineations that orient in two predominant directions, from the top north-northwest to bottom south-southeast and from the bottom north-northwest to top south-southeast. There are several grain-lineations that parallel the direction of the lineations, and several rotation structures, which appear mainly around medium size granules. There is evidence of possible pipe-like pore water flow through the slide (in to, or out of, the slide). There is some minor grain crushing found throughout the slide as well. The lower portion of the sample exhibits a large concentration of small voids.

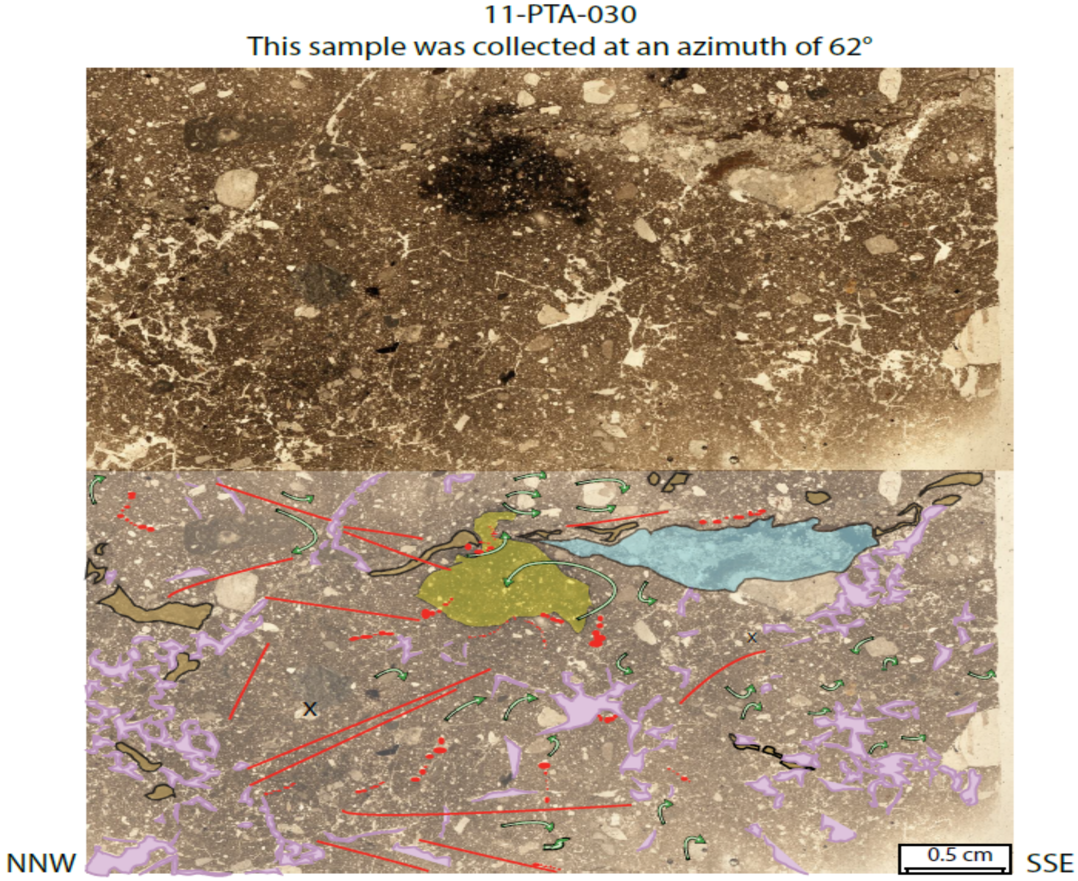

Figure 39. Annotated slide 11-PTA-030.

11-PTA-031

Lineations occur throughout the thin section are oriented predominantly to the top southeast corner (Fig. 40) with some lineations crosscut to the lower southeast corner. There are grain stacks that parallel these lineations, as well as rotation structures, with some stacking up, paralleling the lineations and grain-lineations. The rotations appear more concentrated in the lighter, coarser-grained matrix, however no rotations are observed to have formed near lineations. There are several pressure shadows observed adjacent to some of the larger clasts. There is a weak orientation of apparent a-axis (long axis) of small clasts to the top southeast corner.

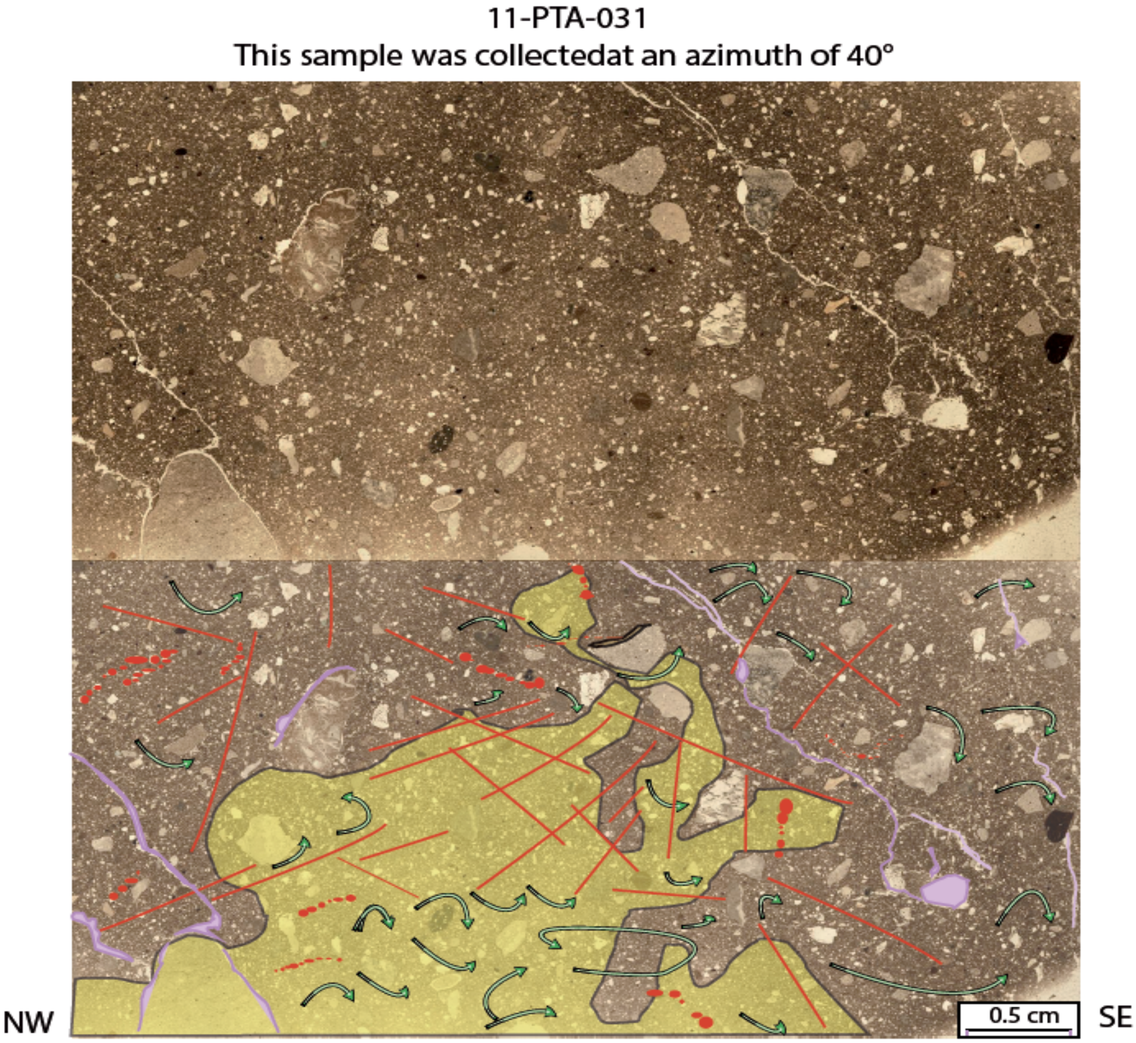

Figure 40. Annotated slide 11-PTA-031.

11-PTA-032

There are lineations that orient to the top northeast corner and bottom northeast corners, with grain-lineations paralleling the lineations angled toward the top northeast corner (Fig. 41). There are several rotation structures that also weakly parallel the orientations of the grain-lineations and lineations. There are several instances of pressure shadows, however, only occurring in the lighter, coarser matrix. Several necking structure was also observed.

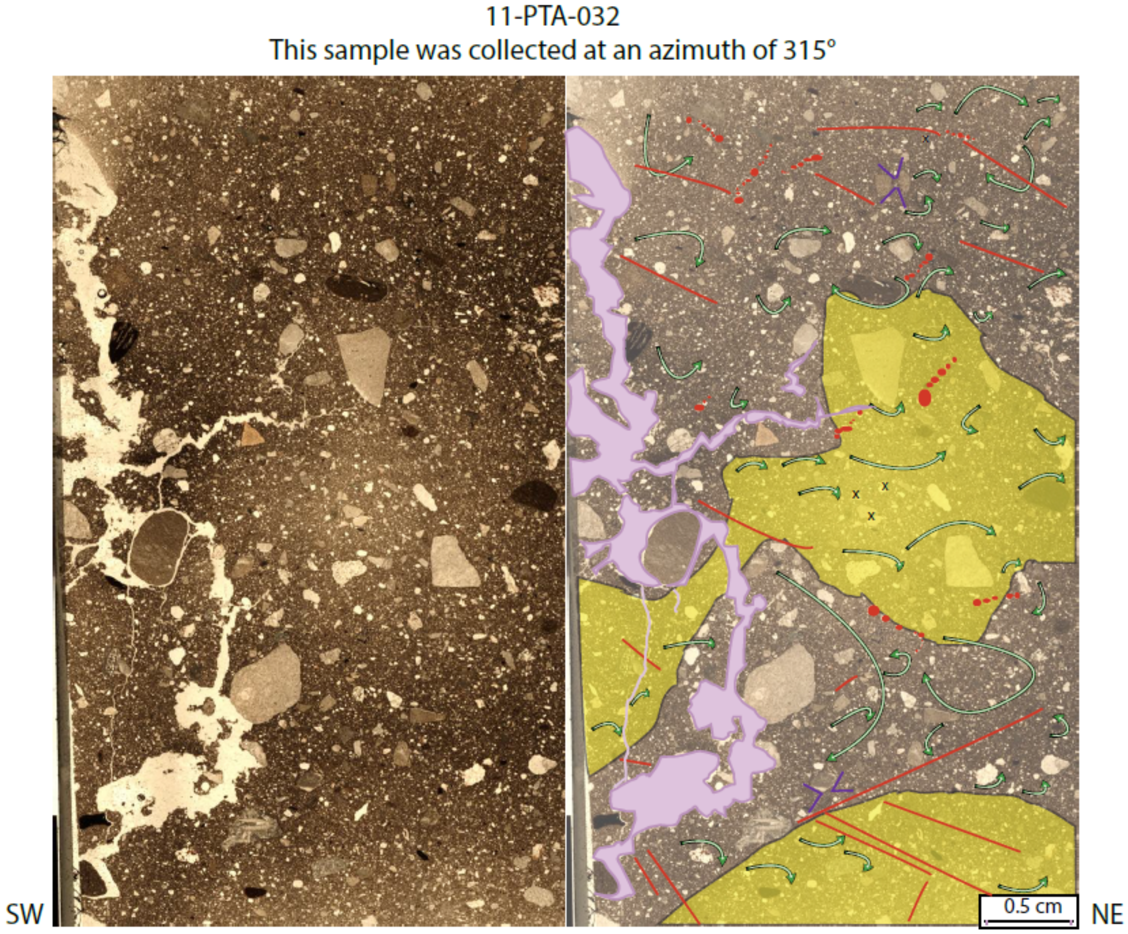

Figure 41. Annotated slide 11-PTA-032.

11-PTA-035

This sample was packed in fine sand for shipping and was impregnated with the sand, which can be seen along the outer edges of the sample (Fig. 42, highlighted in white). There are lineations oriented to the top northeast and lower northeast corners of the slide. Fine-grained grain stacks occur that parallel the orientation of the lineations toward the upper northeast corner, although some have been altered by rotation. There is also rotation structures that have no clear preferred stacking orientation. Finally, a weak orientation to the top northeast can be observed through the apparent a-axis of some of the grains.

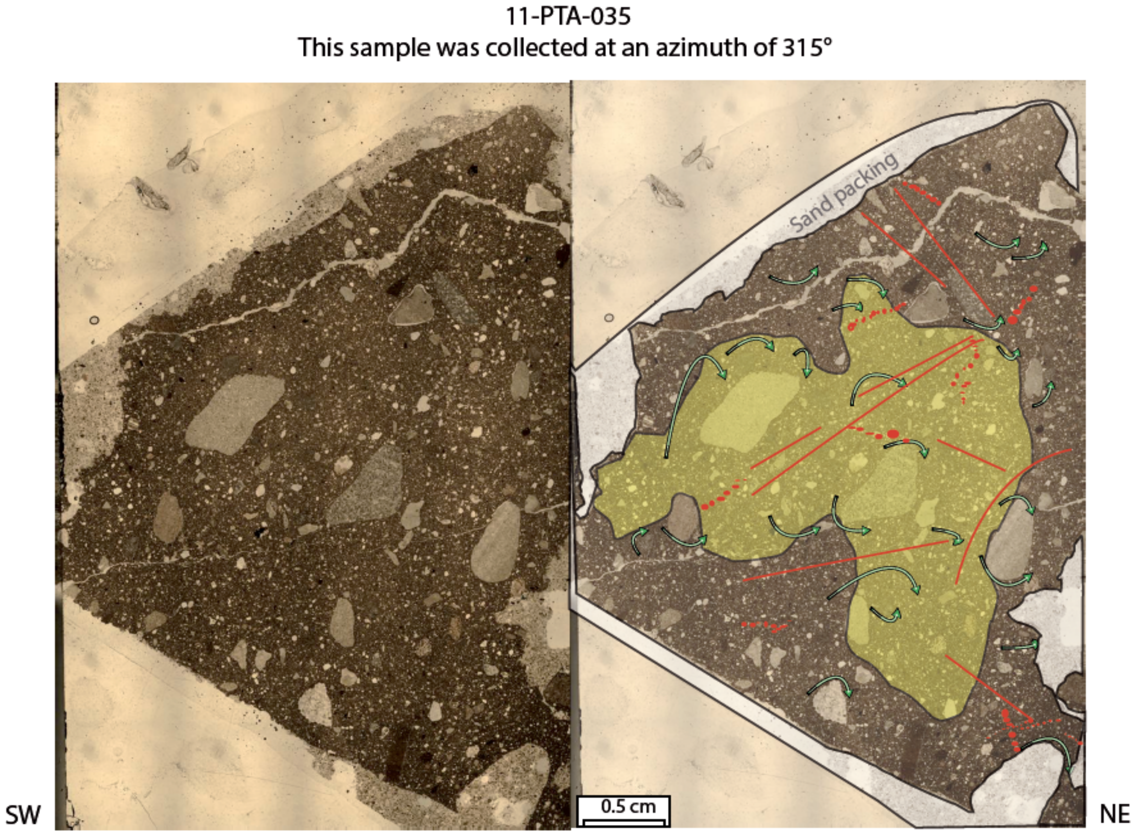

Figure 42. Annotated slide 11-PTA-035.

11-PTA-036

Lineations oriented predominantly to the top northeast corner (Fig. 43). There are also some lineations oriented in the lower northeast direction. Grain-lineations also occur, which parallel the orientations of the lower northeast lineations. There are a few weakly developed rotation structures. A minor amount of grain crushing has occurred throughout the matrix.

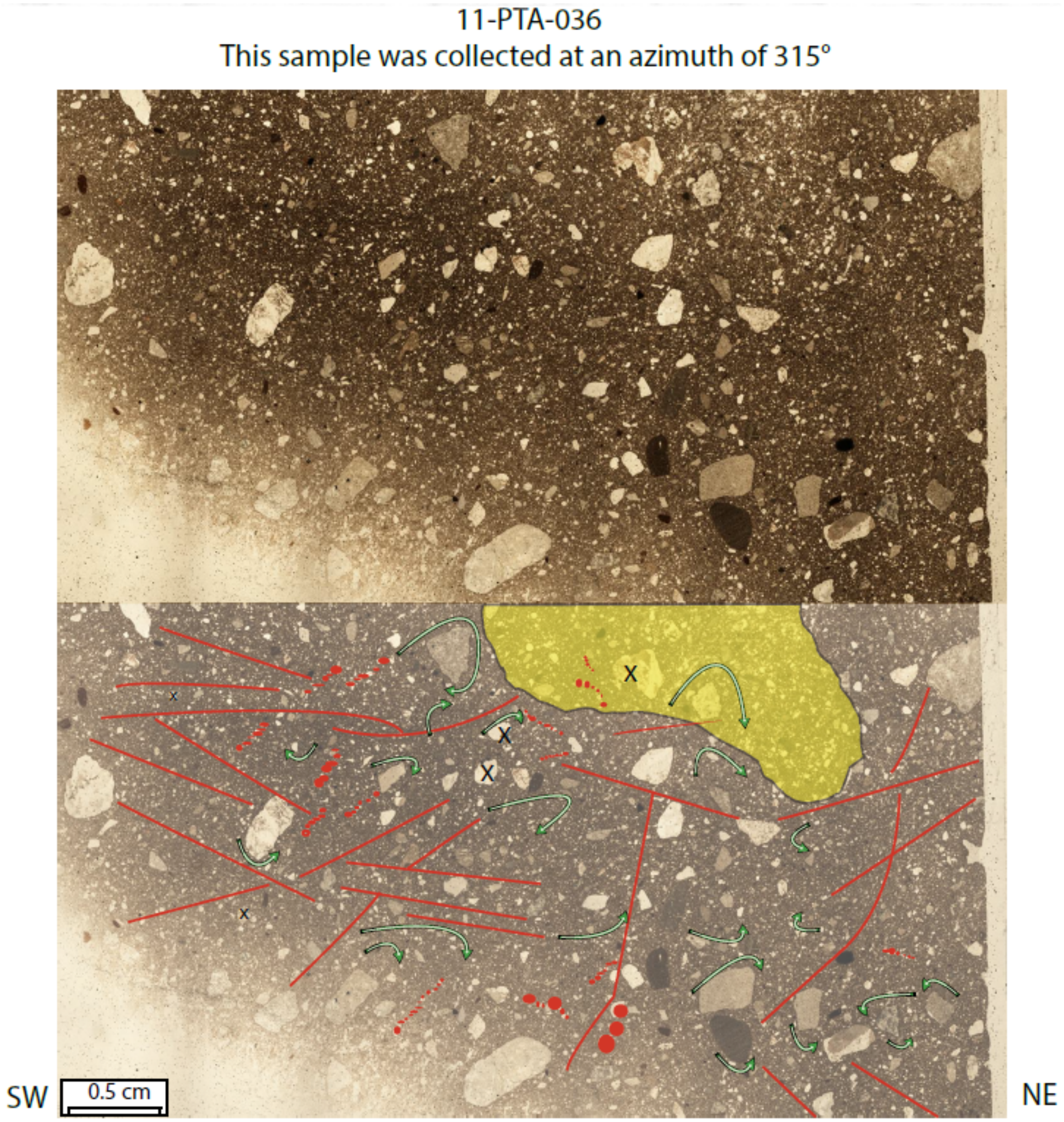

Figure 43. Annotated slide 11-PTA-036.

3.6.4 Unit D

11-PTA-037

There are two large fracture voids, one oriented vertically through the thin section and the other oriented angularly towards the top southwest (Fig. 44). There is also a large void on the northeast side, which developed during the production of the thin section (See Chapter 2.7.4). There are lineations throughout the thin section with predominant orientations to the bottom northeast and top northeast corners. There are a few grain-lineations that align parallel to the lineations oriented to the top northeast. There are also rotation structures with several 'groups' aligned towards the top northeast corner, parallel to the second set of lineations and most grain stacks. There are also shadows and clay accumulations on the southwest side of some larger clasts.

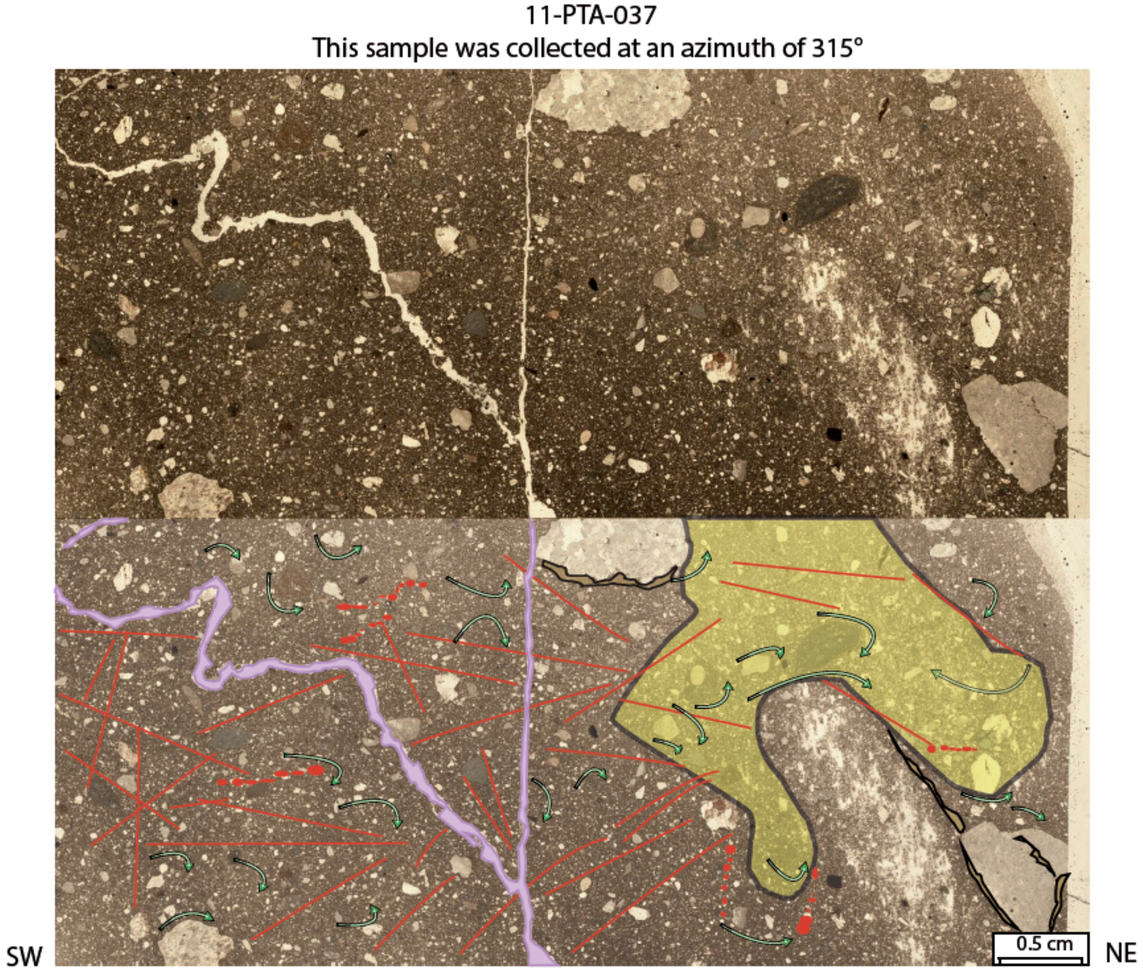

Figure 44. Annotated slide 11-PTA-037.

11-PTA-038

This sample was packed in fine sand for shipping and was impregnated with the sand still surrounding the sample, which can be seen along the outer edges of the sample (Fig. 45, highlighted in white). There are two matrix textures observed in the thin section, a darker clay-rich domain and a lighter coarser domain (Fig. 45, highlighted in yellow). Crosscutting lineations are also present and oriented towards the top northeast and lower northeast corners. Several horizontal fracture voids are noted near the base of the slide. Grain-lineations found within the matrix trend along a horizontal orientation and rotation structures tend to align in a more vertical trend.

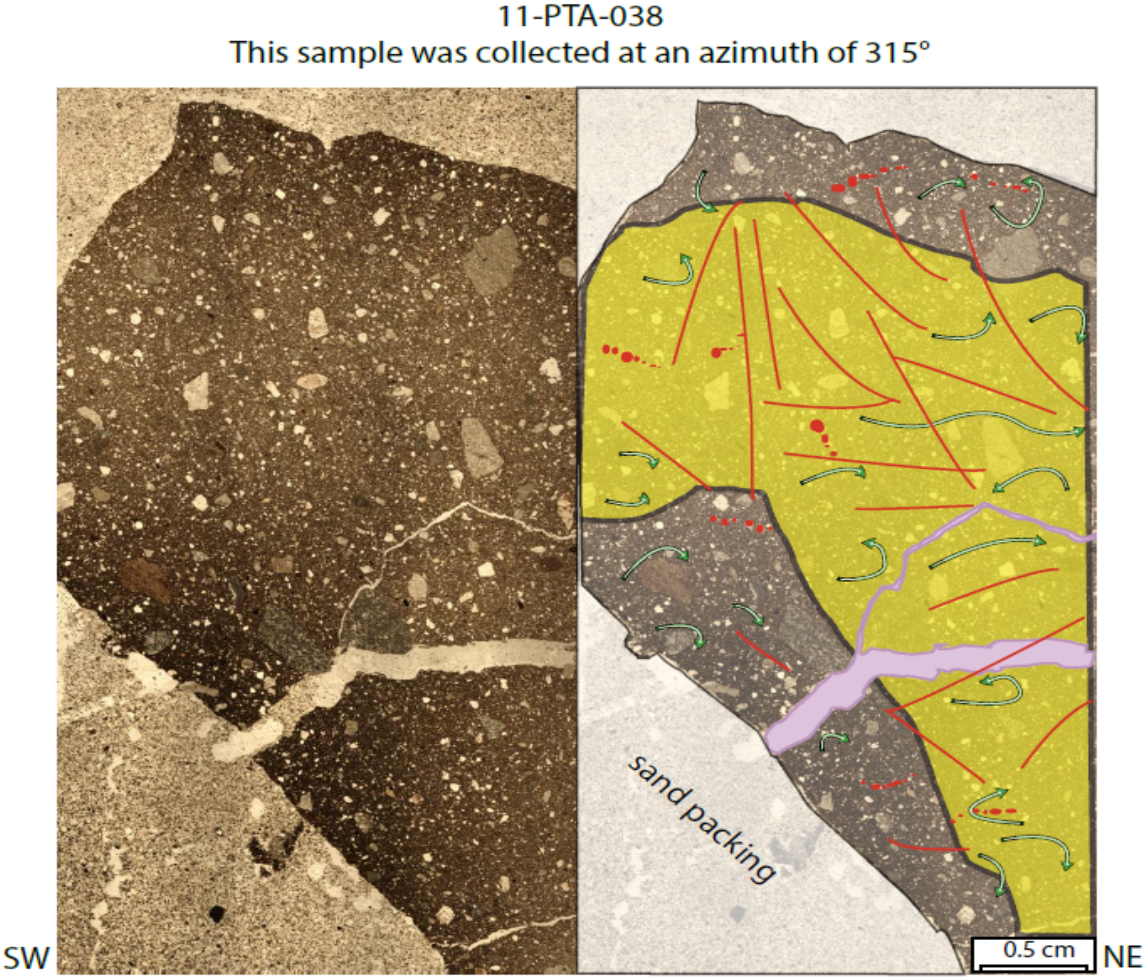

Figure 45. Annotated slide 11-PTA-038.

11-PTA-040

This thin section is highly voidal, with voids oriented in all directions (Fig. 46). A number of short lineations that have a slight preferred horizontal orientation are also present, with a few grain-lineations paralleling the lineations. Rotational structures have no clear orientation and there are a few crushed grains observed throughout the thin section.

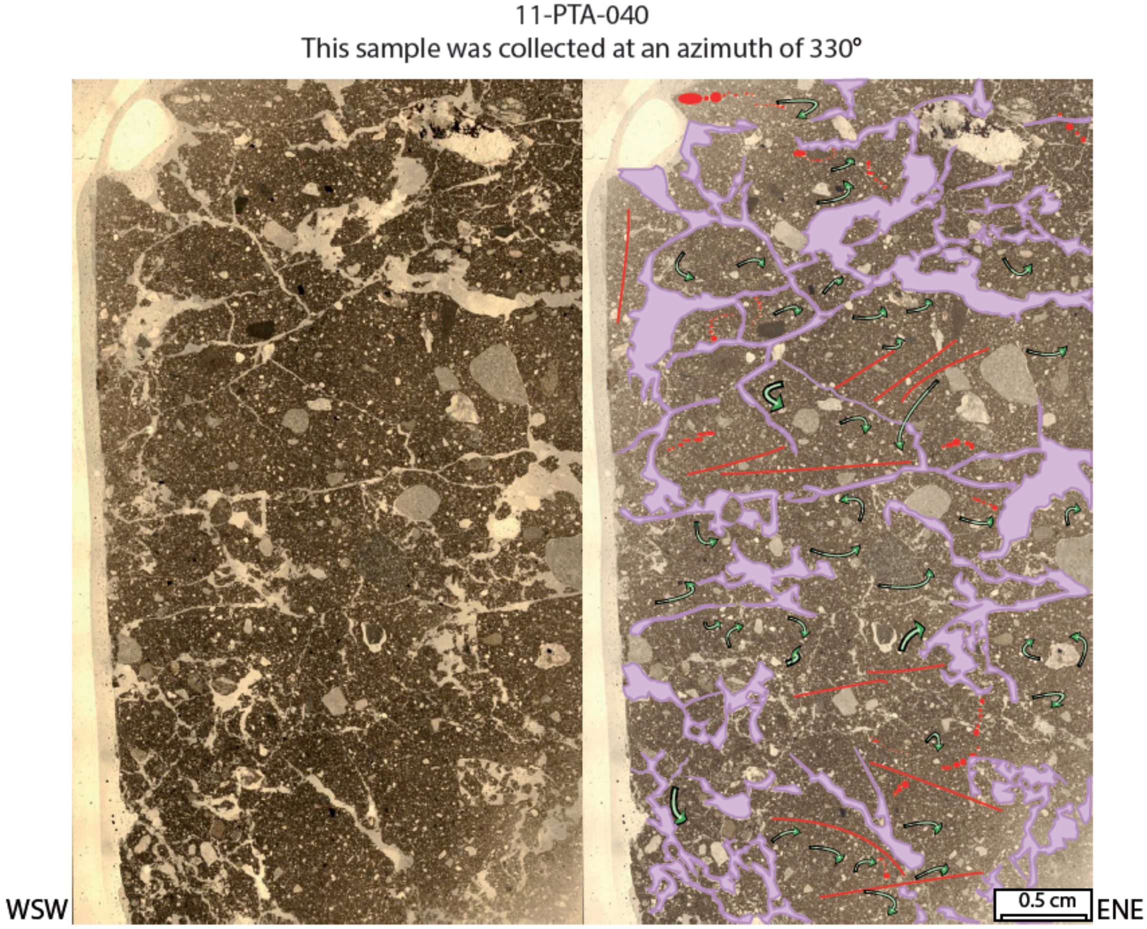

Figure 46. Annotated slide 11-PTA-040.

11-PTA-041

This thin section is also highly voidal, with the voids having a preferred vertical orientation (Fig. 47). There are several short lineations that are oriented toward the lower east-northeast bottom corner. Grain-lineations near the base parallel the short lineations. There are several rotation structures, which appear more abundant in the upper portion of the thin section, as well as some microfractured grains.

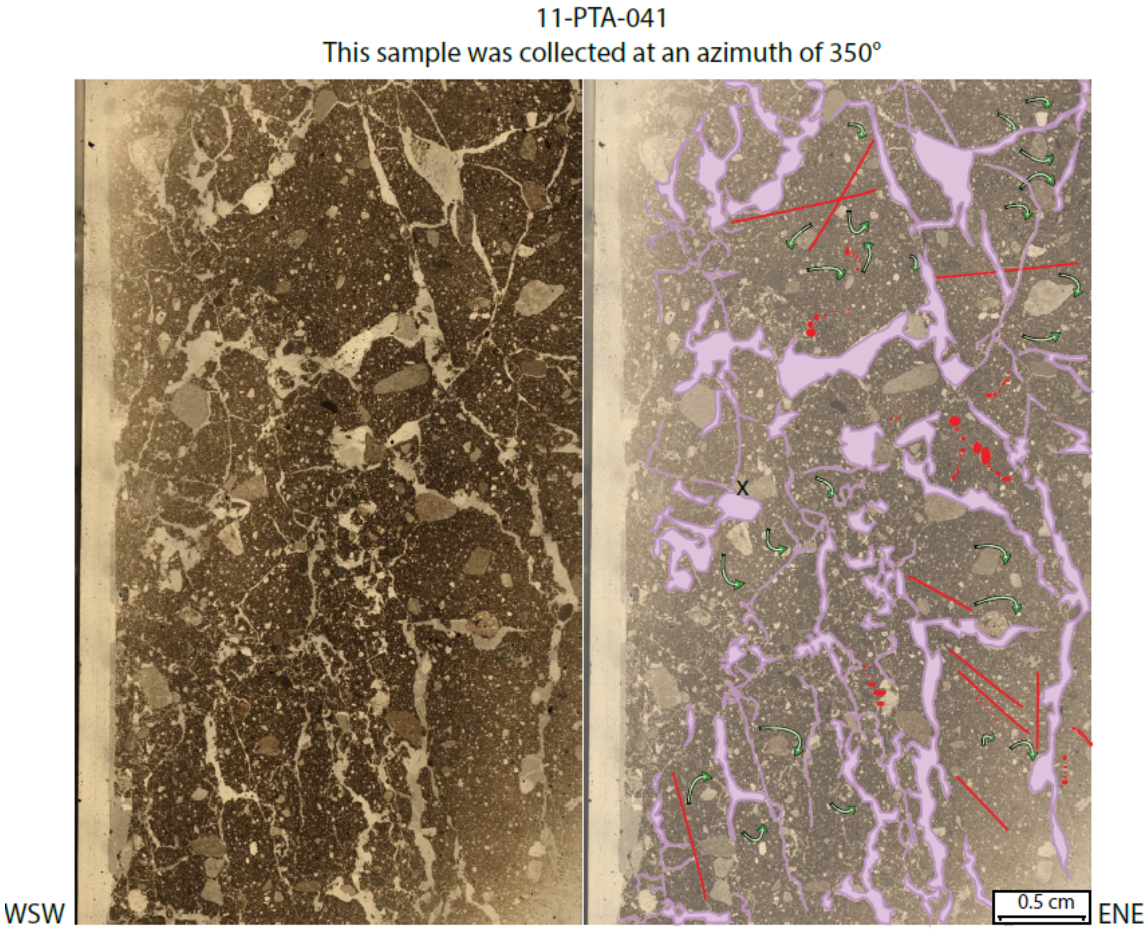

Figure 47. Annotated slide 11-PTA-041.

11-PTA-042

There are abundant voids observed in the thin section (Fig. 47). Several large grains are well rounded and have a similar orientation to the voids. This sample is likely too proximal to the land surface to conclude all structures are glacially influenced. Annotations have not been added to this image due to the large amount of voids that occur within the thin section, likely due to natural soil processes and exposure to anthropologic activity at the former open pit.

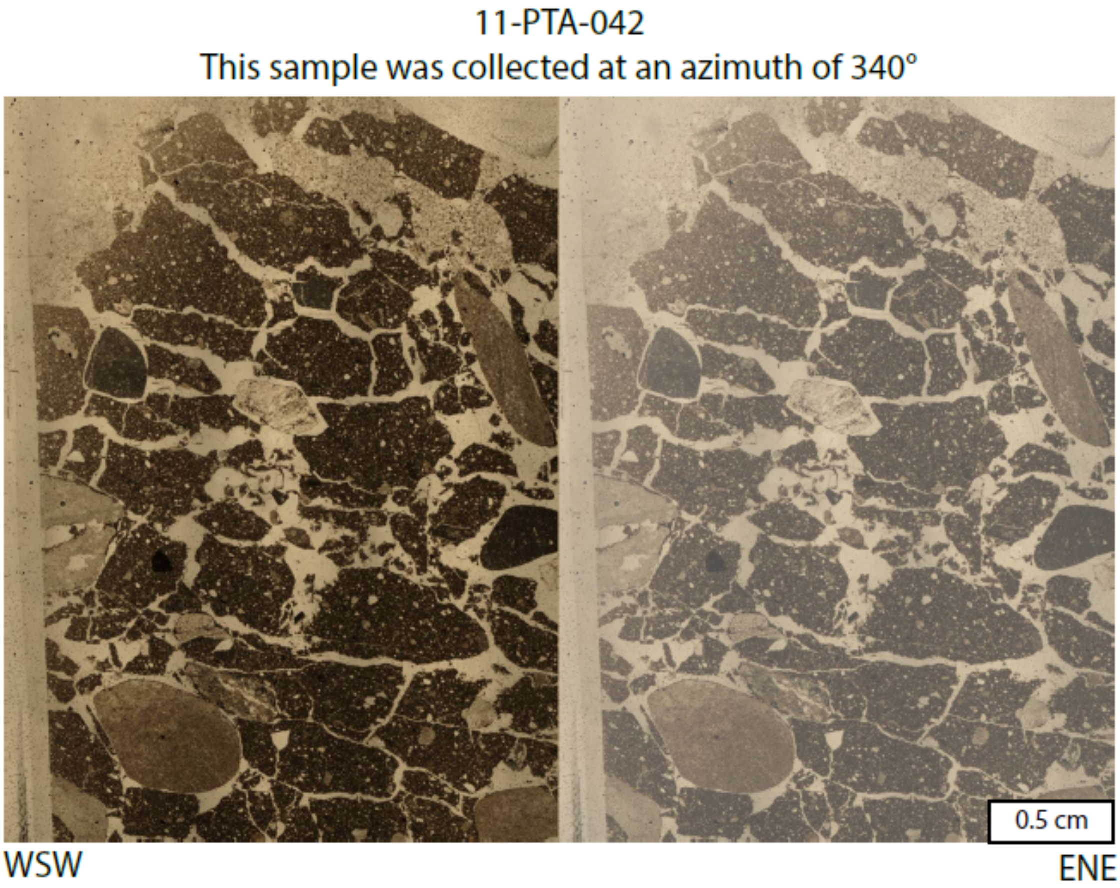

Figure 48. Annotated slide 11-PTA-042.

A summary of the microstructures and their interpretations can be found in Appendix H.

Chapter 4

4.0 DISCUSSION

As initial field observations had suggested, four distinct till units have been identified within the north face at pit-K62 located within the past producing Pine Point mining district. Investigation of the sediment facies displayed few macroscopic sediment structures other than small sand lenses, rip-up clasts, shearing contacts, and two weak boulder horizons. Although the diamicton appears massive and, macroscopically gravity flows and till can be indistinguishable, the micromorphological samples collected from pit K-62 lacked the texturally distinct layering, and tiling structures that have been commonly associated with debris flow (*cf.* Menzies and Zaniewski, 2003; Lachniet et al., 2001) suggesting these sediments were not debris flow diamicton. Therefore, based on the exotic clast lithologies, poor-sorting, striated and polished clasts, the strengths of the clast fabrics, and the unique set of microstructures found within each unit, the entire sedimentary sequence (excluding Unit E and Unit F) is considered till. This chapter will justify the initial field separation of the till units, discuss how the stratigraphic record correlates to the observed erosional record in the area (Oviatt et al., 2011) and discuss the depositional environment of the units.

4.1 Defining Stratigraphy

4.1.1 Units A-B

Based on field observations, the section at pit K-62 was separated into six visually distinguishable units, with Unit A being the lowest in this sequence (Fig 19). Unit A was first separated based on its visibly darker colour (PTA-022-wet: 2.5Y 3/2; dry

10YR 6/2 and PTA-023B- wet: 10YR 6/3; dry: 5Y 5/2) than the overlying unit (wet 2.5Y 5/3; dry 10 YR 7/2). There is also a change in matrix between Unit A (avg: 48.7% sand; 42.6% silt) and Unit B (32.0% sand; 49.6% silt).

Pebbles collected from Unit A are dominated by Precambrian aged Canadian Shield clasts (61.4%), in concentrations not observed in overlying Unit B (29.8%). These clasts suggest a different provenance then the overlying unit, furthering the justification of unit separation. The lithology of these clasts indicates the unit likely originating from somewhere northeast (Fig. 2) within the Canadian Shield. These shield clasts comprised mostly of felsic and mafic granites, but include well-rounded arkosic quartzite pebbles from the Sonsa group (Roscoe et al., 1987) from the eastern part of the Great Slave Lake were also present. The presence of well-rounded arkosic quartzite pebbles and sand lenses within this till indicate early LIS transport had incorporated older fluvial sediments during erosion, possibly pre-glacial Cordilleran derived.

The geochemical results, total carbon content, and heavy mineral analysis show contrasting results between Unit A and Unit B as well. The differences in the LOI values, CO_2 calcite and dolomite percentages, and pyrite/marcasite, kyanite, sillimanite, and sphalerite grain counts between the two units furthers the justification of the unit separation. The sedimentological characteristics of Unit A do not reflect the local bedrock (Oviatt et al. 2013a;2013b), suggesting a more exotic origin, again likely to the northeast near the boundary of the Canadian Shield.

There are slight differences geochemically within Unit A that are likely the result of mixing of debris into the unit over continued deposition. As subglacial debris from distant sources is gradually mixed with entrapped "fresh" material, the geochemical signature of the distance source is diluted, altering the geochemical signature of the sediment overlaying them (Broster, 1986; Stanley, 2009). As a result, PTA-023B has lower concentrations of Zn and Pb then the sample beneath in (PTA-022) and higher %Ca and %Mg values. The increased concentrations of Zn and Pb in unit A are likely the result of ice flowing over the deposit and incorporating either more of the local bedrock, or reworking previously deposited material rich in Pb and Zn. However, without a useable clast fabric from this unit, ice flow correlation is difficult. Unit B has higher %Mg and %Ca concentrations and lower concentrations of Pb and Zn as it was deposited from ice not incorporating eroded mineral rich material from the ore zone. Clast fabric measurements from this unit (290°) agree with this hypothesis.

Micromorphological samples from this unit contained two domains (11-PTA-022; Fig. 29), which could be two separate domains that have not completely homogenized, or could indicate a zone of high shear. However, the structure lacks the banding usually associated with shearing zones and is likely to be a well-reworked sand lenses, due to the presence of only sand size grain and smaller rotation structure at the terminus of the structure (highlighted in yellow). The lowest sample collected from Unit A (PTA-022) contained far more fine particles, than any other sample collected throughout the face, possibly indicating weathered bedrock, proglacial fluvial or lacustrine sediments, or highly eroded material over long transport, which is supported by the clast lithology results. Unit A was also highly compact, and lacks the fissility planes observed in overlying units. 11-PTA-023B does display some voids and fewer fine particles (Fig. 30), and also displays darker portions around some clasts (highlighted in yellow) which could be the result of the migration of fines to low pressure areas when rotation around the clast during shear events (Kilfeather and van der Meer, 2008), or simply the inclusion of another unit which has cohered to the clast.

4.1.2 Units B-C

The initial separation of Unit B from Unit C was based on the visually identifiable shearing contact that was observed between these two units. Geochemically, this unit is indistinguishable from the overlying Unit C, containing levels of Pb-Zn consistent with that of the overlying unit. This consistency is also observed in comparing LOI, calcite and dolomite concentrations, and total carbon concentrations. Heavy mineral analysis shows slightly elevated amounts of hercynite and kyanite, but contained very similar concentrations of all other minerals examined. Pebble lithologies from Unit B coincided with those found in Unit C as well.

The similarities found between these two units when comparing their sedimentological characteristics is a result of the mixing of these units during the erosion, emplacement, and deposition. This can be further demonstrated and visually observed when examining the contact between the two units or the microstructures throughout this unit (Fig. 31; Fig. 32). This unit contains multiple domains and rotation structures, clearly indicating that there is re-working of another domain into this unit and has not quite homogenized. Micromorphological analysis shows this thin section has very few voids, unlike all of the overlying units. This unit also lacks the abundance of lineations that are observed in overlying sediments, but has far more rotation structures than overlying sediments.

Clasts fabric analysis completed in this unit also suggests Unit B was likely deposited from a different flow direction then from Unit C. Unit B clast fabric results indicate a flow direction of 290° (S_1=0.54), whereas the overlying unit tended towards the SW.

Therefore, despite the similarities in geochemistry, heavy minerals, LOI, clast lithology and total C, the differences in microstructures, the shearing contact between the units, and clast fabric differences suggest that Unit B is a separate till unit than the overlying Unit C. The similarities observed in this unit with the overlying unit are a result of the fine grain mixing between the two units. The geochemical, LOI, and total C analysis was done on < 0.063 mm grain size fraction and the heavy mineral analysis was done on < 2.0 mm grain size. The clast lithologies had similar results likely due to their close proximity to the bedrock.

Although this unit appears to be of a different provenance than the underlying Unit A, the same can not be concluded for overlying Unit C, based on its similar sedimentological properties. However, the differences in microstructures, the shearing contact between Units A and B, change in sediment colour, and change in clast fabric direction indicates change in ice dynamics/provenance just after the deposition of Unit B.

4.1.3 Units C-D

Field observations indicated that a boulder horizon and an increase in fissility separated Unit C from Unit D (Fig. 22). However, a minor boulder horizon was also observed within unit D, and was not classified as a separate unit, due in part to the weakness of the boulder horizon, but mainly due to the lack of sedimentological differences above and below this minor boulder horizon.

Geochemically, Unit C was comparable to overlying Unit D, except when comparing Pb and Zn concentrations. In Unit C concentrations of Pb ranged from 20.08 – 41.29 ppm and concentrations of Zn range from 67.3 - 108.8 ppm, whereas concentrations in Unit D range from Pb values of 64.54 - 66.82 ppm and Zn values of 169.8 - 173.5 ppm. The elevated concentrations of Zn and Pb in Unit D suggest the increased inclusion of some of the lead-zinc deposit within the region, or inclusion of higher-grade bedrock into the unit. The absence of higher concentrations of Pb and Zn in Unit C suggest there was less inclusion, or bedrock with a lower concentration of Pb/Zn again supported by the clast fabrics and striations indicating the flow direction did not incorporate material directly above the ore deposit.

Clast fabric results from Unit C further support this interpretation. Fabrics taken within Unit C tend ~ 270° near the top of the unit (PTA-035) and 230-240° lower in the unit (PTA-031 and PTA-034). Although there is a slight variation within the fabrics toward the upper part of the unit, considering the thickness of this unit (~12 m), the slight orientation adjustment does not justify unit separation, particularly when comparing other sedimentological properties mentioned.

Clast fabrics measured from Unit D, less then 5 m above the highest sample from Unit C, oriented ~140° in the lower part of the unit (PTA-037) and 260° in the upper portion of the unit (PTA-042). Although these fabric results do not correlate, and suggest unit separation, the other sedimentological characteristics between these samples do not justify unit separation.

Micromorphological features between these units also show a clear differentiation between units. Unit C contains multiple domains, which is only observed in the lowest samples from Unit D (PTA-037 and PTA-038). The samples from Unit D also lack grain crushing, which is observed throughout the samples taken from Unit C. Furthermore, the samples from Unit C are compact showing few voids, whereas samples from Unit D have abundant voids.

4.2 Correlation with erosional record

Analysis of the clast fabric data (Table 2; Fig. 19) in comparison to the observed glacial landforms in the area, and the erosional record encompassed by the striations within the Pine Point Mining District (Oviatt et al., 2011; Oviatt, 2013), demonstrates that glacial history of the Pine Point region is much more complex than previously reported (Lemmen, 1990; Brown et al., 2011; Paulen et al., 2008). A summary chart of clast fabric directions, striation directions, and landform orientations can be seen in Figure 48.

The erosional record indicates three ice flow trajectories (Fig. 4), the youngest being to the southwest (~ 250°), an intermediate flow to the northwest (~ 300°), a later intermediate flow to the north-northwest (~330°) and a later west-southwest flow (~ 250°). The most well preserved streamlined landforms in the area (Fig. 5) coincide with the latest flow phase (~250°) cross-cutting the landforms parallel to the northwest intermediate flow (~ 300°). These erosional and depositional records recorded within the landscape are re-enforced by the clast fabrics within the till facies (Fig. 48).

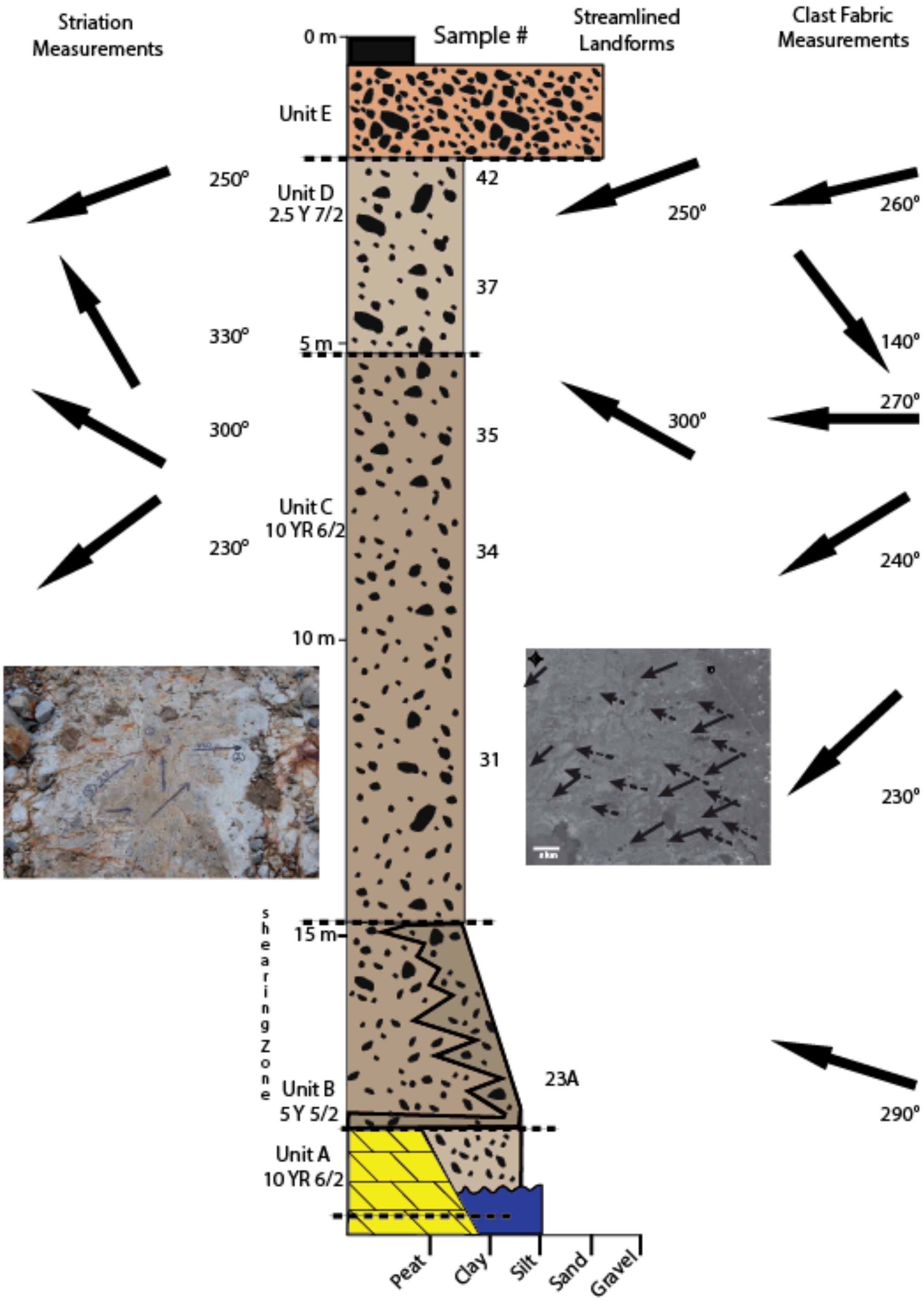

Figure 49. Illustration outlining the general tends of striations, streamlined landforms, and clast fabric results, and their correlation to each other throughout the stratigraphic unit. Note: Striations were sampled at a nearby location. See Oviatt et al. (2011) for details.

Based on the results of the clast fabrics, the upper most sample in unit D (11-PTA-042) did have a moderately-strong correlation with the youngest ice-flow striation direction (Fabric: ~260° S_1 = 0.68; Striation: ~250°), which is similar to the striation as well as in the cross cutting landforms in the area (~250°; Fig. 5). The underlying clast fabric (PTA-037 ~ 140°, S_1=0.60) has an orientation that is parallel to the intermediate striation record (~300°), however was not observed in the streamlined landforms (Fig. 5). The only other observed streamlined landforms were the landforms that had been crosscut (~300°) by the more predominant observable features that orient to the southwest. These landforms coincide with the third oldest striation record (~300°) and are likely related with the sample at the top of Unit C (PTA-035; Fabric~ 270°). Samples 11-PTA-031 and 11-PTA-034 were also taken from Unit C, however had stronger fabrics (S_1=0.77 and S_1= 0.65) that oriented (~240° and ~230°) toward the oldest striation record (~230°). Unit B (11-PTA-023A) was only thick enough to justify a single clast fabric measurement (~290°). This orientation was not observed in the striation record. However, this till unit is only ~2.5 m thick indicating a possible short lived glacial episode or erosion of deposited material by a later ice flow, or was overprinted, or deformed by a later ice flow. The preservation of the dark coloured diamict in the karst collapse structure, and lack of deposited material from this unit on exposed bedrock in the area suggests the latter. The lowest clast measurement taken in Unit A displayed a weak (S_1=0.05) fabric with no clear orientation and was not associated with any striation or landform orientations, and was likely the result of the till flowing or being pushed into the karst depression.

The Pine Point region was not far from a fluctuating ice margin that occupied the Great Slave Lake Basin during the middle Wisconsinan (Dyke and Prest, 1987), it is possible that ice marginal lobate shifts in flow direction could be responsible for changes in ice flow observed throughout the facies.

4.3 Depositional environment

The oldest till (Unit A) preserved in the section had a steeply dipping fabric, making identifying an accurate flow direction impossible (Table 3). The high angularity of the clast fabric and the lack of preservation of this unit outside of the karst collapse structure, suggests this unit flowed down into the depression during deposition, probably at the onset of glaciation, with till exposed on bedrock possibly being removed by later glaciations. Pebble lithology results from this unit resulted in predominantly Canadian Shield clasts, suggesting considerable transport distance (~120 km; Fig. 2), and the presence of well rounded small pebbles and re-worked sand lenses indicates pre-glacial fluvial sediments were likely eroded and incorporated into this unit up-ice.

Microstructures identified in samples taken from this unit displayed strong evidence of polyphase deformation, exhibiting rotation structures, lineations, and grain stacking (Phillips and Auton, 2000). Rotation structures, which result from varying velocity gradients within and between subglacial sediments (Evans, et al., 2006), increase proportionally to the increase in deformation indicating a high degree of deformation stress has been applied to the till. The presence of lineations, which are localized readjustments of the till due to fluctuating shear directions and rates, suggests a high degree of shear-stress has been placed on the till as well. The presence of rotation structures, lineations, necking structures, and grain lineations indicates the till has undergone ductile deformation. The increase of rotation structures within the upper portion of the unit (Fig. 29 and Fig. 30) in conjunction with the lack of fissility in the lower section, indicate that due to either fluctuating shear stress during deposition, or pore water fluctuation, the overlying stress did not penetrate through the entire unit. However, as there is no evidence of pore water microstructures within the samples, there was likely a fluctuation in shear stress during deposition, causing an increase in shear structures in the upper portion of the unit (Table 5). This fluctuation could have also developed as a result of the karst-collapse “sheltering” the lower sample (PTA-022), whereas the upper sample was taken at the top of the collapse feature (PTA-023B), and may not have been protected.

There is also evidence of rafted material within the unit (Fig. 30), indicating during transport and deposition the depositing ice mass eroded, incorporated, and deposited a foreign sediment without fully homogenizing into the till. These structures indicate that this unit was deposited subglacially as part of a deforming bed. The microstructures within this section also indicate a high amount of deformation has occurred, and cross cutting lineations through rotation structures, suggests this till was part of a subglacial deformable bed. This till experienced increased basal shear stress overpowering the bulk shear strength, causing the till to become mobile. This increase in basal shear stress could have resulted from an increases in applied stress, pore-water fluctuations, a change in thermal regime or changing sediment rheology. Traditionally this would be referred to as a basal lodgement till, however it has been more accurately categorized as a Type B-tectomic/mélange till (Menzies, 2012; Fig. 50).

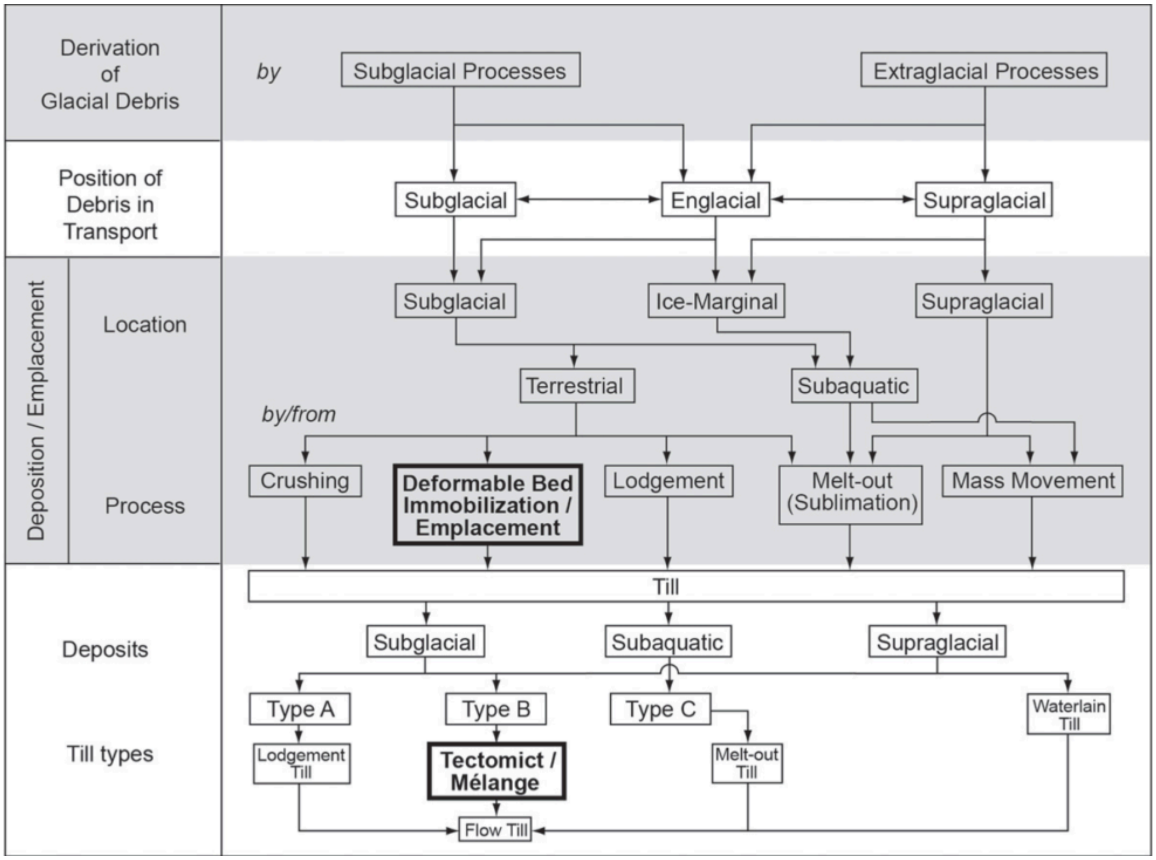

Figure 50. Flow chart exemplifying relationships between till formation, transport, deposition, and classification (Menzies, 2003; Menzies, 2012).

The overlying unit (Unit B) showed macroscopic mixing with Unit A (Fig. 20), and microstructures within the sample give evidence of mixing, and ductile deformation throughout the entire unit, indicating Unit B was being emplaced as it progressively began to immobilized. The microstructure assembly of grain stacks, multi-directional lineations, and the abundance of rotation structures within this unit suggests a polyphase flow (Table 5). The lineations, within this unit cross cut the reworked sediments, indicating the brittle deformation occurred after the ductile mixing of the two units and rotation of some of the grains. The multiple directions of the lineations could possibly be overprinting, however further investigation is required to confirm this.

The fissility in this unit could be a response to unloading of the sediment after the retreat of the ice, or could be a result of the formation of ice lens during winter with the orientation of the fissility planes controlled by the geometry of the migrating freeze front. The fissility could also be an indication of high levels of repeated Riedel shearing, specifically R2 where the shear occurs at 75° to the shearing direction, has been replicated by Thomason and Iverson (2007) in ring shear lab experiments. However this type of fissility would mean that the clast within the thin section would also align to these shear angles, which is not observed, and is therefore highly unlikely. The lack of micromorphological evidence indicating freeze-thaw mechanisms rules out fissility being caused by ice lenses and suggests that the fissility is a result of loading/unloading.

The scavenging of up-ice till units into emplaced till and the assembly of identified microstructures suggests Unit B was emplaced by a mobile bed into underlying immobile (Unit A) bed. Microstructures within this unit (changing orientations of lineations/grain stacks) indicate that this unit has undergone fluctuations in strain rates and possibly directions, classifying this as a Type B- tectomict/mélange till (Fig. 49).

Unit C was the thickest unit and contained a polyphase clast fabric (Table 3). The clasts fabrics from the upper portion of this unit (PTA-035) correlate with striation measurements taken in the Pine Point region and to eroded streamlined landforms (Fig. 50). These relations confirm the relation between the erosional record recorded on the regional bedrock and surficial landforms to the deposition of the upper-portion of thickest unit of till in the area and the flow direction of the ice during this deposition was toward the southwest and west-northwest. Microstructures within the unit support a polyphase flow hypothesis, having evidence of multi-directional lineations, grain stacks, necking structures, and rotation structures. The lineations cross-cut the rotation structures and both domains, indicating the brittle deformation of the sediment occurred after the ductile deformation.

However, the rotation structures are restricted mainly to separate domains, not crossing the domain boundaries indicating that the majority of the ductile deformation occurred before the mixing of the two domains. If the rotation structures developed post-mixing of the two units, the rotation structures would not have been restricted to the single domains, but rather would cross cut between the two units. The majority of the rotation structures occur in clay rich regions of the matrix, which likely had higher pore water content allowing for movement of the fine grains with less resistance (Larsen et al., 2007). The voids within this unit do not have grains paralleling the void direction and are therefore unlikely to be shear induced, but are likely a result of post-depositional unloading, or ice lens formation (van Vile-Lanoë et al., 1984; Sveistrup et al., 2005). There are examples of shear zones within two of the samples (PTA-027 and PTA-028), indicating an increase in shear stress associated with the changing subglacial conditions resulting from the transitional zone created by changing basal ice strain, the rheology of subjacent deforming sediments, and/or temperature changes within the till (Truffer et al., 2000; van der Meer et al., 2003; Larsen et al., 2007; Phillips et al., 2008; Boulton, 2010). The uppermost sample associated with the shearing zone (PTA-030; Fig. 7), shows evidence of pore water escape (Fig. 40). This pore water structure appears to be a pipe-like flow, flowing either E or W (into or out of the slide). This pipe-like flow feature overlies a moderately brecciated matrix. The flow-like structure drained the pore water from the matrix of the unit, increasing the strain on the underlying sediment causing an increase in shear and possibly brecciating the matrix. There are multiple domains found throughout this unit suggesting that this unit was not completely homogenized, further indicating that this unit was emplaced from a mobile bed into an immobile deposited unit (possibly unit B). Microstructures within this unit (changing orientations of lineations/grain stacks) also indicate that this unit has undergone fluctuations in strain rates and possibly directions, classifying this as a Type B- tectomict/mélange till (Fig. 50). It is likely that the continuous ~ 15 m of till that consists of Unit C could be a reflection of the glaciation during the Middle Wisconsinan, however without time scale evidence this can not be said with absolutely certainty.

Clast fabric measurements from Unit D (Table 3; Fig. 19) correlated to bedrock striations in the region and streamlined landforms in the region (Fig. 49). The correlation between these erosional feature's orientation and clast fabric orientations taken from this unit confirm Unit D was deposited by a northwest switching to a more west-southwest polyphase ice flow.

This polyphase flow is further supported by microstructures observed in this unit, such as multi-directions lineations, grain stacks, and rotation structures. The three upper samples (PTA-040, PTA-041 and PTA-042) were highly voidal, both in the horizontal and vertical direction. These types of voidal fractures within the sediment are typical of ice lens formation and melting associated freeze thaw mechanisms (van Vliet-Lanoë et al., 1984; Sveistrup et al., 2005). There is no grain crushing observed in there upper two samples (PTA-040 and PTA-041), which could indicate the overburden stress levels did not reach the critical strength required to induce grain cracking/fracturing (Johnson, 1985; Jaroslav, 2002). Another possible explanation could be the dilatancy of the pore water pressure restricted the grains from coming into contact with one another, although there is no pore-water evidence to support this. Menzies et al., (2012) has suggested that the lack of edge-to-edge crushing could be associated with streaming ice, which, when considering the streamline landforms in the region roughly paralleling clast fabric results from this unit, could be the causative factor, although further investigation would be required to confirm this. The two lower samples from this unit however have few voids, and contain evidence of multiple domains. Microstructures within this unit (changing orientations of lineations/grain stacks) also indicate that this unit has undergone fluctuations in strain rates and possibly directions, suggesting a Type B tectomict/mélange till (Fig. 50).

An argument contesting an additional unit boundary between the lower samples (PTA-037 and PTA-038) and the upper samples (PTA-040, PTA-041, and PTA-042) could be made, considering the changes in clast fabric direction (Fig. 19), increase in voids (Table 5), and the presence of a weak boulder horizon. However, the consistency in geochemical, heavy mineral concentrations, total C contents, and pebble lithologies indicate they should be classified as a single unit.

In summary, all of the units appear to be Type B- tectomict/mélange tills, which have been emplaced as part of a deforming soft sediment subglacial bed, beneath a temperate ice sheet (Fig. 50). However, the upper three units (Unit B, Unit C, and Unit D) show no clear sedimentological differentiation within the tills down the section, although differing till "types" do occur (see differences between Fig. 29 through Fig. 35 and Fig. 36 through Fig. 38). These units have been emplaced into an immobile bed as evident through the multiple domains, and overprinting of lineation/grain stack rotations. The deposition of these units resulted from the slow immobilization of the sediment, due to stress weakening caused by dissipation by accumulation of sediment below the mobile layer of the deforming bed, or through increase in effective stress caused by the loss/drainage of pore water (van der Meer et al., 2003; Piotroswki et al., 2004; Menzies et al., 2012). Clearly, the deposition of the ~ 20 m of sediment would have been emplaced over some considerable time, with changing subglacial conditions, as is evident through the shearing contact between Unit B and Unit C, the boulder horizon between Unit C and Unit D, and the lack of edge-to-edge crushing in Unit D.

In general, the local bedrock appears to be the controlling factor for the Unit A-D's composition, with ice flow fluctuations causing slight changes in each unit's sedimentary characteristics. This is evident through the spiked levels of Pb/Zn in Unit D caused by a northeast/north-northwest flow, which directly crosses known subcropping Pb and Zn deposits (as evident through open pits in these directions; Fig. 6), as opposed to Unit C which had lower concentrations of Pb/Zn resulting from a predominantly westward flow, missing the Pb/Zn deposits (Fig. 6).

The shearing contact between Unit B and Unit C and the reworking/rip-up clasts in Unit C indicate strain rates within the basal-debris increased causing brittle failure within the sediment causing the mixing of the sediments through shearing. The overlying stress also caused rotation furthering the mixing of the units and allowing for rip up clasts to be incorporated into the overlying unit. The boulder horizon, coupled with the change in microstructures between Unit C and Unit D, could indicate an increase in ice velocity. The boulder horizon between Unit C and Unit D suggest the fine particles of the matrix were removed by the combined effects of subglacial meltwater flushing and glacial sliding, isolating larger clasts at the top of a till sheet (Boyce and Eyles, 2000), which could be disturbed and deformed by overriding till after formation (Hicock, 1991). Lian et al., (2003) have linked boulder pavements to ice streaming ice, which form as pore water pressure dropped after the removal of the fine particles, reducing the shear stress, and allowed the ice to advance with less resistance by the subglacial debris (Hicock and Dreimanis 1992; Benn and Evans 1996; Tulaczky et al. 2000). Streamlined landforms support this, however whether the landforms are related has yet to be confirmed. The lack of edge-to-edge crushing could also support this hypothesis, however the high quantity of voids within the upper samples, and limited proof of this correlation (Menzies et al., 2012) further hinders the confirmation of this hypothesis. The presence of Glacial Lake McConnell sediments above Unit D, suggests that, at least Unit D, was deposited during the Late Wisconinan (Lemmen, 1990), and due to the lack of interglacial sediments between any of the underlying units, Unit C and Unit B were deposited by the LIS.

The lowest unit (Unit A), does not appear to be related to overlying units, clast lithology, grain size analysis, heavy mineral concentrates, $CaCO_3$ concentrations, and total C percentages, indicates this unit is very different from overlying units. The pebble lithology in itself indicates a substantial transport distance (Fig. 29; Fig. 2), and confinement of this unit to karst depressions/in close proximity to (>1 m) these karst depressions suggests that this unit was emplaced at the onset of the LIS glaciation.

Chapter 5

5.0 Conclusion

There are four distinct glacial units, throughout the facies at pit-K62, all of which appear to be Type B –tectomict/mélange tills emplaced as part of a deforming soft subglacial bed. The upper three units, (Unit B, Unit C, and Unit D) were emplaced into immobile underlying units, whereas the lowest unit (Unit A) was likely deposited into the karst collapse depression at the base of the section during the onset of glaciation. The overlying units were deposited throughout the continuous glaciation of the Pine Point region throughout the Wisconsinan (Dyke et al., 2002). The relatively thick glacial drift cover resulted from a loss in pore pressure as the LIS left the Canadian Shield and entered the WCSB region. Subglacial water infiltrated the sedimentary bedrock more easily than the less porous/permeable granitic shield bedrock, resulting in deposition. There was then a rapid immobilization of the sediment due to stress weakening caused by dissipation of accumulating sediment (*cf.* King et al., 2007). This deposition occurred throughout the Wisconsinan until the region was inundated by Glacial Lake McConnell ~ 10 ka BP, which resulted in the deposition of littoral beach sediments (Unit E). The separation of the units indicates changes in interactions between the mobile bed and immobile interface driven by shear stress changes at the ice/mobile sediment interface.

The erosional history observed in the striation records and landforms at Pine Point generally correlate with the subglacial depositional sequences, indicating a complete sedimentological record of the LIS during its time covering the Pine Point Mining District. All observed exposures in the Pine Point mining district show continuous sequences of conformable, thick subglacial till deposits, with no occurrences of intertill sediments or tills with oxidized horizons of any kind. South of Pine Point, in western Alberta, there is evidence of only one glaciation, during the Late Wisconsinan (Liverman et al., 1989; Jackson et al., 2011). Southeast of Pine Point, in northeastern Alberta, older glacial sediments are preserved in buried valleys (Andriashek, 2003; Paulen, 2009; Jackson et al., 2011). There is no evidence at Pine Point to support that these multiple tills reflect separate glaciations.

Dyke et al. (2002) map the LIS margin during the Middle Wisconsinan at approximately the edge of the Canadian Shield. Therefore it is postulated, that since there is no evidence of ice-margin advance or retreat sequences in the glacial stratigraphy at Pine Point and that the general depositional and erosional ice flow indicators do not indicate proximity to ice margin position, that the Middle Wisconsinan ice margin was probably north and west of the Pine Point area, possibly occupying the Great Slave Lake basin during the Middle Wisconsinan. The relatively flat bedrock surface, at the eastern margin of the WCSB, provided an environment that was suitable for continuous glacial sedimentation.

5.1 Recommendations

The Pine Point mining district is a truly unique location, offering easy access to thick undisturbed continuous glacial deposits. This research project merely examined a single pit exposure at a site that contains ample access to glacial stratigraphy. There is abundant additional work that could be complete at this site and the larger region. Therefore it is highly recommended that future work continue within this region to increase the understanding of the ice flow history and the ice dynamics within this region.

With regard to this particular study it is recommended that when conducting clast fabric analysis as well as thin section analysis, a cross section of the thin sections (the x and y planes) be produced as well. By having a cross-sectional view of the thin section a micro-fabric could have been completed and compared to the results of the clast macro-fabric.

5.2 Future Works

During this research project, it has become evident that the glacial history of the past producing Pine Point mining district is much more complex then originally thought. A project correlating the lithofacies at Pit K-62 with other facies from other open pit mines within the region would greatly aid in developing an understanding of this complex polyphase glaciation. There are also possible correlations with regional stratigraphy, possibly in the sections exposed on the Buffalo and Hay Rivers, and rudimentary correlations possible with the seismic shothole database collected in the region (Smith and Lesk-Winfeld, 2010) By correlating lithofacies across a region, a three dimensional understanding of the changing glacier margins, changing ice direction, and changing ice dynamics can be more accurately understood. This allows for a more accurate understanding of the past glacial environments in the region to be inferred (*cf.* Boyce and Eyles, 2000).

Secondly, dating the units would allow for a better understanding of the depositional time frame, and allow for easier correlation with current ice margin and glacial lake extents hypotheses. Although finding samples that would allow for carbon dating would be difficult, especially in deforming subglacial beds as the communition of materials in the soft-sediment deforming bed rapidly fractures and destroys any specimens that would allow for this analysis to be completed. The use of Optical Luminescence, Cosmetic Nuclide or another geochronology tool may prove to be more practical in obtaining a relative time frame for the deposition of the sediments.

References

Adams, J.J., Rostron, J.B., and Mendoza, C.A. 2000. Evidence for two-fluid mixing at Pine Point, NWT. Journal of Geochemical Exploration, n. 69-70, p. 103-108.

Allmendinger, R.W., Cardozo, N.C, and Fisher, D. 2013. Structural geology algorithms. Vectors, and tensors. Cambridge, England, Cambridge University Press, p. 289.

Andrews, J.T. 1971. Techniques of till fabric analysis. British Geomorphologic Research Group, Technical Bulletin No. 6, p. 43.

Andriashek, L.D. 2003. Quaternary geological setting of the Athabasca Oil Sands (in situ) Area, Northeast Alberta. EUB/AGS Earth Sciences Report 2002–03, p. 286.

Baroni, C. and Fasano, F. 2006. Micromorphological evidence of warm-based glacier deposition from the Ricker Hills Tillite (Victoria Land, Antarctica). Quaternary Science Review, n. 25, p. 976-992.

Bednarski, J.M. 1993. Preliminary report of the Quaternary geology of the Canadian Shield of Northeastern Alberta. Geological Survey of Canada, Special Paper No. 93-1E, p. 191-196.

Bednarski, J.M. 1999. Quaternary geology of northeastern Alberta. Geological Survey of Canada, Bulletin n. 515, p. 1-29.

Beget, J. 1987. Low profile of the northwest Laurentide Ice Sheet. Arctic and Alpine Research, v. 19, n. 1, p. 81-88.

Bell, R. 1899. Summary Report of the Geological Survey department for the year 1899, by the director. Mackenzie District. Annual Report of the Geological Survey of Canada 12: 103A-110A.

Bell, J.M. 1929. The lead-zinc deposits near Pine Point, Great Slave Lake. Annual western meeting, Edmonton, Alberta. In *The transactions of the Canadian Institute of Mining and Metallurgy and of the Mining Society of Nova Scotia 1929.*

Bell, T., Rogerson, R.J., and Mengel, F. 1989. Reconstructed ice-flow patterns and ice-limits using drift pebble lithology, outer Nachvak Fiord, northern Labrador. Canadian Journal of Earth Science, v. 26, p. 577-590.

Benn, D.I. 1994. Fabric shape and the interpretation of sedimentary fabric data. Journal of Sedimentary Research, v. 64, n. 4, p. 910-915.

Benn, D.I. 1995. Fabric signature of subglacial till deformation, Breidamerkurjokull, Iceland. Sedimentology, v. 42, n. 5, p. 735-747.

Benn, D.I. and Evans, D.J.A. 1996. The interpretation and classification of subglacially-deformed materials. Quaternary Science reviews, v. 15, p. 23-52.

Boulton, G.S. 1976. The origin of glacially-fluted surfaces- observations and theory. Journal of Glaciology, v. 17, p. 287-309.

Boulton, G. 2010. Drainage pathways beneath ice sheets and their implications for ice sheet form and flow: the example of the British Ice Sheet during the Last Glacial Maximum. Journal of Quaternary Science, v. 25, p. 483–500.

Boulton, G.S. and Hindmarsh, R.C.A. 1987. Sediment deformation beneath glaciers; rheology, and geological consequences. Journal of Geophysical Research, v. 92, n. B9, p. 9059-9082.

Bostock, H.H. 1964. A provisional physiographic map of Canada. Geological Survey of Canada. Special paper No. 64-35.

Bostock, H.S. 1970. Physiographic regions of Canada. Geological Survey of Can- ada, Map 1254A, scale 1:5,000,000.

Boyce, J.I. and Eyles, N. 2000. Architectural element analysis applied to glacial deposits: internal geometry of a late Pleistocene till sheet, Ontario, Canada. Geological Society of America Bulletin, v. 112, p. 98-118.

Brabec, D. 1983. Evaluation of soil anomalies by discriminate analysis in geochemical exploration for carbonate-hosted lead-zinc deposits. Economic Geology, v. 78, p. 333-339.

Bridgland, D.R. 1986. Clast lithological analysis. Quaternary Research Association Technical Guide No. 3, p. 207.

Broster, B.E. 1986. Till variability and compositional stratification: examples from the Port Huron lobe. Canadian Journal of Earth Sciences, v. 23, p. 1823-1841.

Brown, V.H., Stokes, C.R., and Ó'Cofaigh, C. 2011. The Glacial Geomorphology of the north-west Laurentide Ice Sheet, Journal of Maps, v.7, p. 409-428.

Campbell, N. 1966. The lead-zinc deposits of Pine Point. Canadian Mining and Metallurgical Bulletin, v. 59, p. 953-960.

Cardozo, N. and Allmendinger, R.W. 2013. Spherical projections with OSXStereonet. Computers and Geoscience, v. 51. p. 193-205. Doi: 10.106/j.cageo.2012.07.21

Carr, S.J. 1999. The micromorphology of Last Glacial Maximum sediments in the Southern North Sea. Catena, v. 35, n. 2-4, p. 123-145.

Carr, S.J. 2001. Micromorphological criteria for discriminating subglacial and glaciomarine sediments: evidence from a contemporary tidewater glacier, Spitsbergen. Quaternary International, n. 86, p. 71-79.

Carr, S.J. 2004. Micro-scale features and Structures. *In:* Evans, D.J.A and Benn, D.I. [*Eds*.] A practical guide to the study of glacial sediments. Arnold, London, UK, p. 115-144.

Carr, S.J. and Lee, J.R. 1998. Thin section production of diamicts: Problems, and solutions. Journal of Sedimentary Research, v. 68, n. 1, p. 217-220.

Carr, S.J., Haflidason, H., and Sejrup, H.P. 2000. Micromorphological evidence supporting late Weichselian glaciation of the northern North Sea. Boreas, v. 29, n. 4, p. 315-328.

Carr, S.J. and Rose, J. 2003. Till fabric patterns and significance; particle response to subglacial stress. Quaternary Science Reviews, v. 22, n. 14, p. 1415-1426.

Carver, R.E. 1971. Heavy Mineral Separation. In: Carver, R.E.(*Ed.)* Procedures in Sedimentary Petrology. Chichester, Wiley. New York, p. 427-452.

Cashman, S. and Cashman, K. 2000. Cataclasis and deformation-band formation in unconsolidated marine terrace sand, Humboldt County, California. Geology, v. 28, n. 2, p. 111-114.

Craig, B. G. 1965. Glacial Lake McConnell and the surficial geology of parts of Slave River and Red- stone River map-areas, District of Mackenzie. Geological Survey of Canada, Department of Mines and Technical Surveys, Bulletin 122.

Cumming, G.L., Kyle, J.R., and Sangster, D.F. 1990. Pine Point: A case history of lead isotope Homogeneity in a Mississippi Valley-Type district. Economic Geology, v. 85, p. 133-144.

Dowdeswell, J.A. and Sharp, M. 1986, Characterization of pebble fabrics in modern terrestrial glaciagenic sediments. Sedimentology, v. 33, p. 699-710.

Dreimanis, A. 1962. Quantitative gasometric determination of calcite and dolomite by using Chittick apparatus. Journal of Sedimentary Petrology, v.32, p.520-529.

Dreimanis, A. 1982. INQUA- Commission on genesis and lithology of Quaternary deposits. Work Group (1)- genetic classification of tills and criteria for their differentiation. Progress report on activities 1977-1982, and definitions of glacigenic terms. In C. Schluchter (*Ed*.) INQUA Commission on genesis and lithology of Quaternary deposits. Report on activities 1077-1982. Zurich, p. 12-31.

Dreimanis, A., Knox, K.S., Moretti, F.J., and Reavely, G.H. 1957. Heavy mineral studies in tills of Ontario and adjacent areas. Journal of Sedimentary Research, v.27, p. 148-161.

Dyke, A. S. 2004. An outline of North American deglaciation with emphasis on central and northern Canada. *In:* J. Ehlers and P.L. Gibbard (*Eds.*), *Quaternary Glaciations - Extent and Chronology, Part II. North America*. Elsevier B.V., Amsterdam, Development in Quaternary Science Series, v. 2, p. 373-424.

Dyke, A.S. and Prest, V.K. 1987. Late Wisconsinan and Holocene history of the Laurentide Ice Sheet. Geographie physique et Quaternaire, v. 41, n. 2, p. 237-263.

Dyke, A.S., Andrews, J.T., Clark, P.U., England, J.H., Miller, G.H., Shaw, J., and Veillette, J.J. 2002. The Laurentide and Innuitian Ice Sheets during the Last Glacial Maximum. Quaternary Science Reviews, v. 21, p. 9-31.

Eaton, D.W. and Hope, J. 2003. Structure of the crust and upper mantle of the Great Slave Lake shear zone, northwestern Canada, from teleseismic analysis and gravity modeling. Canadian Journal of Earth Sciences, v. 40, p. 1203-1218.

Evans, D.J.A. and Benn, D.I. (*Eds.)* 2004. A practical guide to the study of Glacial Sediments. Arnold, London.

Evans, D.J.A, Phillips, E.R., Hiemstra, J.F., and, Auton, C.A. 2006. Subglacial till: Formation, sedimentary characteristics and classification. Earth-Science Reviews, v. 78, p. 115-176.

Fitzpatrick, E.A. 1969. Some aspects of soil evolution in north-eastern Scotland. Soil Sciences, v.109, p. 403-408.

Fitzpatrick, E.A. 1984. Micromorphology of Soils. London, Chapman and Hall, p. 433.

Gleeson, S.A. and Turner, W.A. 2007. Fluid inclusion constraints on the origin of the brines responsible for Pb-Zn mineralization at Pine Point and coarsenon-saddle and saddle dolomite formation in southern Northwest Territories. Geolfuids, v. 7, p. 51-68.

Girard, I., Klassen, R.A., and Laframboise, R. 2004. Sedimentology laboratory manual, Terrain Sciences Division. Open File 4823, Geological Survey of Canada.

Gwyn, Q.H.L. and Dreimanis, A. 1979. Heavy mineral assemblages in tills and their use in distinguishing glacial lobes in the Great Lakes region. Canadian Journal of Earth Science, v. 16, p. 2219-2235.

Hannigan, P. 2007. Metallogeny of the Pine Point Mississippi Valley-Type Lead-Zinc District, Southern North West Territories. *In:* W.D. Goodfellow (*Ed.*), *Mineral Deposits of Canada: A Synthesis of Major Deposit-Types, District Metallogeny, the*

Evolution of Geological Provinces, and Exploration Methods. Geological Association of Canada, Mineral Deposits Division, Special Publication No. 5, p. 609-632.

Hart, J.K. 1994. Till fabric associated with deformable beds. Earth Science Processes and Landforms, v. 19, n. 1, p. 15-32.

Hart, J.L. 2007. An investigation of subglacial shear zone processes from Weybourne, Norfolk, UK. Quaternary Science Reviews, v. 26, p. 2354-2374.

Hart, J.K, Khatwa, A., and Sammonds, P. 2004. The effect of grain texture on the occurrence of microstructural properties in subglacial till. Quaternary Science Review, v.23, p. 2501- 2512.

Heginbottom, J.A. and Dubreuil, M-A. 1993. A new permafrost and ground ice map for the National Atlas of Canada. Permafrost, Sixth International Conference, Proceedings, p. 255–60.

Hicock, S.R. 1991. On subglacial stone pavements in till. Journal of Geology, v. 99, p. 607-619.

Hicock, S.R. and Dreimanis, A. 1992. Deformation till in the Great Lake Region; implications for rapid flow along the south-central margin of the Laurentide Ice Sheet. Canadian Journal of Earth Science, v. 27, n. 7, p. 1565-1579.

Hiemstra, J.F. and van der Meer, J.J.M. 1997. Pore-water controlled grain fracturing as an indicator for subglacial shearing in tills. Journal of Glaciology, v. 43, n. 145, p. 446-454.

Hiemstra, J.F. and Rijsdijk, K.F. 2003. Observing artificially induced strain: implications for subglacial deformation. Journal of Quaternary Science, v. 18, n. 5, p. 373-383.

Hirvas, H. and Nenonen, K. 1990. Field methods for glacial indicator tracing. *In:* R. Kujansuu and M. Saarnisto (*Eds.*), *Glacial Indicator Tracing*. Rotterdam, p. 217-248.

Holmes, C.D. 1941. Till Fabric. Bulletin of the Geological Society of America, v. 52, p. 1299-1354

Hooyer, T.S. and Iverson, N.R. 2000. Clast-fabric development in a shearing granular material: implications for subglacial till and fault gouge. Geological Society of America Bulletin, v. 112, p. 638-692.

Iverson, N.R, and Iverson, R.M. 2001. Distributed shear of subglacial till due to Coulomb slip. Journal of Glaciology, v. 47, n. 158, p. 481-488.

Iverson, N.R., Moore, P.L., Hooyer, T.S., Thomason, J.F., and McLoughlin, M.P. 2003. Laboratory studies of till mechanical behavior and fabric evolution during shear. XVI

INQUA congress: shaping the Earth; A Quaternary perspective. Reno, NV, USA. July 23-30, 2003, Congress of International Union for Quaternary Research, v. 16, p. 124.

Jackson, L.E., Andriashek, L.D., and Phillips, F.M. 2011. Limits of successive Middle and Late Pleistocene continental ice sheets, Interior Plains of southern and central Alberta and adjacent areas. *In:* J. Ehlers, P.L. Gibbard and P.D. Hughes (*Eds.*), *Quaternary Glaciations – Extent and Chronology: A Closer Look.* Elsevier B.V., Amsterdam, Development in Quaternary Science Series, v. 15, p. 575-589.

Jaroslave, K.L. 2002. Notes on the effect of grain crushing on the granular soil behaviour. Engineering Geology, v. 63, p. 93-98.

Jeffery, G.B. 1922. The motion of ellipsoidal particles immersed in a viscous fluid. Proceedings of the Royal Society: Mathematical, physical, and engineering sciences. v. 102, n. 715, p. 161-179.

Johnson, K.L. 1985. Contact Mechanics. Cambridge University Press, Cambridge, p. 452.

Kemp, R.A. 1985. Soil micromorphology and the Quaternary. Quaternary Research Association, Technical Guide No. 2, p. 80.

Kent, D. M. 1994. Paleogeographic evolution of the cratonic platform- Cambrian to Triassic. Geological Atlas of the Western Canadian Sedimentary Basin. Mossop, G.D., and Shetsen, I. [*Comp.*], p. 69-86. Calgary: Canadian Society of Petroleum Geologists and the Alberta Research Council.

Kilfeather, A.A. and van der Meer, J.J.M. 2008. Pore size, shape and connectivity in tills and their relationship to deformation processes. Quaternary Science Review, v.27, p.250-266.

King, E.C., Woodward, J., and Smith, A.M. 2007. Seismic and radar observations of subglacial bed forms beneath the onset zones of Rutford Ice Stream, Antarctica. Journal of Glaciology, v.53, n. 183, p. 665-672.

Kleman, J. and Glasser, N.F. 2007. The Subglacial thermal organization (STO) of ice sheets. Quaternary Science Reviews, v.26, p.285-597.

Krebs, W. and Macqueen, R. 1984. Sequence of digenetic and mineralization events, Pine Point lead-zinc property, Northwest Territories, Canada. Bulletin of Canadian Petroleum Geology, v. 32, p. 434-464.

Krumbein, W.C. 1938. Size frequency distributions of sediment and the normal phi curve. Journal of Sedimentary Petrology, v. 8, p. 84-90.

Krumbein, W.C. and Pettijohn, F.J. 1938. Manual of Sedimentary Petrography. Appleton-Centuary Company, p. 549.

Kubiëna, W.L. 1938. Micropedology. Collegiate Press, Ames, Iowa, pp. 1-243

Lachniet, M.S., Larson, G.J., Lawson, D.E., Evenson, E.B., and Alley, R.B. 2001. Microstructures of sediment flow deposits and subglacial sediments: a comparison. Boreas, v.30, n. 3, p. 254-262.

Larsen, N.K., Piotrowski, J.A., and Christiansen, F. 2006. Microstructures and microshears as proxy for strain in subglacial diamicts: implications for basal till formation. Geology, v. 34, p. 889-892.

Larsen, N.K., Piotrowski, J.A., and Menzies, J. 2007. Microstructural evidence of low-strain, time transgressive subglacial deformation. Journal of Quaternary Science. v. 22, n. 6, p. 593-608.

Lee, J. and Kemp, R. 1993. Thin sections of unconsolidated sediments and soils: a recipe. Center for environmental Analysis and management (CEAM). Royal Holloway, University of London. CEAM Technical Report, v. 2, p 1-32.

Leighton, I.D., Hiemstra, J.F., and Weidemann, C.T. 2012. Recognition of micro-scale deformation structures in glacial sediments- pattern perception, observer bias and the influence of experience. Boreas, v. 42, p. 463-469.

Lemmen, D.S. 1990. Surficial materials associated with glacial Lake McConnell, southern District of Mackenzie. *In:* Current Research, Part D, Geological Survey of Canada, Paper 90-1D, p. 79-83.

Lemmen, D.S. 1998a. Surficial geology, Klewi River, District of Mackenzie; Northwest Territories. Geological Survey of Canada, “A” Series Map 1905, scale 1:250 000.

Lemmen, D.S. 1998b. Surficial geology, Buffalo Lake, District of Mackenzie; Northwest Territories. Geological Survey of Canada, “A” Series Map 1906, scale 1:250 000.

Lemmen, D.S., Duk-Rodkin, A., and Bednarski, J.M., 1994. Late glacial drainage systems along the northwestern margin of the Laurentide Ice Sheet. Quaternary Science Reviews, v. 13, p. 805-828.

Lian, O.B. and Hicock, S.R. 2000. Thermal conditions beneath parts of the last Cordilleran Ice Sheet near its center as inferred form subglacial till, associated sediments, and bedrock. Quaternary International, v. 68-70, p. 147-162.

Lindholm, R.C. 1987. A practical approach to sedimentology. London, Allen and Unwin, p. 269.

Liverman, D.G.E., Catto, N.R. and Rutter, N.W. 1989. Laurentide glaciation in west-central Alberta: a single (Late Wisconsin) event, Canadian Journal of Earth Sciences, vol. 26, p. 266-274.

March, A. 1932. Mathematische theorie der regelung nach der korngestalt bei affiner deformation. Zeitsschrift für Kristallographie, v. 81, p. 285-297.

Mathews, W.H. 1974. Surface profiles of the Laurentide Ice Sheet in its marginal areas. Journal of Glaciology, 13: 37-43.

McClenaghan, M.B. and DiLabio, R.N.W. 1996. Ice-flow history and glacial dispersal patterns, southeastern Cape Breton Island, Nova Scotia: implications for mineral exploration. Canadian Journal of Earth Science, v. 33, p. 351-362.

McClenaghan, M.B., Thorleifson, L.H., and DiLabio, R. N. W. 2000. Till geochemical and indicator mineral methods in mineral exploration. Ore Geology Reviews, v. 16, p. 145-166.

McClenaghan, M.B., Lavin, O.P., Nichol, I., and Shaw, J. 1992. Geochemistry and clast lithology as an aid to till classification, Matheson, Ontario, Canada. Journal of Geochemical Exploration. v. 42, p. 237- 260.

McClenaghan, M.B., Parkhill, M.A., Averill, S.A., Pronk, A.G., Seaman, A.A., Boldon, R., McCurdy, M.W., Rice, J.M. 2013. Indicator mineral abundance data for till, and stream sediment samples from the Sisson W-Mo deposit, New Brunswick. Geological Survey of Canada. Open File 7387, p. 18. Doi:10.4095/292670.

McClenaghan, M.B., Oviatt, N.M., Averill, S.A., Paulen, R.C., Gleeson, S.A., McNeil, R.J., McCurdy, M.W., Paradis, S. and Rice, J.M. 2012. Indicator mineral abundance data for bedrock, till and stream sediment samples from the Pine Point Mississippi Valley-Type Zn-Pb deposits, Northwest Territories; Geological Survey of Canada, Open File 7267, 1 CD-ROM. doi:10. 4095/292121

McMartin, I. and Paulen, R.C. 2009. Ice-flow indicators and the importance of ice-flow mapping for drift prospecting. *In:* R.C. Paulen and I. McMartin (*Eds.*), *Application of Till and Stream Sediment Heavy Mineral and Geochemical Methods to Mineral Exploration in Western and Northern Canada*. Geological Association of Canada, Short Course Notes 18, p. 15-34.

Menzies, J. 1998: Microstructure s within subglacial diamictons. *In:* Kostrzewski, A. (*Ed.*): Relief and Deposits of Present-day and Pleistocene Glaciation of the Northern Hemisphere – Selected Problems, 153–166. Adam Mickiewicz University Press, Geography Series no. 58. Poznan, Poland.

Menzies, J. 2000. Micromorphological analysis of microfabrics and microstructures indicative of deformational processes in glacial sediments. *In*: Maltman, A.J., Hubbard, B., and Hambrey, M.J., (*Eds*.) Deformation of Glacial Materials. Geological Society special Publication No. 176. London, p. 224-257.

Menzies, J. 2012. Strain pathways, till internal architecture and microstructures-perspectives on a general kinematic model- a 'blueprint' for till development. Quaternary Science Reviews, v.50, p. 10-12.

Menzies, J. and Maltman, A.J. 1992. Microstructures in diamictons – evidence of subglacial bed conditions. Geomorphology*,* v. 6, p. 27-40.

Menzies, J., Zaniewski, K., and Dreger, D. 1997. Evidence from microstructures of deformable bed conditions within drumlins, Chimney Bluffs, New York State. Desimentary Geology, v. 111, n. 1-4, p. 161-175.

Menzies, J. and Zaniewski, K. 2003. Microstructures within a modern debris flow deposit derived from Quaternary glacial diamicton- a comparative micromorphological study. Sedimentary Geology, v. 157, p. 31- 48.

Menzies, J. and Ellwager, D. 2011. Insights into subglacial processes inferred from the micromorphological analyses of complex diamicton stratigraphy near Illmensee-Lichtenegg, Hochsten, Germany. Boreas, v. 40, n. 2, p. 271-288.

Menzies, J., van der Meer, J.J.M., and Rose, J. 2006. Till- as a glacial "tectomict", its internal architecture, and the development of a "typing" method for till differentiation. Geomorphology, v. 75, p. 172-200.

Menzies, J., van der Meer, J.J.M., Domack, E., and Wellner, J.S. 2010. Micromorphology: As a tool in the detection analyses and interpretation of glacial sediments and man-made materials. Proceedings of the Geologist; Association, v. 121, p. 281-292.

Menzies, J., Gao, C., and Kodors, C. 2012. Micromorphology of a Middle Pliocene till from the James Bay Lowlands, Canada, evidence of fast ice stream or surge behaviour. Proceedings of the Geologists' Association, v.124, p. 790- 801.

Miller, H. 1884. On boulder glaciation. Royal Physical Society, Edinburgh Proceedings, v. 8, p. 156-189.

Milner, H.B. 1962. (*Ed.*) Sedimentary Petrography. London, Allen and Unwin, p. 129.

Murphy, C.P. 1986. Thin section preparation of soils and sediments. AB Academic. University of Michigan, p 149.

Nelson, J., Paradis, S., Chirstensen, J., and Gabites, J. 2002. Canadian Cordilleran Mississippi Valley-type deposits: A case for Devonian-Mississippian back-arc hydrothermal origin. Economic Geology, v. 97, p. 1013-1036.

Neudorf, C.M., Brennand, T.A., and Olav, B.L. 2013. Till-forming processes beneath ports of the Cordilleran Ice Sheet, British Columbia, Canada: macroscale and microscale evidence and a new statistical technique for analyzing microstructure data. Boreas, v.24, p. 848-875.

Ó'Cofaigh, C., Dowdeswell, J.A., Allen, C.S., Hiemstra, J.F., Pudsey, C.J., Evens, J., and J.A. Evans, D. 2005. Flow dynamics and till genesis associated with a marine-based Antarctic paleo-ice stream. Quaternary Science Reviews. v. 24, n. 5-6, p. 547-561.

Okulitch, A.V. (compiler) 2006. Phanerozoic bedrock geology, Slave River, District of Mackenzie, Northwest Territories. Geological Survey of Canada, Open File 5281, scale 1:1,000,000.

Oviatt, N.M. 2013. Characterization of Indicator Minerals and Till Geochemical Dispersal Patterns Associated with the Pine Point Pb-Zn Mississippi Valley-type Deposits, Northwest Territories, Canada. Masters thesis, University of Alberta, p. 212.

Oviatt, N.M., and Paulen, R.C. 2013. Surficial Geology, Brenynat Point, NTS 85-B/15, Northwest Territories. Geological Survey of Canada Canadian Geoscience Map 114, 2013. Scale 1:50 000. Doi 10.4095/000000.

Oviatt, N. M., Paulen, R.C., McClenaghan, M.B., Gleeson, S.A., and Paradis, S. 2011. Drift Prospecting Research at the Pine Point Pb-Zn Mississippi Valley Type (MVT) Deposit, Northwest Territories. Conference paper, Geohydro 2011, Quebec City.

Oviatt, N.M., McClenaghan, M.B., Paulen, R.C., and Gleeson, S.A. 2013a. Till geochemical signatures of the Pine Point Pb-Zn Mississippi Valley-type district, Northwest Territories. Geological Survey of Canada, Open File 7320, p. 59.

Oviatt, N.M, McClenaghan, M.B., Paulen, R.C., Gleeson, S.A., and Averill, S.A. 2013b. Indicator minerals in till and bedrock samples from the Pine Point Mississippi Valley Type district, NWT. Geological Survey of Canada, Open File 7423, p. 87.

Paradis, S., Turner, W.A., Coniglio, M., Wilson, N., and Nelson, J.L, 2006. Stable and radiogenic isotopic signatures of mineralized Devonian carbonate rocks of the northern Rocky Mountain and Western Canadian Sedimentary Basin. In: Hanngian, P.K. [*Ed.*] Potential for carbonate-hosted lead-zinc Mississippi Valley-type if you read this I will buy you a beer mineralization in northern Alberta and southern Northwest Territories. Geoscience Contributions, Targeted Geoscience Initiative, Geological Survey of Canada, Bulletin no. 591, p. 75-103.

Parent, M., Paradis, S.J., and Doiron, A. 1996. Pamplisest glacial dispersal trains and their significance for drift prospecting. Journal of Geochemical Exploration, v. 56, i. 3, p. 123-140.

Passchier, S. 2000. Soft-sediment deformation features in core from CRP-2/2A, Victoria Land Basin, Antarctica. Terra Antarctica, v.7, n.3, p. 401-412.

Paulen, R.C. 2009. Drift prospecting in northern Alberta - A unique glacial terrain for exploration. In: Paulen, R.C. and McMartin, I. (*Eds*.), Application of Till and Stream Sediment Heavy Mineral and Geochemical Methods to Mineral Exploration in Western and Northern Canada. Geological Association of Canada, GAC Short Course Notes 18, p. 185-205.

Paulen, R.C., Plouffe, A., and Smith, I.R. 2008. Diamond and base metal indicator minerals in glacial sediments of northern Alberta, Canada. EXPLORE, v. 138, p. 1-7.

Phillips, E. and Auton, C.A. 2000. Micromorphological evidence for polyphase deformation of glaciolacustrine sediments from Strathspey, Scotland. In: Maltman, A.E., Hubbard, B., and Hambrey, M.J. (*Eds*.) Deformation of glacial materials. Geological Society of London, London, UK, p. 279-292.

Phillips, E., Lee, J.R., and Burke, H., 2008. Progressive proglacial to subglacial deformation and syntectonic sedimentation at the margins of the Mid-Pleistocene British Ice Sheet: evidence from north Norfolk UK. Quaternary Science Reviews, v. 27, p. 1848–1871.

Piotrowski, J.A. and Tulaczyk. 1999. Subglacial conditions under the last ice sheet in northwest Germany: ice-bed separation enhanced basal sliding? Quaternary Science Reviews v. 18, p. 737-751.

Piotrowski, J.A., Larsen, N.K., and Junge, F.W. 2004. Reflections on soft subglacial beds as a mosaic of deforming and stable spots. Quaternary Science Review, v. 23, n. 9, p. 993-1000.

Prest, V.K., Grant, D.R., and Rampton, V.N. 1968. Glacial map of Canada. Geological Survey of Canada, “A” Series Map 1253, scale 1: 5 000 000.

Reinardy, B.T.I., Hiemstra, J.F., Murray, T., Hillenbrand, C., and Larter, R.D. 2011. Till genesis at the bed of an Antarctic Peninsula palaeo- ice stream as indicated by micromorphological analysis. Boreas, v. 40, p. 498-517.

Rice, J.M., Paulen, R.C., Menzies, J.M., McClenaghan, M.B., and Oviatt, N.M., 2013. Glacial stra- tigraphy of the Pine Point Pb-Zn mine site, Northwest Territories; Geological Survey of Canada, Current Research 2013-5, 14 p. doi: 10.4095/292184

Ringrose, T. and Benn, D.I. 1997. Confidence regions for fabric shape diagrams. Journal of Structural Geology, v. 19, p. 1527-1536.

Rhodes, D., Lantos, E.A., Lantos J.A., Webb, R.J., and Owens, D.C. 1984. Pine Point ore bodies and their relationship to the stratigraphy, structure, dolomitization and karstification of the Middle Devonian Barrier Complex. Economic Geology, v. 79, p. 991-1055.

Roberts, D.H. and Hart, J.K. 2005. The deforming bed characteristics of a stratified till assemblage in northeast Angila, UK: Investigating controls on sediment rheology and strain signatures. Quaternary Science Reviews, v. 24, n. 1-2, p. 123-140.

Roedder, E. 1968. Temperature, salinity, and origin of the ore-forming fluids at Pine Point, Northwest Territories, Canada, from fluid inclusion studies. Economic Geology, v. 63, n. 5, p. 439-450.

Roscoe, S.M., Ganhi, S.S., Charbonneau, B.W., Maurice, Y.T., and Gibb, R.A. 1987. Mineral resource assessment of the area in the East Arm (Great Slave Lake) and Artillery Region, N.W.T., Proposed as a National Park (NTS 75 J,K,L,M,N,O). Geological Survey of Canada, Open File 1434, p. 99.

Ruszczynska-Szenajch, H., Trzcinski, J., and Jarosinka, U. 2003. Lodgement till deposisiton and deformation investigation by macroscopic observation, thin-section analysis and electron microscope study at site Debe, central Poland. Boreas, v. 32, p. 339-415.

Shepard, F.P. 1954. Nomenclature based on sand-silt-clay ratios. Journal of Sedimentary Petrology, v. 24. N. 3, p.151-158.

Skall, H. 1975. The paleoenvironment of the Pine Point lead-zinc district. Economic Geology, v. 70, p. 22-47.

Shetsen, I. 1984. Application of till pebble lithology to the differentiation of glacial lobes in southern Alberta. Canadian Journal of earth Science, v. 21, p.920-933.

Shilts, W.W. and Kettles, I.M. 1990. Geochemical-mineralogical profiles through fresh and weathered till. *In*: Kujansuu, R. and Sarnisto, M. (*Eds.*) Glacier indicator tracing. Balkema, Rotterdam, p. 187-216.

Smith, D.G. 1994. Glacial Lake McConnell: paleogeography, age, duration and associated river deltas, Mackenzie River Basin, western Canada. Quaternary Science Reviews, v.13, p.829-843.

Smith, I.R. and Lesk-Winfield, K. 2010: Drift isopach, till isopach, and till facies reconstructions for Northwest Territories and northern Yukon. Geological Survey of Canada, Open File 6324.

Spirito, W.A., McClenaghan, M.B., Plouffe, A., McMartin, I., Campbell, J.E., Paulen, R.C., Garrett, R.G. and Hall, G.E.M. 2011. Till sampling and analytical protocols for GEM projects: from field to archive. Geological Survey of Canada, Open File 6850.

Stanley, C.R. 2009. Geochemical, Mineralogical, and Lithological Dispersal Models in Glacial Till: Physical Process Constraints and Application in Mineral Exploration. *In:* R.C. Paulen and I. McMartin (*Eds.*), Application of Till and Stream Sediment Heavy Mineral and Geochemical Methods to Mineral Exploration in Western and Northern Canada. Geological Association of Canada, GAC Short Course Notes 18, p. 185-205.
Sveistrup, T.E., Haraldsen, T.K., Langohr, R., Marcelino, V., and Kværner, J. 2005. Impact of land use and seasonal freezing on morphological and physical properties of silty Norwegian soils. Soil and Tillage Research, v. 81. n. p. 39-56.

Tamerlane Ventures, Incorporated. 2013. Pine Point Project- Mine site History. Accessed December 4, 2013 from: http://www.tamerlaneventures.com/index.php/pine-point-properties-66/property-history-properties-65

Thomason, J.F. and Iverson, N.R. 2006. Microfabric and microshear evolution in deformed till. Quaternary Science Reviews, v. 25, p. 1027-1038.

Truffer, M., Harrison, W.D., and Echelmeyer, K.A., 2000. Glacier motion dominated by processes deep in underlying till. Journal of Glaciology, v. 46, p. 213–221.

Tulaczyk, S., Kamb, B., and Engelhardt, H. F. 2000: Basal mechanics of Ice Stream B, Antarctica. Journal of Geophysical Research B105, 463–481.

van der Meer, J.J.M. 1987. Micromorphology of glacial sediments as a tool in distinguishing genetic varieties of till. Geological Survey Finland Special Paper 3, p. 77-89.

van der Meer, J.J.M. 1993. Microscopic evidence of subglacial deformation. Quaternary Science Reviews, v. 12, i. 13, p. 553-587.

van der Meer, J.J.M. 1996. Micromorphology. *In*: Menzies, J. (*Ed*.) Past Glacial Environments, sediments forms, and techniques. Vol.2. Butterworth-Heinemann, Ltd. Jordan Hill, Oxford.

van der Meer, J.J.M. 1997. Particle and aggregate mobility in till: Microscopic evidence of subglacial processes. Quaternary Science Review, v. 16, n. 8, p. 827-831.

van der Meer, J.J.M. and Menzies, J. 2006. Sixth International workshop on the micromorphology of glacial sediments. Department of Geosciences, Hamilton College, Clinton, New York, p. 1-83.

van der Meer, J.J.M. and Menzies, J. 2011. The micromorphology of unconsolidated sediments. Sedimentary Geology, v. 238, n. 3-4, p. 213-232.

van der Meer, J.J.M., Menzies, J., and Rose, J. 2003. Subglacial till: the deforming glacier bed. Quaternary Science Reviews, v.22, p. 1659–1685.

van Vilet-Lanoe , B., Coutard, J.P., and Pissart, A. 1984. Structures caused by repeated freezing and thawing in various loamy sediments: a comparison of active, fossil and experimental data. Earth Surface Processes and Landforms, v. 9, p. 553–565.

Vincent, J-S. and Klassen, R.W. 1989. Introduction, *In:* Chapter 2 Quaternary Geology of the Canadian Interior Plains (Fulton, R.J. Comp.)*. In:* Quaternary Geology of Canada and Greenland. 1989. *In*: Wheeler. J.O. (*Ed*.). Canadian Government Publishing Center Supply and Services Canada. Ottawa, ON.

Walden, J. 2004. Particle lithology (or mineral and geochemical analysis). *In:* Evans, D.J.A., and Benn, D.I. (*Eds.)* A Practical guide to the study of glacial sediments. Hodder Education, London, UK, p. 145-181.

Winsborrow, M.C.M., Clark, C.D., and Stokes, C.R. 2004. Ice Streams of the Laurentide Ice Sheet. Géographie physique et Quaternaire, v. 58, p. 269-280.

Wolfe, S.A., Huntley, D.J., and Ollerhead, J. 2004. Relict Late Wisconsinan dune fields of the northern Great Plains, Canada. Geographie Physique et Quaternaire, v. 58, p. 323-336.

Woodcock, N.H. 1977. Specifications of fabric shapes using an eigenvalue method. Geological Society of America Bulletin, v. 88, n.9, p. 1231-1236.

Appendix A

Grain size distribution

Method: Camsizer & Lecotrac LT100

	Weight (g)	Size Fraction (mm) (Reported as % weignt of <2mm)							
Sample No.	Dry split	> 2mm	2-0.063mm	< 0.063mm	2-1.4	1.4-1	1-.71	.71-.50	.50-.35
11-PTA-042	464.945	83.420	131.785	249.740	1.550	1.666	1.643	2.081	2.320
11-PTA-037	435.606	52.441	118.095	265.070	1.422	1.473	1.583	1.936	2.025
11-PTA-035	363.429	62.059	100.585	200.785	1.861	1.721	1.821	1.761	1.981
11-PTA-030	367.688	58.383	107.851	201.454	1.454	1.510	1.626	2.091	2.247
11-PTA-025	368.617	40.229	110.766	217.623	1.739	1.651	1.884	1.995	2.198
11-PTA-023B	402.176	32.670	144.957	224.549	1.391	1.682	1.904	2.304	3.081
11-PTA-023A	412.502	52.456	115.184	244.862	1.532	1.710	1.710	1.957	2.285
11-PTA-022	373.510	48.473	189.068	135.969	1.816	1.754	2.205	4.094	6.861

	Size Fraction (mm) (Reported as % volume of <2mm)								
Sample No.	.35-.25	.25-.18	.18-.12	.12-.088	.088-.063	.063-.044	.044-.031	.031-.016	.016-.008
11-PTA-042	2.904	3.462	5.174	6.909	6.832	7.690	6.618	10.852	8.154
11-PTA-037	2.473	3.056	4.443	6.248	6.163	6.846	6.232	10.552	8.446
11-PTA-035	2.594	3.178	4.311	6.352	7.797	4.423	5.008	9.901	8.817
11-PTA-030	2.792	3.105	4.459	7.379	8.204	7.015	6.066	9.774	7.712
11-PTA-025	2.723	3.409	4.994	6.695	6.442	7.101	6.029	9.938	7.916
11-PTA-023B	4.458	4.458	4.904	6.667	8.380	6.304	5.704	10.208	8.497
11-PTA-023A	2.685	3.012	4.100	6.123	6.879	7.228	6.294	10.193	8.077
11-PTA-022	10.554	9.739	7.862	6.960	6.324	5.270	4.354	7.759	6.166

Appendix A

Grain size distribution

Method: Camsizer & Lecotrac LT100

	Weight (g)	) (Reported as % weignt of <2mm)			% of Bulk Sample	wt. % Sand-Silt-Clay of <2mm		
Sample No.	.008-.004	.004-.002	.002-.001	< .001	% Pebbles	% Sand	% Silt (63-2um)	% Clay (<2um)
11-PTA-042	8.049	8.476	9.196	6.423	17.942	34.542	49.840	15.619
11-PTA-037	8.757	9.247	10.436	8.664	12.039	30.821	50.080	19.099
11-PTA-035	9.708	10.122	10.714	7.932	17.076	33.376	47.978	18.646
11-PTA-030	8.194	8.795	9.707	7.868	15.878	34.869	47.556	17.575
11-PTA-025	8.354	8.784	9.689	8.459	10.913	33.730	48.122	18.148
11-PTA-023B	9.173	9.297	7.828	3.759	8.123	39.230	49.183	11.587
11-PTA-023A	8.633	9.151	10.023	8.409	12.717	31.991	49.576	18.433
11-PTA-022	6.312	6.049	4.491	1.432	12.978	58.168	35.910	5.922

wt. % Sand-Silt-Clay of <2mm

Sample No.	% Sand	% Silt (63-4um)	% Clay (<4um)
11-PTA-042	34.542	41.363	24.095
11-PTA-037	30.821	40.833	28.346
11-PTA-035	33.376	37.856	28.768
11-PTA-030	34.869	38.761	26.370
11-PTA-025	33.730	39.338	26.932
11-PTA-023B	39.230	39.886	20.884
11-PTA-023A	31.991	40.425	27.583
11-PTA-022	58.168	29.860	11.971

APPENDIX B

Munsell Coulour

		Wet		Dry	
Sample No.	Unit	Color	Description	Color	Description
11-PTA-042	D	10YR 5/3	brown	2.5Y 7/2	light grey
11-PTA-037	D	10YR 5/3	brown	2.5Y 7/2	light grey
11-PTA-035	C	2.5Y 5/3	light olive brown	10YR 6/2	light brownish grey
11-PTA-030	C	2.5Y 5/3	light olive brown	10YR 7/2	light gray
11-PTA-025	C	2.5Y 5/3	light olive brown	10YR 6/2	light brownish grey
11-PTA-023A	B	2.5Y 5/3	light olive brown	10YR 7/2	light gray
11-PTA-023B	A	10YR 6/3	pale brown	5Y 5/2	olive gray
11-PTA-022	A	2.5Y 3/2	brown	10YR 6/2	light brownish grey

APPENDIX C

Carbon and Loss on ignition data

Validity of results: ± (0.1 %C + 5% of concentration)

Loss on ignition: 500°C for 1 hour

Total %C & Inorganic %C: 1350‘ Method: CR-412

Sample No.	Unit	Total C	Inorganic C	Organic C	Loss on	Pb	Zn	Cr	Ti	Mg	Ca
		(+- 0.1%)	(+- 0.1%)	(+- 0.2%)	Ignition %	ppm	ppm	ppm	%	%	%
11-PTA-042	D	9.03	8.91	0.12	1.30	66.82	173.5	12.6	0.028	6.63	18.46
11-PTA-037	D	8.91	8.74	0.17	1.30	64.54	169.8	12.7	0.028	6.42	18.03
11-PTA-035	C	8.55	8.13	0.42	1.15	20.08	67.3	14.6	0.025	5.57	18.02
11-PTA-030	C	8.62	8.29	0.33	1.16	41.29	108.8	14.4	0.029	6.46	18.26
11-PTA-025	C	9.14	8.83	0.31	1.15	39.34	84.1	12.5	0.021	6.59	19.66
11-PTA-023A	B	8.80	8.40	0.40	1.30	26.75	77.6	13.3	0.023	6.14	18.27
11-PTA-23B	A	1.82	1.39	0.43	2.09	12.27	64.2	24.5	0.034	1.49	3.15
11-PTA-22	A	2.60	2.10	0.40	2.10	37.3	149.4	17.6	0.021	1.92	4.88

APPENDIX D

$CaC0_3$ Concentrates by CM 5015 Coulometer/Acid evolution.

Validity of results:

Total CO_2%	± (0.05 %CO_2 + 5% of concentration)
Calcite CO_2%	± (0.05 %CO_2 + 5% of concentration)
Dolomite CO_2%	± (0.1 %CO_2 + 5% of concentration)
$CaCO_3$ equ. %	± (0.05 % + 5% of concentration)
$CaMg(CO_3)_2$ equ.	± (0.1 % + 5% of concentration)

Sample No.	Unit	Total CO_2%	Calcite CO_2%	Dolomite CO_2%	$CaCO_3$ equ	$CaMg(CO_3)_2$ equ.	Ratio Calcite/Dolomite
11-PTA-042	D	31.80	7.24	24.56	16.46	51.46	0.32
11-PTA-037	D	30.83	7.83	23.00	17.80	48.18	0.37
11-PTA-035	C	29.21	8.98	20.23	20.42	42.38	0.48
11-PTA-030	C	29.59	7.74	21.84	17.61	45.76	0.38
11-PTA-025	C	31.59	7.65	23.94	17.39	50.16	0.35
11-PTA-023A	B	30.57	7.94	22.63	18.06	47.40	0.38
11-PTA-023B	A	4.83	1.19	3.64	2.71	7.62	0.36

APPENDIX E

Summary of base metal indicator mineral grain counts

Sample Number	Unit	Pyrite/ Marcasite	Cpy	Sphal- erite	Galena	Hercynite	Arsenopyrite/ Loellingite	Barite	Kyanite	Silli- manite	Staur- olite
11-PTA-042	D	20	0	0	0	4	1	0	80	0	0
11-PTA-037	D	10	0	5	7	22	0	0	60	10	1
11-PTA-035	C	3000	1	100	10	3	0	3	3	150	1
11-PTA-030	C	3000	0	400	30	0	0	0	5	10	0
11-PTA-023A	B	3000	2	400	14	20	0	0	20	40	2
11-PTA-023B	A	5000	0	120	0	6	0	0	250	250	10

Normalized table of base metal indicator mineral grain counts to 10 kg

Sample Number	Unit	Pyrite/ Marcasite	Cpy	Sphal- erite	Galena	Hercynite	Arsenopyrite/ Loellingite	Barite	Kyanite	Silli- manite	Staur- olite
11-PTA-042	D	16	0	0	0	3	1	0	62	0	0
11-PTA-037	D	7	0	3	5	15	0	0	41	7	1
11-PTA-035	C	2256	1	75	8	2	0	3	2	113	1
11-PTA-030	C	2128	0	284	21	0	0	0	4	7	0
11-PTA-023A	B	2041	1	272	10	14	0	0	14	27	1
11-PTA-023B	A	3333	0	80	0	4	0	0	167	167	7

APPENDIX E

Bulk sample weights

Sample Number	Unit	Weight (kg)			
		Bulk Rec'd	Table Split	+2 mm Clasts	Table Feed
11-PTA-042	D	12.9	12.9	1.6	11.3
11-PTA-037	D	14.5	14.5	2.6	11.9
11-PTA-035	C	13.3	13.3	2.2	11.1
11-PTA-030	C	14.1	14.1	1.9	12.2
11-PTA-023A	B	14.7	14.7	2.2	12.5
11-PTA-023B	A	15.0	15.0	1.6	13.4

Appendix F

Clast Fabric Field Measurements

11-PTA-022			
Azimuth	**Plunge**	**Azimuth**	**Plunge**
101	10	280	4
8	59	46	38
351	69	61	57
91	14	77	50
76	48	190	60
160	62	64	15
231	75	64	10
131	81	251	58
4	60	24	0
62	10	195	57
85	67	19	63
152	9	36	61
80	39	214	8
58	10		
144	1		
169	74		
65	42		
57	59		
34	9		
114	74		
69	18		
159	61		
16	39		
91	54		
311	61		
146	50		
48	51		
166	35		
148	76		
259	11		
69	63		
15	36		
84	49		
201	9		
86	15		
59	46		
180	51		

11-PTA-023B			
Azimuth	**Plunge**	**Azimuth**	**Plunge**
54	40	188	0
56	31	143	16
111	46	186	9
69	81	46	54
12	19	224	29
351	3	144	4
284	4	155	5
83	41	154	0
350	29	141	3
351	36	206	11
174	58	146	14
36	44	141	10
325	38	196	5
15	46		
261	22		
279	32		
125	61		
129	10		
294	40		
286	40		
281	9		
346	0		
149	28		
301	19		
325	6		
291	1		
166	21		
111	0		
112	1		
118	2		
99	18		
161	1		
114	4		
116	14		
110	6		
130	50		
113	10		

Clast Fabric Field Measurements

11-PTA-031			
Azimuth	**Plunge**	**Azimuth**	**Plunge**
64	17	23	15
63	19	51	3
94	26	54	7
57	12	152	11
5	3	36	12
64	6	57	18
191	14	59	10
199	27	35	4
101	28	56	7
183	17	36	6
49	4	19	9
47	7		
55	11		
48	4		
61	5		
43	15		
37	14		
26	1		
352	24		
276	22		
33	30		
45	14		
64	26		
42	1		
54	27		
13	15		
189	6		
96	19		
251	5		
63	26		
132	1		
49	2		
29	8		
54	16		
7	7		
44	37		
4	38		
42	22		
61	19		

11-PTA-034			
Azimuth	**Plunge**	**Azimuth**	**Plunge**
239	23	227	12
359	51	199	33
194	24	38	19
311	42	31	34
2	3	207	40
222	9	306	13
228	36	64	7
20	12	147	35
234	4	253	30
15	12	69	6
53	25	233	38
67	15		
237	4		
23	2		
275	1		
273	22		
284	14		
53	21		
260	4		
55	4		
75	14		
39	20		
16	19		
342	44		
45	42		
213	14		
57	1		
346	50		
250	25		
28	13		
255	23		
34	20		
234	9		
204	53		
278	10		
54	2		
14	14		
257	44		
58	24		

Clast Fabric Field Measurements

11-PTA-035			
Azimuth	**Plunge**	**Azimuth**	**Plunge**
301	4	326	17
29	26	334	36
346	32	326	31
17	9	49	25
296	2	309	15
314	23	33	24
312	7	9	16
297	14	223	43
272	22	270	4
259	20	266	15
273	12	13	11
63	25		
268	9		
19	19		
286	7		
285	37		
268	34		
271	37		
332	47		
257	13		
56	18		
19	30		
353	37		
20	24		
58	19		
32	24		
283	21		
343	22		
282	15		
22	13		
38	8		
312	36		
237	9		
271	26		
46	37		
276	16		
47	3		
292	15		
264	24		

11-PTA-037			
Azimuth	**Plunge**	**Azimuth**	**Plunge**
171	6	346	16
34	24	334	6
321	21	319	19
335	14	155	14
184	36	157	14
324	9	295	6
342	40	244	6
51	9	191	9
112	14	349	11
342	9	354	16
228	24	189	11
359	49	134	16
335	55	329	54
52	4		
336	14		
274	14		
196	31		
144	16		
169	6		
4	25		
349	54		
314	16		
262	18		
311	18		
131	23		
26	11		
181	26		
289	40		
21	13		
206	15		
311	9		
334	18		
212	10		
142	23		
337	17		
191	28		
325	16		
190	56		
262	14		

Clast Fabric Field Measurements

11-PTA-042				
Azimuth	**Plunge**	**Azimuth**	**Plunge**	
335*	28*	164	8	*cobble
333	18	239	14	
75	1	298	3	
154	4	61	9	
147	6	191	6	
356	19	59	1	
55	6	57	1	
69	14	66	9	
119	21	94	17	
63	18	91	10	
49	28	246	17	
105	9	74	4	
76	17	256	6	
75	11			
79	1			
249	9			
62	1			
15	3			
26	23			
198	6			
246	7			
269	9			
44	2			
104	6			
44	6			
72	1			
116	1			
41	17			
30	12			
89	39			
78	28			
232	2			
294	7			
224	14			
245	7			
212	4			
174	10			
81	39			
234	11			

APPENDIX G

Pebble lithology counts from samples taken from Pit-K62, Pine Point

		SHIELD														
			Felsic		Mafic		Meta		Meta		Arkosic quartzite					
			intrusive		intrusive		volcanic		sediment		Fe rich		undiff.		Vein quartz	
Sample	Unit	n	n	%	n	%	n	%	n	%	n	%	n	%	n	%
11-PTA-042	D	338	51	15.09	10	2.96	0	0.00	3	0.89	0	0.00	0	0	1	0.30
11-PTA-037	D	402	65	16.17	15	3.73	2	0.50	3	0.75	0	0.00	0	0	6	1.49
11-PTA-035	C	378	66	17.46	8	2.12	0	0.00	10	2.65	11	2.91	0	0	0	0.00
11-PTA-030	C	408	84	20.59	13	3.19	4	0.98	23	5.64	9	2.21	0	0	0	0.00
11-PTA-023A	B	346	76	21.97	4	1.16	3	0.87	13	3.76	7	2.02	0	0	0	0.00
11-PTA-023B	A	363	152	41.87	25	6.89	6	1.65	15	4.13	22	6.06	1	0	3	0.83

		PALEOZOIC								CORDILLERA			CRETACEOUS					Total
		Carbonaceous				Dolomitized						Grey		Ironstone				n
		Limestone		mudstone		green shale		limestone		Quartzite		dolomite		Siderite		Other		
Sample	Unit	n	%	n	%	n	%	n	%	n	%	n	%	n	%	n	%	
11-PTA-042	D	177	52.37	0	0.00	0	0.00	0	0.00	0	0.00	95	28.11	0	0.00	1	0.30	338
11-PTA-037	D	96	23.88	0	0.00	0	0.00	0	0.00	0	0.00	215	53.48	0	0.00	0	0.00	402
11-PTA-035	C	156	41.27	0	0.00	0	0.00	0	0.00	0	0.00	127	33.60	0	0.00	0	0.00	378
11-PTA-030	C	92	22.55	0	0.00	0	0.00	0	0.00	0	0.00	183	44.85	0	0.00	0	0.00	408
11-PTA-023A	B	158	45.66	0	0.00	0	0.00	0	0.00	0	0.00	84	24.28	0	0.00	1	0.29	346
11-PTA-023B	A	52	14.33	0	0.00	0	0.00	0	0.00	0	0.00	86	23.69	0	0.00	1	0.28	363

Sample	Comments
11-PTA-042	2 sulphide grains, and one massive sulphide pebble, one tillite
11-PTA-037	4 sulphide grains, and 1 massive sulphide pebble
11-PTA-035	4 sulphide grains, and 1 massive sulphide pebble
11-PTA-030	
11-PTA-023A	1 Hematite p
11-PTA-023B	1 Cordillera Quartzite, 1 calcite, 2 massive sulphide Pebble

Appendix H

*Azimuth of sample was unavailable; arrows indicate general direction relative to slide orientation.

Sample	Unit	Description	Interpretation	Figure
11-PTA-022	A	• Single domain • Small vug-like voids • Multi-directional lineations (NE ↘ and NE ↗) • Grain lineations (NE↘ and NE↗) • Rotation structures • Necking structures	-High degree of shear exerted on till -Evidence of reworking and possible overprinting -Polyphase deformation -Unit was deposited subglacially as part of a deforming bed -Type B mélange till	Figure 29
11-PTA-023B	A	• Single domain with additional domains "clinging" to some clasts • Fracture voids • Lineations • Grain lineations • Rotation structures		Figure 30
11-PTA-023	A/B	• Contact between Unit A and Unit B • Reworked Unit A into Unit B • Lineations • Rotation structures	-Unit A being reworked and deformed into Unit B by a subglacial deforming bed	Figure 31
11-PTA-023A	B	• Multiple domains • Small voids • Multi-directional lineations (↔and ↕)* • Rotation structures • Grain stacks • Microfractured and fragmented grains	-Polyphase deformation -Evidence of possible overprinting -evidence of reworking -loading/ unloading fissility -Unit was emplaced subglacially by a mobile bed into an underlying (Unit A) bed -Type B mélange till	Figure 32

11-PTA-025	C	• Multiple domains • Abundant voids • Lineations • Rotation structures • Single fractured grain	-Thickest unit -Polyphase flow -Shearing zones -Pore-water movement -High degree of shearing exhibited on the till -Fluctuation in amount of shear exhibited on shear throughout the unit -Evidence of reworking -Emplaced from a mobile bed into an immobile bed (Unit B) causing some shearing -Type B Mélange till	Figure 33
11-PTA-026	C	• Multiple domains • Fracture and vug-like voids • Multi-directional lineations (S ↘ and S↗) • Grain lineations (S ↗ and S↘) • Rotation structures • Till balls and clay accumulations • Fractured grains		Figure 34
11-PTA-027	C	• Multiple domains • Fracture voids • Lineations • Grain lineations • Rotation structures • Deformation banding		Figure 35
11-PTA-028	C	• Multiple domains • Fracture voids • Mutli-directional lineations (N↘ and N↗) • Grain lineations (N↘ and N↗) • Rotation structures • Necking structures • Shear banding • Micro-fractured grains		Figure 36

11-PTA-029	C	• Multiple domains • Large vug-like voids • Thin fracture voids • Multi-directional lineations (S↘ and S↗) • Grain lineations (S↘ and S↗) • Rotation structures • Necking structures • Pressure shadows	-Thickest unit -Polyphase flow -Shearing zones -Pore-water movement -High degree of shearing exhibited on the till -Fluctuation in amount of shear exhibited on shear throughout the unit -Evidence of reworking -Emplaced from a mobile bed into an immobile bed (Unit B) causing some shearing -Type B mélange till	Figure 37
11-PTA-030	C	• Single domain • Voids throughout thin section • Multi-directional lineations (NW↘and NW↗) • Grain lineations (NW↘and NW↗) • Rotation structures • Clay accumulations • Pipe-like pore water movement • Minor grain crushing		Figure 38
11-PTA-031	C	• Multiple domains • Multi-directional lineations (SE↘ and SE↗) • Grain lineations (SE↗ and SE↘) • Rotation structures • Pressure shadows • Thin fracture voids		Figure 39
11-PTA-032	C	• Multiple domains • Multi-directional lineations (NE↘ and NE↗) • Grain lineations (NE↗) • Rotation structures • Pressure shadows • Necking structure • Multiple fracture and vug like voids		Figure 40

11-PTA-035	C	• Sand-packed • Thin fracture voids • Multiple domains • Multi-directional lineations (↘ and ↗)* • Grain stacks (predominantly fine-grained)(↗) • Rotation structures • Weak clast orientation (↗)*	-Thickest unit -Polyphase flow -Shearing zones -Pore-water movement -High degree of shearing exhibited on the till -Fluctuation in amount of shear exhibited on shear throughout the unit -Evidence of reworking -Emplaced from a mobile bed into an immobile bed (Unit B) causing some shearing -Type B mélange till	Figure 41
11-PTA-036	C	• Multiple domains • Absence of voids • Multi-directional lineations (NE↘ and NE↗) • Grain lineations (NE↗) • Weak rotation structures • Crushed grains		Figure 42
11-PTA-037	D	• Multiple domains • Large fracture voids • Multi-directional lineations (NE↘ and NE↗) • Grain lineations (NE↗) • Rotation structures (NE↗) • Pressure shadows	-Polyphase deformation -Freeze thaw mechanism on samples closest to the surface -Possible streaming ice -Evidence of reworking in lower samples -Type B mélange till	Figure 43
11-PTA-038	D	• Sand-packed • Multiple domains • Fracture voids • Multi-directional lineations (↘and ↗)* • Grain lineations (↔) • Rotation structures		Figure 44

11-PTA-040	D	• Single domain • High abundance of fracture voids • Short lineations • Grain lineations • Rotation structures • Crushed grains	-Polyphase deformation -Freeze thaw mechanism on samples closest to the surface -Possible streaming ice -Evidence of reworking in lower samples -Type B mélange till	Figure 45
11-PTA-041	D	• Single domain • High abundance of fracture voids • Short lineations • Grain lineations • Rotation structures • Crushed grains		Figure 46
11-PTA-042	D	• Abundance of fracture voids • Unable to complete accurate micromorphological interpretations		Figure 47